Optical Second Harmonic Generation Studies on a New Class of Molecular Materials: Diaminodicyanoquinodimethanes

A Thesis
Submitted for the Degree of
DOCTOR OF PHILOSOPHY

by

M. RAVI

School of Chemistry
University of Hyderabad
Hyderabad 500 046
INDIA

June 1997

To my parents

.... the study of chemistry is profitable,
not only inasmuch as it promotes the material interests of mankind,
but also because it furnishes us with insight
into those wonders of creation which immediately surround us,
and with which our existence, life and development,
are most closely connected.

- Justus Von Liebig

CONTENTS

			Page No.
Declaration			**i**
Certificate			ii
Acknowledgements			iii
Abbreviations			**v**
Synopsis			**vi**
Chapter	**1**	**Introduction**	
	1.1	Historical Background	1
	1.2	The Concept of Optical Nonlinearity	5
	1.3	Second Order Nonlinear Optical Materials	12
	1.4	Strategies to Obtain Noncentrosymmetric Structures for Quadratic NLO Applications	18
	1.5	Methods for the Computation of Molecular Hyperpolarisabilities	**24**
	1.6	Experimental Techniques to Measure SHG	**30**
	1.7	Layout of the Thesis	**37**
		References	**40**
Chapter	**2**	**Computation of Molecular Hyperpolarisability and the Study of Structure-Property Relationships**	
	2.1	Background	47
	2.2	Computation of Molecular Hyperpolarisabilities	51
	2.3	Dependence of Hyperpolarisability on the Quinonoid - Benzenoid Character	55

2.4 Dependence of Hyperpolarisability on the Molecular Twist 67
2.5 Conclusion 78
References **80**

Chapter 3 Synthesis and Characterisation
3.1 Background 83
3.2 Synthesis 85
3.3 Characterisation 89
3.4 Conclusion 95
References 97

Chapter 4 Experimental Determination of Molecular Hyperpolarisability
4.1 Background 99
4.2 Determination of Excited State Dipole Moments using a Simple Solvatochromic Method 100
4.3 Estimation of Hyperpolarisabilities using Extrapolation from the Two-level Model 112
4.4 Determination of Hyperpolarisability using EFISHG Technique 120
4.5 Conclusion 126
References 128

Chapter 5 Materials from Achiral Molecules: Crystal Structures and Powder SHG Studies
5.1 Background 131
5.2 Crystal Structures of DPIDQ, DPZDQ and DMDQ 13 3

5.3 Solvate Switchable Powder SHG in DPDQ 142
5.4 Conclusion 151
References 153

Chapter 6 Materials from Chiral Molecules: Crystal Structures and Powder SHG Studies
6.1 Background 155
6.2 Crystal Structures and Powder SHG Studies of MBPDQ and PMPDQ 158
6.3 Dual Influence of Intermolecular H-bonding on the SHG in DHPDQ 166
6.4 Influence of the Placement of the Stereogenic Centre and Enhanced SHG in DMPDQ 178
6.5 Conclusion 187
References 189

Chapter 7 Overview of the Present Work and Future Prospects 191

Appendix 197
List of Publications

DECLARATION

I hereby declare that the matter embodied in this thesis is the result of investigations carried out by me in the School of Chemistry, University of Hyderabad, Hyderabad under the supervision of Dr.T.P.Radhakrishnan.

In keeping with the general practice of reporting scientific observations, due acknowledgments have been made wherever the work described is based on the findings of other investigators.

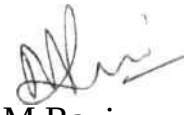

M.Ravi

CERTIFICATE

This is to certify that the work described in this thesis entitled ***Optical Second Harmonic Generation Studies on a*** *New* ***Class of Molecular Materials : Diaminodicyanoquinodimethanes*** has been carried out by *Mr. M. Ravi*, under my supervision and the same has not been submitted elsewhere for any degree.

Dr. T. P. Radhakrishnan
(Thesis Supervisor)

DEAN
School of Chemistry

ACKNOWLEDGMENTS

I am at loss of words to express my gratitude to Dr.T.P.Radhakrishnan, my *guru*, for the constant encouragement, inspiring guidance and for the freedom he gave me in carrying out my research. I am grateful to him for suggesting an exciting research problem. My association with him is a memorable one in my life.

I am deeply indebted to Dr.D.Narayana Rao. School of Physics for his cooperation throughout my research work in carrying out SHG experiments. Without his help 1 couldn't have completed my work effectively. I also thank Dr.A.Samanta for his suggestions and involvement in solvatochromic studies.

I thank Prof. P.S.Zacharias, Dean, my M.Phil supervisor, Prof.R.Jagannathan and all other faculty members of the School of Chemistry for their support. I thank all my teachers at Tara Colllege, Sangareddy and Department of Chemistry, Osmania University for their wonderful teachings from which I benefited very much.

I am grateful to Dr.Shmuel Cohen and Prof.Israel Agranat, Hebrew University of Jerusalem, for solving the crystal structures. I thank Prof.J.Chandrasekhar for providing a computer program for some of the calculations and Prof.C.Reichardt, for his generous gifts of betaine dye.

It is a great pleasure to thank my labmates: Dr.Satya Prasanna, Prasad, Dr.Sirish, Anitha, Arounagiri, Sastry, Giribabu, Palas, Sonika, Nachimuthu, Asha and Laser labmates: Rammohan, Nirmal, Ranita and Shiva for their cooperation and friendship. I thank Mr.Venugopal Rao for his help in carrying out EFISHG experiments.

I take this opportunity to thank my classmates and friends Shankar Rao, Prasanna, Krishna, Satish Kumar and Balaram. I thank all research scholars and friends for the cheerful and enlivening atmosphere they maintained and for making my stay at the RS hostel unforgettable.

I thank the non-teaching staff of the School for their assistance during my research work.

I thank the CSIR, New Delhi for financial help and DST for providing the funding to build the EFISHG setup.

Finally I thank my parents, sisters, brothers, Sunny and all other family members for their love and encouragement.

ABBREVIATIONS

AM1	Austin Model 1
CI	configuration interaction
CPHF	coupled perturbed Hartree-Fock
CS	crystal structure
CT	charge transfer
DADQ	7,7-diamino-8,8-dicyanoquinodimethane
DHPDQ	7,7-di[*R*(-)-3-hydroxypyrrolidino]-8,8-dicyanoquinodimethane
DMDQ	7,7-dimorpholino-8,8-dicyanoquinodimethane
DMPDQ	7,7-di[*S*(+)-2-methoxymethylpyrrolidino]-8,8-dicyanoquinodimethane
DMSO	dimethylsulphoxide
DPDQ	7,7-dipyrrolidino-8,8-dicyanoquinodimethane
DPIDQ	7,7-dipiperidino-8,8-dicyanoquinodimethane
DPZDQ	7,7-dipiperazino-8,8-dicyanoquinodimethane
EFISHG	electric field induced second harmonic generation
FF	finite field
HRS	hyper Rayleigh scattering
MBPDQ	7-[(*S*)-α-methylbenzylamino]-7-pyrrolidino-8,8-dicyanoquinodimethane
NLO	nonlinear optics
PMPDQ	7-[(*S*)-methoxymethylpyrrolidino]-7-pyrrolidino-8,8-dicyanoquinodimethane
QBC	quinonoid - benzenoid character
SHG	second harmonic generation
SOS	sum-over-states
TCNQ	7,7,8,8-tetracyanoquinodimethane
THF	tetrahydrofuran

SYNOPSIS

Currently there is tremendous interest in developing new materials for a wide variety of nonlinear optical (NLO) applications in the areas of optoelectronics and photonics. Most of the materials commercially used today are based on inorganic compounds. Compared to these inorganic materials, many organic and organometallic molecular materials have much higher NLO efficiencies and faster response times and are amenable to a wider range of synthetic protocols. However, the organic materials are often handicapped by problems such as poor crystal growth characteristics, low thermal stability and damage threshold, inadequate transparency windows etc.. Therefore there is a great need to investigate and develop novel molecular materials that circumvent these difficulties.

This thesis presents the systematic investigation of a class of push-pull diamino substituted dicyanoquinodimethane systems as novel molecular materials for quadratic NLO applications. The results of these studies are presented in seven chapters. We describe below the salient features of the contents of each chapter. In Chapters 2 - 6, the first Section provides some background information about the contents of the Chapter.

CHAPTER 1: INTRODUCTION

Section 1 presents the historical background of the field of nonlinear optics and the development of organic materials for quadratic NLO applications. Basic concepts of nonlinear optics including second harmonic generation (SHG) and linear electro-optic effects are discussed in Section 2. The materials for second harmonic generation including organic, inorganic and organometallic compounds reported by various groups are reviewed in Section 3. Various approaches to obtain noncentric structures for designing materials for quadratic NLO applications like SHG are summarised in Section 4. The computaional methods to calculate molecular hyperpolarisabilities are discussed in Section 5. In Section 6, the experimental techniques to measure SHG in solution and powders are outlined. The final section of this chapter presents the layout of this thesis.

CHAPTER 2: COMPUTATION OF MOLECULAR HYPER-POLARISABILITY AND THE STUDY OF STRUCTURE-PROPERTY RELATIONSHIPS

The molecular hyperpolarisabilties, β are commonly computed using semiempirical or *ab initio* procedures employing the sum-over-states (SOS) and coupled Hartree-Fock (CPHF) methods. The methodologies which we have adopted for the computation of β are presented in Section 2. The (3 values computed for several derivatives of push-pull quinodimethanes

which we have synthesised, are presented and the results discussed in this Section. We have investigated the effect of push-pull groups and electrostatic environment on β using model calculations on a prototypical system, namely, 7,7-diamino-8,8-dicyanoquinodimethane. This effect is quantified by the definition of a quinonoid-benzenoid character and the results are presented in Section 3. We have also carried out some analysis of the dependence of β on the molecular structure of these push-pull quinonoid compounds. Crystal structure studies on several compounds have shown that these molecules possess a strong twist between the plane containing the donor group N atoms and the plane containing the conjugating unit and dicyanomethylene group. Calculations have been carried out on a model system, DPDQ to study the dependence of β on the molecular twist. Section 4 presents the results of these studies and the analysis of the unusual variation of β observed, using the two-level model.

CHAPTER 3: SYNTHESIS AND CHARACTERISATION

In this chapter, we present the synthesis and characterisation of achiral and chiral derivatives of push-pull diamino substituted dicyanoquinodimethane we have investigated in this study. These compounds are very easily synthesised and offer tremendous flexibility in derivatisation. These novel materials we have investigated have higher thermal stability than many of the well-known organic NLO materials.

They are also amenable to easy crystal growth. Their synthesis and spectroscopic characterisation details are presented in this Chapter.

CHAPTER 4: EXPERIMENTAL DETERMINATION OF MOLECULAR HYPERPOLARISABILITY

The two-level model for β shows that change in dipole moment on excitation of a molecule strongly influences and often determines the hyperpolarisability. We have proposed a simple procedure for the solvatochromic determination of the change in dipole moments of organic molecules on excitation and this practically convenient procedure is described in Section 2. We utilised this procedure together with simple electronic absorption studies, to determine experimentally, the two-level approximation to the p of some of our quinonoid systems. This simple solvatochromic method is discussed in Section 3 along with an analysis of the results in view of the earlier computed p. We have also assembled the set up to carry out Electric Field Induced Second Harmonic Generation (EFISHG) study of molecular p in solution. Details are presented in Section 4 along with studies carried out on a representative quinonoid molecule.

CHAPTER 5: MATERIALS FROM ACHIRAL MOLECULES: CRYSTAL STRUCTURES AND POWDER SHG STUDIES

In Section 2, we present the study of powder SHG and crystal structures of the various materials we have studied based on achiral quinonoid compounds. Several of these compounds had centrosymmetric lattices and showed no SHG. However, DPDQ in one of its polymorphic forms showed an unusual and novel phenomenon of solvate switchable SHG and this is discussed in Section 3.

CHAPTER 6: MATERIALS FROM CHIRAL MOLECULES: CRYSTAL STRUCTURES AND POWDER SHG STUDIES

Section 2 presents the crystal structures and the results of the powder SHG studies on the materials we have developed from chiral quinonoid systems. SHG dependence on particle sizes showed that these materials are capable of phase-matchable SHG. In Section 3 we discuss the dual influence of intermolecular H-bonding on the SHG capability in DHPDQ. Molecular engineering was successfully employed to improve the SHG capability in this class of compounds (see table below). Interesting and useful correlation of the crystal structures and the SHG, extracted from these studies are discussed in Section 4. (See Chapter 6 for the molecular structure of these compounds.)

Compound	Space group	SHG/U
MBPDQ	$P2_1$	3
DHPDQ	$P2_12_12_1$	13
PMPDQ	$P2_12_12_1$	28
DMPDQ	$P2_1$	55

CHAPTER 7: OVERVIEW OF THE PRESENT WORK AND FUTURE PROSPECTS

This chapter presents an overview of the present investigation on a new class of molecular materials for SHG. These materials have several positive features like easy synthesis, high thermal stability, optical transparency and moderate to strong phase-matchable SHG. Investigation of these materials have also revealed some important practical guidelines for the fabrication of molecular materials for SHG. Future direction for research in this area are also outlined in this Chapter.

CHAPTER 1

INTRODUCTION

1.1 HISTORICAL BACKGROUND

Reflection, refraction and diffraction are the commonly observed interactions of light with matter. These are said to occur in the domain of linear optics, since the magnitude of the observed effects change linearly with the light intensity. Light absorption and photochemical events such as photosynthesis can also be described as one-photon linear optical processes. Nonlinear optics (NLO) is the study of the interaction of intense electromagnetic fields with matter which causes the modification of the optical properties such as refractive index, and leads to output fields that are different from the input field in phase, frequency, amplitude or polarisation. When the field is applied externally, it is called an electro-optic effect[2], and the earliest observations of such effects were the variation of refractive index as a linear (Pockels effect) and a quadratic (Kerr effect) function of the applied electric field. When the electric field associated with an incident electromagnetic radiation gives rise to an NLO response, the observed effect is an all-optical one, and such phenomena could be observed only with the advent of lasers in the 1960's. Availability of high power lasers stimulated extensive research on the nonlinear optical properties of materials. Nonlinear susceptibilities $\chi^{(}$ and $\chi^{(\ )}$ describe terms in the polarisation, proportional to the square and the cube of the electromagnetic field respectively. The susceptibility $\chi^{(2)}$ is responsible for second harmonic generation (SHG), a typical nonlinear optical process; it involves the conversion of an input optical wave into an output wave of double the input frequency. For example, such a process could produce green light (532 nm)

from a Nd:YAG laser operating at 1064 nm. The $\chi^{(2)}$ vanishes in materials with inversion symmetry whereas all materials have a nonvanishing value of $\chi^{(3)}$. The cubic nonlinearity leads to a large variety of nonlinear effects, including third harmonic generation, four wave mixing, phase conjugation *etc*..[3-5]

SHG was first observed in single crystal quartz by Franken and coworkers[6] in 1961. Giordmaine[7] and Maker *et al*[8] demonstrated SHG in KDP crystals which were commercially grown for Pockels-type electro-optic shutters. Subsequently other NLO effects like parametric oscillation were discovered which provide tunable beams in the infra red by parametric down conversion from 1.06 urn wavelength. Parametric amplification was observed in lithium niobate ($LiNbO_3$) single crystals in 1965.[10] Materials with large $\chi^{(}$, which can be used farther into the infra red, include proustite (Ag_3AsS_3), tellurium, indium antimonide *etc*..[5]

The first observation of SHG in an organic material (benzopyrene) was made in 1964 by Rentzepis and Pao.[11] The potential of organics was revealed by further studies on hexamethylenetetramine,[12] hippuric acid[13] and benzil. In 1968 a systematic approach was developed to quantify and classify the SHG in powders of organic and inorganic compounds by Kurtz and Perry. The analysis of nonlinear interference processes in crystals known as the Maker fringe method[8] was developed by Jerphagnon and Kurtz in 1970.[16] Demonstration of electric field induced second harmonic generation (EFISHG) in centrosymmetric media such as fluids by

Hauchecorne *et al* in 1971[17] showed that it is possible to measure individual molecular nonlinearities in solution by breaking the centre of symmetry upon application of high electric field pulses. Exploration of nonlinear optical organic materials changed from a random scanning process into a systematic search with the work of Davydov *et al*[19] which established the connection between enhanced nonlinearities and charge transfer in conjugated molecules.

Extensive early work on organic NLO materials was carried out by the research groups at CNET, France and Bell Laboratories, USA. The organic molecules with their inherent flexibility and synthesis potential are ideal candidates for 'crystal engineering'.[20] Theoretical methods were developed to analyse the correlation between molecular structure and nonlinearity and to relate the molecular hyperpolarisabilities to bulk susceptibilities. Simple ideas such as the two-level model[22] for molecules with intramolecular charge transfer were put forward which turned out to be extremely useful in the synthetic design of new NLO systems. From the late 1970's upto now, fundamental work on solutions has continued ' ; however the focus has shifted from purely molecular studies to the problem of designing molecular materials. Several organic molecules have been found to have appreciable NLO capabilities (see Sec. 1.3). One of the early successes in this direction was the fabrication of two crystalline materials with NLO efficiency higher than that of $LiNbO_3$ by one order of magnitude; MAP (methyl-(2,4-dinitrophenyl)-aminopropanoate)[24] and MNA (2-methyl-4-nitroaniline). * Strong SHG and tunable parametric amplification was

observed in POM (3-methyl-4-nitropyridine-1 -oxide)[26] and NPP (N-(4-nitrophenyl)-(L)-prolinol) crystals.[27] NPP and the parent structure PNP (nitro-4-pyridino-2-(L)-prolinol) are examples of optimal structures for phase-matched nonlinear interactions[28] where the molecules are ideally oriented with respect to the crystalline symmetry axis so as to maximise the effective nonlinear coefficients. NPP has a nonlinear coefficient (d) of 200 x 10^{-9} esu which leads to two orders of magnitude higher efficiency (d n" ; n = refractive index) than lithium niobate. Recent research has focused on developing new materials with good practical attributes such as thermal and chemical stability and crystal growth characteristics. This has led to the growth of single crystals [9] of NPP, MAP and POM and detailed characterisation of their nonlinear susceptibility tensor. However, investigations of the powder NLO characteristics by the Kurtz and Perry method have been widely used for screening the large number of available and new materials. ' " - Recently nondipolar noncentrosymmetric molecules with octupolar moments have emerged as interesting new candidates ; the system with the highest static hyperpolarisability reported so far is a ruthenium complex with chiral ligands.[37] The NLO properties of poled polymers, polymers incorporated in sol-gel matrices,[41-42] liquid crystalline polymers[38] and Langmuir-Blodgett films[43], polymeric photorefractive materials[44] have also been under extensive investigation. Polymers with extended conjugation such as polyacetylene, polyphenylenevinylene, polythiophene, polydiacetylene and macrocyclic systems like Phthalocyanines and porphyrines have emerged as some of the best materials for third order NLO applications.[45]

Nonlinear optical effects are widely used in optoelectronic devices which have innumerable applications in telecommunications, fast switches, optical computing, optical data storage, optical information processing *etc*.. The emerging area of photonics is expected to fully exploit a variety of nonlinear optical phenomena and materials. The basic capability of NLO materials to effect the modulation and amplification of optical signals should lead to a dominant role for them in future information technology.

1.2 THE CONCEPT OF OPTICAL NONLINEARITY

When the electric field of an electromagnetic radiation typically in the optical range of frequencies, interacts with a material, it induces a dipole moment in the material. The dipole moment induced per unit volume is called 'polarisation'. At low electric fields, the macroscopic polarisation *ie.* polarisation of the bulk medium, P is linearly related to the field by the proportionality constant, $\chi^{(1)}$, known as the linear electric susceptibility. At high fields typically those associated with lasers, contribution of the nonlinear (second and higher order) terms become significant.[46] Higher order susceptibilities $\chi^{(n)}$ (n > 1) are inherently much smaller than $\chi^{(1)}$; they become much smaller as n increases. The polarisation along the 1th axis can therefore be generally represented as:

$$P_i = \chi_{ij}^{(1)} E_j + \chi_{ijk}^{(2)} E_j E_k + \chi_{ijkl}^{(3)} E_j E_k E_l + \ldots\ldots \qquad (1.1)$$

Since the electric field and the polarisation are vectors, the n order macroscopic electric susceptibility ($\chi^{(n)}$) that relates the components of the polarisation to the applied field is an (n+1) order tensor. In Eqn.1.1, the indices i, j, k, and 1 refer to the coordinate framework of the bulk material.

Fig. 1.1 (a) illustrates the linear and nonlinear polarisation with respect to electric field. The asymmetric polarisation response to a symmetric electric field in a nonlinear medium is shown in Fig.l.l(b). The Fourier decomposition of this nonlinear polarisation comprising of

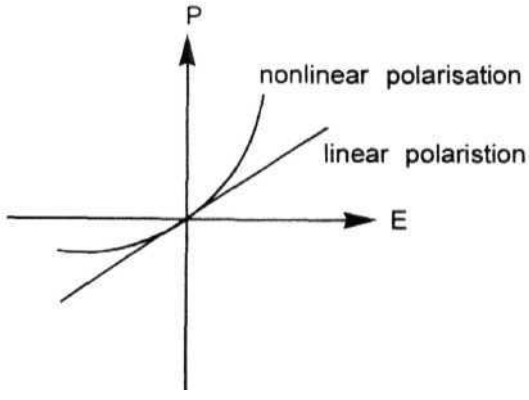

Figure l.l(a): *linear and nonlinear polarisation vs electric field*

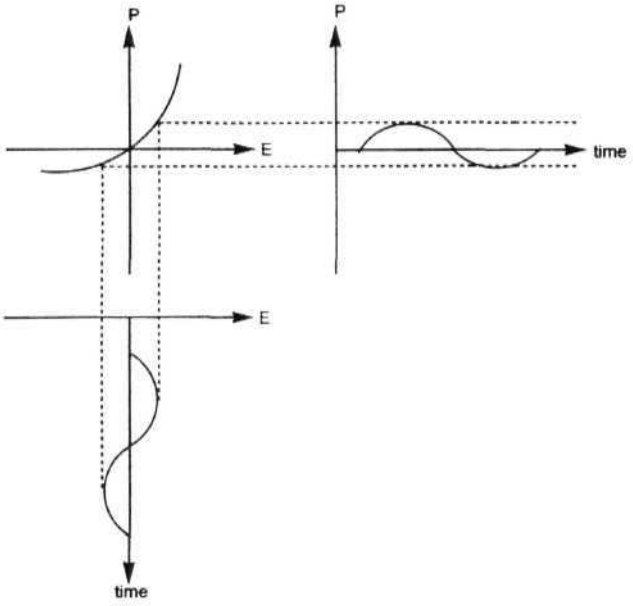

Figure 1.1 (b): *Asymmetric polarisation response to a symmetric electric field*

components of zero frequency, the fundamental frequency, the second harmonic frequency, the third harmonic frequency *etc.* is shown in Fig.l.l(c). The effects upto the second order which are easily observed experimentally are called the optical rectification ($\chi^{(2)}$ (0; ω,ω)), linear electro-optic effect ($\chi^{(2)}$ (-co; co,0)), second harmonic generation ($\chi^{(2)}$ (-2co; co,co)) and third harmonic generation ($\chi^{(3)}$ (-3co; co,co,co)).

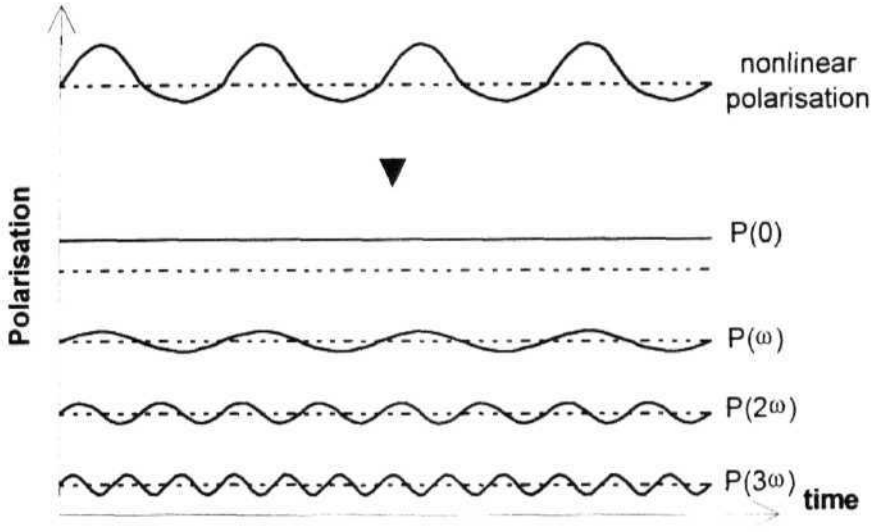

Figure l.l(c): *The Fourier decomposition of nonlinear polarisation and the components of P(x)at frequencies 0, ω, 2ω and 3d)*

In this thesis we deal exclusively with second order nonlinear optical properties of organic materials. We provide below brief descriptions of the second order effects such as linear electro-optic effect and second harmonic generation. The work presented in the thesis focuses mainly on second harmonic generation studies.

Linear electro-optic effect

The linear electro-optic effect or Pockels effect is usually described in terms of the tensor r_{ijk} which is related to the susceptibility, $\chi^{(\,)}(-\omega;\omega,0)$, through the dielectic constant tensor (E) components as:

$$\chi^{(2)}_{ijk}(-\omega;\omega,0) = -(1/2)\varepsilon_{ii}(\omega)\varepsilon_{jj}(\omega)r_{ijk}(-\omega;\omega,0) \qquad (1.2)$$

The Pockels effect is the linear change in the index of refraction of a system in the presence of an external electric field. The ij^t component of the change in the dielectric constant is related to the electric field component E_k by the coefficient, r_{ijk} as follows:

$$\Delta\left(\frac{1}{\varepsilon_{ij}}\right) \equiv \frac{1}{\varepsilon_{ij}} - \frac{1}{\varepsilon_{ij}(0)} \cong -\frac{\Delta\varepsilon_{ij}}{\varepsilon_{ij}^2} = r_{ijk}E_k \qquad (1.3)$$

Here, $\varepsilon_{ij}(0)$ is the ij^{th} component of the dielectric constant in the absence of the external dc field and the approximation is valid in the limit where field induced changes in the dielectric constant are small. The experimental determination of the linear electro-optic coefficient is based on the simplification, $\Delta n = n^3.r.E/2$. Tensor subscripts have been omitted for simplicity. Δn is the induced change in the refractive index, n is the refractive index in zero field. r the electro-optic coefficient, and E the applied modulating field. The small changes in the refractive index are

measured by detecting phase shift of the light traversing the material, which is defined by:

$$\phi = \left(\frac{2\pi}{\lambda}\right)\Delta n l \qquad (1.4)$$

where 1 is the optical path length. Various groups have studied the electro-optic effects in organic molecular crystals and polymers. Devices based on these effects found early technological application as modulators, for example in Q-switches of pulsed lasers. Due to their large optical nonlinearities, organic materials in appropriately designed wave guide structures can be used for electro-optic modulation and switching functions.

Second harmonic generation (SHG)

The phenomenon of frequency doubling or second harmonic generation can be visualised as follows. If the applied electric field is of frequency ω, it can be represented as sinωt and the quadratic terms are seen to have a 2ω dependence.

$$E \propto \sin \omega t$$

$$E^2 \propto \sin^2 \omega t \; (= \frac{1}{2}(1 - \cos 2\omega t))$$

There is an important symmetry constraint for observing second harmonic generation or other quadratic (in general any even order) NLO effects. In systems having a centre of symmetry, reversal of the electric field should exactly reverse the polarisation *ie.* P(-E) = -P(E). From Eqn.1.1 it can be seen that this is possible if and only if all terms with even powers of E becomes zero. In a noncentric system, no such equality exists. This implies that quadratic and other even order effects are possible only in noncentrosymmetric systems. In a gaseous or liquid state where random fluctuations create a centre of symmetry one needs an alignment of molecules using an external field to break the centre of inversion and observe second order effects. For second harmonic generation, a coefficient d_{ijk} is often defined as follows:

$$d_{ijk}(-2\omega;\omega,\omega) = (1/2)\chi^{(2)}_{ijk}(-2\omega;\omega,\omega) \qquad (1.5)$$

Relation between macroscopic and microscopic nonlinearities

In organic molecules, the microscopic polarisation is defined by the induced molecular dipole moment ρ_i which depends on the molecular polarisability, a and hyperpolarisabilities, β, y *etc.* as follows:

$$\rho_i = \alpha_{ij}E_j + \beta_{ijk}E_jE_k + \gamma_{ijkl}E_jE_kE_l + \ldots\ldots \qquad (1.6)$$

The molecular property of significance for the second harmonic generation is the first hyperpolarisability tensor, β_{ijk}. Using the oriented gas model a connection between the molecular hyperpolarisability tensor β_{ijk} and the bulk nonlinear coefficient $\chi_{IJK}^{(2)}$ nas been worked out. The unit cell nonlinearity per molecule, b_{IJK}, introduced by Zyss and Oudar is related to the bulk nonlinear coefficient, d_{IJK} *(ie.* χ_{IJK}) / 2) as follows:

$$d_{IJK} = N f_I^{2\omega} f_J^{\omega} f_K^{\omega} b_{IJK} \qquad \textbf{(1.7)}$$

$$b_{IJK} = \frac{1}{N_g} \sum_{ijk} \left(\sum_{s=1}^{Ng} Cos\theta_{Ii}^{(s)} \, Cos\theta_{Jj}^{(s)} \, Cos\theta_{Kk}^{(s)} \right) \beta_{ijk} \qquad (1.8)$$

where N_g is the number of equivalent position in the unit cell and N is the number of molecules in the crystal unit volume. The angle between the crystallographic axis, I and the microscopic axis, i is denoted by θ_{Ii}. The local field factors (f) essentially correct for the difference between an applied field that would be felt by the molecule in free space and the local field existing in the bulk material. These factors usually take the form of the well known Onsager[48] or Lorentz[49] correction fields.

1.3 SECOND ORDER NONLINEAR OPTICAL MATERIALS

Most of the materials developed initially for nonlinear optical applications were based on inorganic systems. Ferroelectric materials lacking a centre of symmetry were prime candidates. In inorganic materials,

the optical and acoustic phonons as well as the electronic polarisation contribute to the NLO effects. The NLO effects in inorganics can be interpreted only at a bulk level; extension of the atomic or ionic polarisabilities to the bulk NLO properties is complicated. There has been a growing interest in developing π-conjugated organic molecules for nonlinear optical applications as discussed in Sec.1.1 above. Fig.1.2

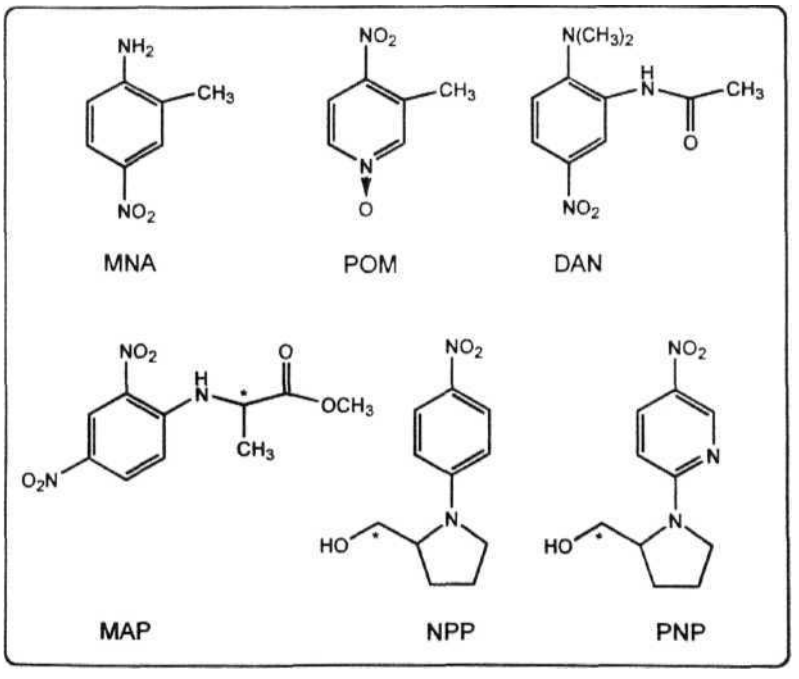

Figure 1.2: *Well known organic NLO molecules*

provides the molecular structures of some well known systems. It has been established that push-pull organic molecules have very high values of β_{ijk} and when they crystallise in noncentrosymmetric space group, they possess large nonlinear susceptibility. The nonlinearity in these systems is dominated by electronic polarisation effects alone. In the solid state, these organic compounds form molecular crystals in which the molecules interact through weak intermolecular forces and retain their individual identity to a high degree.

In organic NLO active molecules with their strongly delocalised *n*-electron system and the 'donor - conjugating unit - acceptor' framework, the physical mechanism of charge transfer that leads to the nonlinear effects can be easily understood in terms of the Mulliken resonance structures as illustrated in Fig. 1.3. When the molecule is polarised by an applied field parallel to the axis along which the substituents exist, the electronic polarisation response will be asymmetrically distorted (solid line) under the cooperative influence of the donor and acceptor groups, as compared to the symmetric response of an unsubstituted benzene (broken line). This asymmetry in the polarisation gives rise to the harmonic frequencies of the field radiated by the molecular dipole oscillations. These simple considerations have led to the development of a vast number of organic molecular crystals and polymers as candidates for NLO applications.

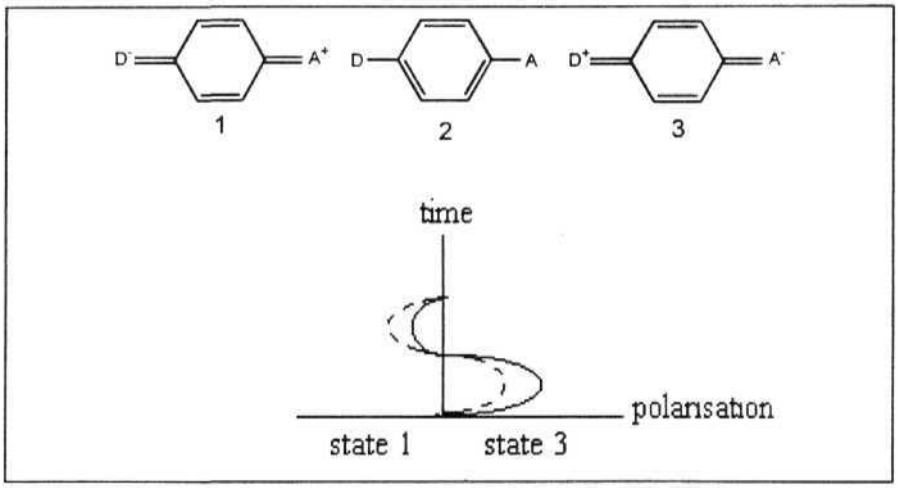

Figure 1.3: *Origin of the nonlinear polarisation in donor-acceptor substituted molecules. The broken line shows the linear response for unsubstituted benzene*

Table 1.1 provides data on the powder second harmonic generation capability of a number of inorganic and well known organic materials (Fig. 1.2). The values for the inorganic systems are quoted with reference to quartz and the values for the organic materials with reference to urea, as is the common practice. The two series of data may be compared given the fact that urea shows approximately 400 times stronger SHG than quartz.

Table 1.1: *Powder SHG values for some well known inorganic materials (relative to quartz; urea included for comparison) and organic materials (relative to urea)*

Material	$I^{2\omega} / I^{2\omega}_{quartz}$	Materials	$I^{2\omega} / I^{2\omega}_{urea}$
$(NH_4)H_2PO_4$	15	Urea	1
$LiNbO_3$	600	MAP	5
KIO_3	1200-2400	POM	13
Ag_2HgI_4	1500	MNA	22
$KNbO_3$	2000	DAN	115
$PbTiO_3$	2400	PNP	140
Urea	400	NPP	150

The quadratic NLO active molecules are mostly based on donor-acceptor substituted aromatics; benzene, stilbenes, diaryl acetylenes, diacetylenes and biaryls are commonly used frameworks. In addition to the above materials, many more organic and organometallic compounds have been examined by the powder SHG method or their molecular hyperpolarisabilities have been measured using EFISHG/HRS techniques, or both. A variety of salts especially with pyridinium and stilbazolium cations have been studied for their second order nonlinear optical properties. A growing number of organometallic compounds have been found to have good powder SHG intensities; ferrocenes, metal carbonyl and metal carbonyl pyridine complexes, octahedral and square-planar metal complexes

are interesting examples.[50] Octupolar molecules are emerging as a new class of molecules with promising NLO properties. Though the investigations for designing crystals for efficient NLO properties is still in their early stages, the molecular hyperpolarisabilities, β, of this class of molecules have been studied by various groups." Recently there has been a report on novel NLO chromophores with through space (as opposed to *n*-conjugative) interactions between the donor and acceptor groups which showed promising NLO properties/

The second order nonlinear optical capability is often characterised by the figure of merit defined as d /n (d = second order coefficient and n = refractive index of the material). Fig. 1.4 shows that the nonlinear organic materials are superior in the visible and near infrared regions of the electromagnetic spectrum. However it may be noted that organic materials have posed some inherent problems such as poor crystal growth characteristics and relatively low thermal stabilities. Also in many cases, they absorb in the visible or near UV region of the electromagnetic spectrum, making the SHG at these wavelengths inefficient. A lot of effort is being put into overcoming these limitations of organic materials, so that they can compete with inorganic materials which at present dominate the area of technological applications.

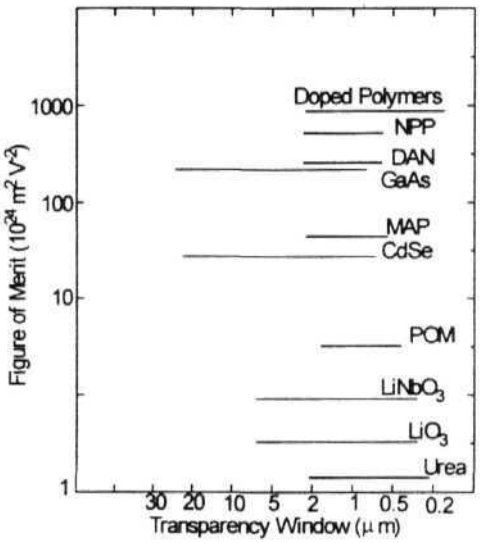

Figure1.4: *Figure of merit and transparency range of some second order NLO materials (the Y-axis scale below 10 has been expanded for clarity)*

1.4 STRATEGIES TO OBTAIN NONCENTROSYMMETRIC STRUCTURES FOR QUADRATIC NLO APPLICATIONS

In Sec. 1.2, we have already noted that a noncentrosymmetric structure is essential for a material to show second order nonlinear optical properties. Amorphous and glassy solids are, in general, centrosymmetric.

Majority of crystalline organic materials are also centrosymmetric. A variety of techniques have been attempted to induce a noncentric lattice formation. Thin films can be prepared as noncentrosymmetric structures, using special techniques. Some of the popular strategies that have been developed to induce noncentrosymmetry in bulk structures are: (i) inclusion of chirality in the molecule, (ii) utilisation of crystal engineering techniques that exploit weak intermolecular forces, (iii) electric field poling of thin films or polymer films in which the molecules of interest are bound physically or chemically and (iv) preparing X, Z or alternate type Langmuir-Blodgett (LB) films. These methods are discussed in some detail below.

Inclusion of Chirality

The utility of chirality for the fabrication of NLO organic materials was recognised very early in the case of amino acids and sugars.[3a] Molecular chirality guarantees the crystallisation of a pure enantiomer in one of the 21 noncentrosymmetric space groups. Achiral molecules generally crystallise in a centric lattice, though some important exceptions are known, *eg.* urea ($P\bar{4}2_1m$), benzil (P32), m-nitroaniline, mNA (Pbc2,), MNA (Cc), POM ($P2_12_12_1$) and 3-acetamido-4-dimethylaminonitrobenzene, DAN ($P2_1$). On the other hand, a pure enantiomer must crystallise in an enantiomorphous space group, and there are plenty of examples of such systems. Some well known cases are (2,4-dinitrophenyl-(L)-alaninemethylester, MAP (P2,), NPP ($P2_1$) and PNP ($P2_1$).[3b] Though a mixture of equal quantities of a pair of enantiomers *ie.* a racemate, usually

crystallises in centrosymmetric space groups some cases of crystallisation in enantiomorphous space groups are also known. We note that the optical activity of a molecule only guarantees a noncentric lattice structure, but does not guarantee usefulness as a material for SHG. This is because, the polarisable part of the molecules may still be aligned almost antiparallel resulting in near cancellation of the NLO response of the molecules that are so aligned. It is important to have the NLO chromophores turned away from an antiparallel alignment to generate good SHG capability. In spite of this, the utilisation of optical activity appears to be one of the most successful techniques for the generation of noncentric crystal structures, especially when used in conjunction with one of the following techniques.

Intermolecular H-bonding and van der *Waal interactions*

Hydrogen bonding is a well known crystal engineering tool to obtain desired crystal packing. In the field of NLO too it has been used often to get optimised noncentric structures in the organic crystals. The hydrogen bond bridges two atoms that have high electronegativities (such as O, N) and this can strongly influence the crystal structure and the spectroscopic properties of the molecules. Some examples of NLO systems where H-bonding has been crucial are, 2-(a-methylbenzylamino)-3,5-dinitropyridine (MBADNP),[53] *o*-nitroaniline and its derivative, MAP and urea. Urea is an extreme case of a hydrogen bonded network.[3a] The urea molecule which has eight atoms, is involved in eight hydrogen bonds (four to each carbonyl and one each from each of the hydrogens). In urea the hydrogen bonding

has played a crucial role in evolving a noncentric crystal structure." Even though H-bonding affects the crystal structure in many significant ways, it is known to have negligible effect on the molecular hyperpolarisabilities. Some theoretical investigations[5] do however indicate that in special cases molecular β's are influenced mildly by H-bonding. The weak interactions between iodo and nitro groups which form supramolecular synthons were also exploited for designing materials for SHG. [6]

Poling of doped polymer films

Polymer films with exceptionally large second order nonlinearities can be produced by the poling process.[7] An efficient NLO chromophore molecule is either doped in a host polymer matrix or covalently linked as pendant groups on a polymer backbone. The polymer is then cast as a film usually by spin coating techniques. Subsequently the film is subjected to a strong external dc electric field and heated to the glass transition temperatures of the polymer. At this point, the chromophores are aligned parallel by the field and locked into position when the film is cooled to room temperature with the external field on. The poling thus leads to the alignment of doped molecules in the polymers film according to the Boltzmann distribution law. The oriented molecular dipoles produce a polarisation, $P = N\mu\langle\cos\theta\rangle$, where N is the number density of the molecules, μ, the ground state dipole moment, and 0, the angle between the dipole and the direction of the poling field. This method can also be used for functionalised and cross-linkable polymer matrices. The resulting

polymeric material is of high optical quality and suitable for wave guided electro-optic devices. The main problem associated with the poled polymer is the metastability of the system. After the external field is removed, the poled orientation of the chromophores slowly gets randomized over a period of time, and hence the noncentrosymmetry generated is lost. This destroys the quadratic NLO capability. Post-poling treatments such as cross-linking have to be undertaken to arrest the depoling process.

Langmuir-Blodgett films

Another approach to the construction of efficient thin film-based SHG materials has been to incorporate NLO chromophores into acentric X or Z type Langmuir-Blodgett (LB) films.[5] This approach offers far greater net chromophore alignment than is possible in a poling field (where the net alignment is statistical). LB films are built up from amphiphilic molecules, *ie.*, molecules having both a hydrophilic and a hydrophobic part. The preparation of the LB film consists of the following steps. The amphiphilic molecule is first dissolved in a solvent immiscible with water and the solution spread onto the clean water surface in a Langmuir trough. The solvent is left to evaporate leaving the molecules spread on the water surface. The Langmuir trough is equipped with a mobile barrier to compress the film laterally. The film is gradually compressed to a surface pressure just below its collapse pressure. Because of their long aliphatic chains the molecules cannot dissolve in water and due to their hydrophilic group, they cannot leave the water surface. Hence they form a compact,

monomolecular and in many instances stable film at the water-air interface. When a hydrophilic substrate previously immersed is slowly raised through the monolayer, deposition takes place with the hydrophilic group attached to the substrate and the hydrophobic part sticking out. Subsequent dipping create a head-to-head or tail-to-tail arrangement of the amphiphiles deposited as multilayers on the substrate. By the above method one prepares an LB film which is basically a centrosymmetric one (called Y-type). Such films are not suitable for optical second harmonic generation. X and Z type films with a head-to-tail arrangement and hence a noncentric bulk arrangement can be prepared with relatively low polarity hydrophilic groups or with special functionalisation of the hydrophobic chain ends. Another approach is to prepare alternate layered film of the type A-B-A-B-A-B, wherein one of the molecules A or B is the active NLO chromophore and the other is just a binding spacer unit.

Several specific methods other than the ones described above for the preparation of noncentric materials have been reported in the literature. Salt formation of NLO chromophores with strongly dipolar counterions has been found useful to create net alignment of the active molecule.[60] Inclusion of the NLO chromophores in noncentric or chiral host lattices such as urea, thiourea, tri-o-thymotide, cyclophosphazene, deoxycholic acid and perhydrotriphenylene (PHTP) has given rise to SHG active materials.[61] Recently, inclusion of polar organic molecules in molecular sieve hosts has been investigated as a means of creating self-assembled aggregates of molecules that possess the noncentrosymmetry required for materials to

exhibit second harmonic generation. There have been reports of polymorphic materials where strongly polar solvents have produced crystal structures which were noncentric whereas less polar solvents gave centric arrangements. Recently self assembly techniques involving covalent linkages and layer-by-layer fabrication has been reported to yield robust noncentric systems highly suited for application like SHG and electro-optic effects.[64]

1.5 METHODS FOR THE COMPUTATION OF MOLECULAR HYPERPOLARISABILITIES

As discussed in the previous Section, the growing thrust on the development of organic materials for NLO applications such as SHG has brought to focus the necessity of understanding molecular nonlinearities better. This should enable designing molecules which will be better candidates for fabricating the NLO materials. Molecular hyperpolarisabilities are amenable to computational studies and a variety of approaches have been developed for this purpose. We discuss below some salient features of these methods and outline some simple guidelines for molecular design that have emerged from such investigations.

Reliable theoretical predictions of the magnitude of molecular hyperpolarisabilities may provide useful guidelines for the synthetic chemist and may orient the search towards previously unexplored species of

potential interest. There are two basic methodologies that can be used to compute β. These techniques are based on (i) generalized finite field elaborations of coupled Hartree-Fock schemes in which the perturbation is included in the Hamiltonian (the finite field (FF) " or coupled perturbed Hartree-Fock (CPHF)[46] method) and (ii) perturbative schemes in which the calculations are carried out on the free (independent of field) molecules and the response involves the coupling of excited states (the sum-over-states (SOS) method). Both the methods have been used extensively for the calculation of β in conjunction with semiemipirical as well as *ab initio* molecular orbital methods. The semiempirical methods which we have adopted in this thesis, to calculate molecular hyperpolarisabilities are described below.

Coupled Hartree-Fock methods

These methods are derivative methods which rely on the fact that the static first, second and third order polarisability tensor components can be obtained as the first, second and third order derivatives of a given dipole moment component μ_i with respect to the field, F.

$$\alpha_{ij}(0) = \left(\frac{\partial \mu_i}{\partial F_j}\right)_{F\to 0} \qquad (1.9)$$

$$\beta_{ijk}(0) = \left(\frac{\partial^2 \mu_i}{\partial F_j \partial F_k} \right)_{F \to 0} \tag{1.10}$$

$$\gamma_{ijkl}(0) = \left(\frac{\partial^3 \mu_i}{\partial F_j \partial F_k \partial F_l} \right)_{F \to 0} \tag{1.11}$$

These derivatives can be computed either numerically or analytically. The method to calculate the derivatives numerically is usually called the finite field method. CPHF methods generally refer to the use of analytical gradients to compute a, β and y. The CPHF method is equivalent to the time-dependent Hartree-Fock (TDHF) procedure for static calculations[4] ; this method is implemented in recent versions of the MOPAC program such as MOPAC93.[66]

An analogous formulation for the a, β and y coefficients can be obtained by examining the molecular energy expansion, rather than dipole expansion with respect to the field. The molecular dipole moment is the negative field derivative of the energy. Hence, p, for example can be written as :

$$\beta_{ijk}(0) = \left(\frac{\partial^2 \mu_i}{\partial F_j \partial F_k} \right) = \frac{\partial^2}{\partial F_j \partial F_k} \left(-\frac{\partial E}{\partial F_i} \right)$$

$$= \left(\frac{\partial^3 E}{\partial F_j \partial F_k \partial F_l} \right)_{F \to 0} \qquad 0.12)$$

Both the methods (dipole expansion and energy expansion) are implemented in earlier versions of the MOPAC program (MOPAC 6.0, Ref. 67). The FF computations are usually carried out at zero excitation frequency *ie.* they provide the static hyperpolarisabilities.

Sum-over-states *method*

As an alternative to directly coupling the applied field to the molecular Hamiltonian, NLO responses can also be computed using standard perturbation theory. In the uncoupled formulation, electronic excited states created by the perturbing laser field are treated as an infinite sum over unperturbed particle-hole states. The SOS perturbation theory expression for the hyperpolarisability calculation is given by Eqn. 1.13.

$$\beta_{ijk}^{2\omega} = -\frac{e^3}{2} \sum_{p} \sum_{n,n'} \left[\frac{r_{gn}^{\ i} r_{nn'}^{\ j} r_{n'g}^{\ k}}{(E_n - E_g - 2\hbar\omega)(E_{n'} - E_g - \hbar\omega)} \right] \qquad (1.13)$$

where the subscripts i, j, k are the Cartesian components, $\mathbf{r_{ab}}$ corresponds to the dipole integral involving the states a and b, and the E values represent the electronic energies and $\hbar\omega$, the energy of the exciting radiation. The summation over p generates six terms obtained by permutation of the pairs

(i, -2ω), (j,ω) and (k,ω). The diagonal terms are so chosen that they correspond to the difference between the excited (n) and ground state (g) dipole moments (Δμ), hence the indices n and n' may be restricted to run over the excited states only. Thus r_{nn} are given by

$$-\frac{\Delta\mu}{e} = r_{nn} = \langle n|r|n\rangle - \langle g|r|g\rangle \qquad (1.14)$$

Consideration of only a single excited state within the SOS method leads to a particularly simple theoretical model as discussed below.

Oudar and Chemla[22] showed that, in the push-pull π-organic chromophores with large (3, the excited states strongly influence the NLO response. They assumed that the anomalously large response observed in these donor/acceptor substituted chromophores was dominated by the intramolecular charge transfer interaction between the donor and the acceptor groups. The second order response was assumed to arise as a sum of two contributions.

$$\beta = \beta_{add} + \beta_{ct} \qquad (1.15)$$

where β_{add} is the additive portion accounting for the interaction between the individual substituents and the π-conjugation network and β_{ct} is the contribution arising from the interaction of donor and acceptor moieties. The charge transfer term along the molecular dipole axis was described in

terms of a two level interaction between the ground state (g) and the first excited state (e) and can be represented by a simplification of Eqn.1.13 as shown below.

$$\beta_{ci} = \beta_{2level} = \frac{3e^2}{2m} \frac{\Delta E_{ge} f_{ge} \Delta \mu_{ge}}{\left[\left(\Delta E_{ge}\right)^2 - \left(2\hbar\omega\right)^2\right]\left[\left(\Delta E_{ge}\right)^2 - \left(\hbar\omega\right)^2\right]} \qquad (1.16)$$

where ftco is the energy of the laser radiation, ΔE_{ge} is the energy difference between the ground state and the first excited state, f_{ge} is the oscillator strength of this transition and $\Delta\mu_{ge}$ the difference in dipole moments between the ground and the first excited state.

The 2-level model is a particularly simple model for a complex property such as the hyperpolarisability. It provides remarkable chemical insight into the nonlinear response of a push-pull molecule. Theoretical studies on various systems indicate that the two-level charge transfer model is very useful in predicting semi-quantitatively the molecular β values. However, several cases are also known where the 2-level model does not provide any meaningful predictions. Since quantities such as ΔE_{ge}, f_{ge} and $\Delta\mu_{ge}$ are easily accessible by computations or simple spectroscopic techniques, evaluation of β_{2level} is very convenient. This provides an insight into the nonlinear response of the molecule and is of great utility in the screening of candidates to develop novel NLO materials.

1.6 EXPERIMENTAL TECHNIQUES TO MEASURE SHG

For complete determination of the nonlinear susceptibility tensor components, second harmonic generation studies have to be carried out on a single crystal. Rotation of a crystal with respect to the incident laser beam gives rise to the second harmonic beam following a Maker fringe pattern. Phase matching angles and χ tensor components can be extracted by measuring the SHG from different faces of a polished single crystal. Kleinman symmetry conditions[69] can be utilised to determine the number of independent tensor components to be evaluated. Such detailed studies are limited by the fact that good optical quality large crystals have to be available and accurate polishing of the crystal faces must be achieved. The Kurtz and Perry powder technique is a convenient method for screening large number of powdered materials for second order nonlinear optical activity without having to grow large single crystals. This powder technique and the popular techniques for the measurement of hyperpolarisability in solution, namely, electric field induced second harmonic generation (EFISHG) and hyper-Rayleigh scattering (HRS) are described below.

Kurtz-Perry powder technique

In this technique, an appropriate laser beam (typically a Nd:YAG beam at 1064 nm) is directed onto a powdered sample, and the emitted light is collected using a parabolic mirror, filtered and measured with a suitable

detection system (usually consisting of a photomultiplier tube, lockin amplifier and personal computer) (Fig.1.5). Urea or quartz is usually used

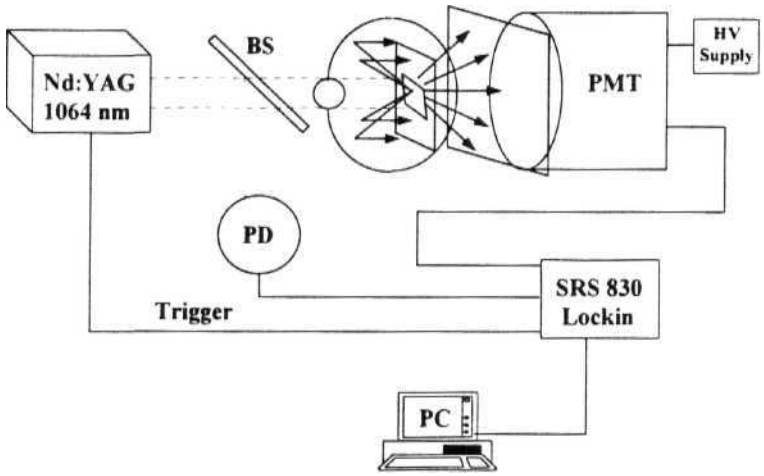

Figure 1.5: *Schematic diagram of the setup for Kurtz-Perry powder SHG measurement*

for calibrating the SHG intensity. Using this technique, general trends can be observed and candidates for detailed studies indentified. This powder SHG technique requires the following condition to be met: r « L « D, where, r is the average powder particle size, L is the powder sample thickness and D is the laser beam diameter. This condition ensures that the fundamental beam strikes a large number of particles of random orientation, thus effecting a significant statistical average. The Kurtz-Perry method

allows identification of the phase-matchability of a material. Phase-matchability refers to the fact that $n_{2\omega} - n_{\omega} \rightarrow 0$ for certain directions of propagation ($n_{2\omega}$ and n_{ω} are the refractive indices at 2ω and ω). For powder samples with large average particle sizes, Kurtz and Perry showed that, in the case non phase-matchable materials, the intensity of the generated second harmonic light, $I_{2\omega}$ follows :

$$I_{2\omega} \propto (d_{ijk}^2) l_c^2 / r \tag{1.17}$$

where (d_{ijk}) is the angular average of the second order polarisability tensor and l_c is the average coherence length defined as $\lambda/[4(n_{2\omega}-n_{\omega})]$. For phase-matchable materials it was shown that,

$$I_{2\omega} \propto (d_{eff}^2) \sin(\theta_m) / \kappa \tag{1.18}$$

where (d_{eff}) is the effective nonlinear coefficient for phase-matched SHG, θ_m is the phase-matching angle, and κ is given by

$$\kappa = (\omega n_{\omega} / c) \sin \rho \tag{1.19}$$

where co is the angular frequency of the fundamental wave, c is the speed of light and p is the angle between the sphere and ellipse index surfaces (p is commonly referred to as the walk-off angle). Eqns. 1.17 and 1.18 are valid only when the average powder grain size is much greater than the characteristic interaction length for SHG. For an average powder grain size

much less than the characteristic SHG interaction length, the SHG intensity for both phase-matchable and non phase-matchable materials is directly proportional to the average grain size, *ie.* $I_{2\omega} \propto (d^2)\, r$, where d^2 is d_{ijk}^2 for non phase-matchable or d_{eff}^2 for phase-matchable materials.

The dependence of SHG intensity on the average particle size of the powder is illustrated in Fig. 1.6 for phase-matchable and non phase-matchable materials. The salient feature to be noted here is that for particle sizes much greater than the average SHG interaction length *(ie.* to the right of $r = l_c$), $I_{2\omega}$ for phase-matchable materials is independent of the particle

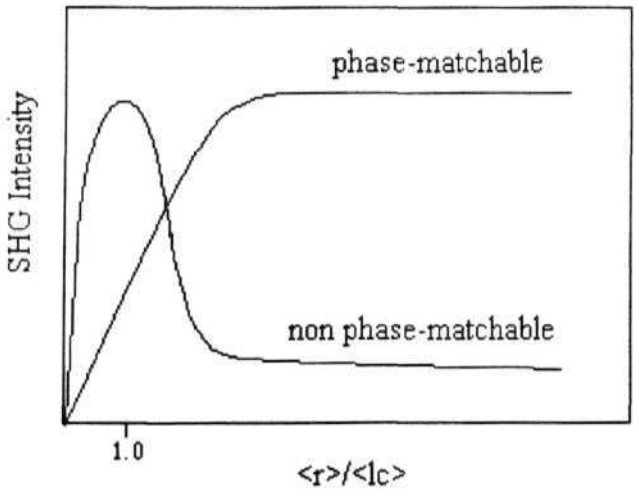

Figure 1.6: *The dependence of SHG intensity on the average particle size, <r> for phase-matchable and non phase-matchable materials; $<l_c>$ is the average coherence length (Ref. 15)*

size (Eqn.1.18) whereas $I_{2\omega}$ for non phase-matchable materials varies inversely with the particle size (Eqn. 1.17).

Several materials have been found to be phase-matchable. For example $LiNbO_3$, KIO_3, Ag_2HgI_4, $(NH_4)H_2PO_4$, urea, NPP and MNA.[15] Furthermore, a detailed analysis of powder SHG of saccharide materials and their phase-matching capabilities was carried out by Bourhill *et al.*[34] This powder SHG technique has found an interesting use in terms of a reverse role of identifying crystal lattice symmetry. Since the powder technique is capable of detecting SHG and thus identifying acentric structures, it can be used as a sensitive and reliable tool for establishing the presence or absence of centre of symmetry in the crystal lattice. However one should exercise caution in using such results, since changes of chemical composition on powdering the crystals, for example by loss of solvate molecules, modification of surface features *etc.* should be taken into account.

EFISHG

Second harmonic generation, the most widely used technique to measure the molecular hyperpolarisabilities, is forbidden in isotropic liquids due to the presence of a centre of inversion. Electric field induced second harmonic generation in solution is used to evaluate the molecular second order nonlinearities when the molecules have a permanent dipole moment and thus are amenable to alignment in a strong electric field. A fundamental laser beam is directed on the solution with a synchronous pulsed dc electric

field applied across the sample and the intensity of second harmonic light produced is measured. The dc field orients the molecular dipoles and thus breaks the centrosymmetric nature of the bulk solution thus allowing quadratic NLO effects to be observed. In the presence of two optical fields and a static electric field, the second harmonic intensity from the solution is related to the molecular polarization at 2ω produced by the electric fields. This molecular polarization is given by

$$P_i^{2\omega} = \beta_{ijk} E_j^{\omega} E_k^{\omega} + \gamma_{ijkl} E_j^{\omega} E_k^{\omega} E_l^0 \tag{1.20}$$

where β_{ijk} and γ_{ijkl} are the molecular first and second order hyperpolarisabilities respectively (see Eqn.1.1). The relationship between the molecular polarisation and the measured macroscopic polarisation of the solution is obtained by statistically averaging the contribution of the individual molecules and is given by

$$P_i^{2\omega} = \chi_{ijkl}^{(3)}(-2\omega;\omega,\omega,0) E_j^{\omega} E_k^{\omega} E_l^0 \tag{1.21}$$

where $$\chi_{ijkl}^{(3)} = \sum N_s f_s^0 (f_s^{\omega})^2 f_s^{2\omega} \left(\gamma + \frac{\beta\mu}{5kT}\right)_s \tag{1.22}$$

where s refers to the molecular species in solution, f's are the appropriate local field factors, N_s is the number density, kT the Boltzman factor and μ the ground state dipole moment. y is the scalar part of the second

hyperpolarisability tensor and is often neglected in the case of donor-acceptor substituted molecules with large β's, since γ /($\beta\mu/5kT$) « 0.1.

In order to determine β accurately, one must also determine the ground state dipole moment, μ either experimentally or by quantum chemical computations. The experimental details and EFISHG setup which we have fabricated and the analysis of the results to determine the β are presented in Sec.4.4.

HRS

Another technique that has become popular of late, is hyper-Rayleigh scattering. Second order light scattering in isotropic samples and centrosymmetric molecules in liquid phase have been known for some time. Persoon's group has developed the application of hyper-Rayleigh scattering, *ie.* incoherently scattered second harmonic generation for the determination of β of NLO chromophores. In this technique, a fundamental laser beam is focused onto a solution sample taken in a thermostatted cylindrical cell. The second harmonic scattered light that is generated is collected by an efficient system of optics and measured using appropriate detection system and analysed to finally determine the p.[73] Since the technique relies on incoherent scattered light, caution has to be exercised in eliminating influences of other Photophysical two-photon processes such as fluorescence and stimulated Raman emission. HRS technique normally provides an averaged β value and tensorial components

can be extracted by utilising appropriately polarised light sources and detection systems. This method is particularly useful over the traditional EFISHG technique, when measurements are to be carried out on octupolar molecules, ionic systems *etc.*.[74]

1.7 LAYOUT OF THE THESIS

This thesis presents the systematic investigation of a class of push-pull diamino substituted dicyanoquinodimethane systems as novel molecular materials for quadratic NLO applications. The results of these studies are presented in the next six chapters. We describe below the salient features of the contents of each chapter.

Chapter 2

The methodologies which we have adopted for the computational studies of β are presented in Sec.2.2. The (3 values computed for several derivatives of push-pull quinodimethanes which we have synthesised, are presented and the results discussed in this Section. We have investigated the effect of the push-pull groups and the electrostatic environment on p using model calculations presented in Sec.2.3. We have also carried out some analysis of the dependence of p on the molecular structure of these push-pull quinonoid compounds. Calculations have been carried out on a model system, to study the dependence of p on the molecular twist. Sec.2.4

presents the results of these studies and the analysis of the unusual variation of β observed.

***Chapter** 3*

In this chapter, we present the synthesis and characterisation of achiral and chiral derivatives of push-pull diamino substituted dicyanoquinodimethane we have investigated in this study. Their linear optical properties are also presented in this Chapter.

Chapter 4

We have proposed a simple procedure for the solvatochromic determination of the change in dipole moments of organic molecules on excitation and this practically convenient procedure is described in Sec.4.2. We utilised this procedure, together with simple electronic absorption studies, to determine experimentally, the two-level approximation to the p of some of our quinonoid systems. This simple solvatochromic method is discussed in Sec.4.3 along with an analysis of the results in view of the computed p. We have also assembled the set up to carry out Electric Field Induced Second Harmonic Generation (EFISHG) study of molecular β in solution. Details are presented in Sec.4.4 along with preliminary studies carried out on a representative quinonoid molecule.

Chapter 5

In Sec.5.2, we present the crystal structures of the various materials we have studied based on achiral quinonoid compounds. The unusual and novel phenomenon of solvate switchable SHG observed in one of the systems is discussed in Sec.5.3.

Chapter 6

Sec.6.2 presents the crystal structures and the results of the powder SHG studies on the materials we have developed from two chiral quinonoid systems. In Sec.6.3 we discuss the dual influence of intermolecular H-bonding on the SHG of another chiral quinonoid system. Molecular engineering leading to enhanced solid state SHG in yet another chiral compound is described in Sec.6.4.

Chapter 7

This chapter presents an overview of the present investigation on a new class of molecular materials for SHG. The positive features like easy synthesis, high thermal stability, optical transparency and moderate to strong phase-matchable SHG observed in these materials are highlighted. Future direction for research in this area are also outlined in this Chapter.

REFERENCES

1. (a) Zernike, F.; Midwinter, J.E. *Applid Nonlinear Optics*, John Wiley, New York, 1973. (b) Boyd, R.W. *Nonlinear Optics,* Academic Press, New York, 1992.
2. (a) Singer, K.D.; Lalama, S.L.; Sohn, J.E.; Small, R.D. in *Nonlinear Optical Properties of Organic Molecules and Crystals*, Chemla, D.S.; Zyss, J. (Eds), Academic Press: New York, 1987, Vol.1, p. 437 and references therein. (b) Prasad, P.N.; Williams, D.J. *Introduction to Nonlinear Optical Effects in Organic Molecules and Polymers* Wiley, New York, 1991.
3. *Nonlinear Optical Properties of Organic Molecules and Crystals,* Chemla, D.S.; Zyss, J. (Eds), Academic Press: New York, 1987, (a) Vol. l.(b)Vol. 2.
4. Eaton, D.F. *Science* **1991,** *253,* 281.
5. Bloembergen, N. *Ann. Rev. Mater. Sci.* **1993,** *22,* 1.
6. Franken, P.A.; Hill, A.E.; Peters, C.W.; Weinrich, G. *Phys. Rev. Lett.* **1961,5,** 118.
7. Giordmaine, J.A. *Phys. Rev. Lett.* **1962,** *8,* 19.
8. Maker, P.D.; Terhune, R.W.; Nisenhoff, M.; Savage, CM. *Phys. Rev. Lett.* 1962,5,21.
9. Bloembergen, N. *Nonlinear Optics,* Benzamin, Massachusetts, 1965.
10. Giordmaine, J.A.; Miller, R-C. *Phys. Rev. Lett.* **1965**, *14*, 973.
11. Rentzepis, P.M.; Pao, Y.H. *Appl. Phys. Lett.* **1964,** *5,* 156.

12. Heilmeir, G.H.; Ockman, N.; Braunstein, R.; Kramer, D.A. *Appl Phys. Lett.* 1964,5,229.
13. Orlov, R.Y. *Sow Phys. - Crystallogr. (Engl. Transl),* **1966,** *11*, 410.
14. Gott, J.R. *J. Phys.* **1971,** *B4,* 116.
15. Kurtz, S.K.; Peryy, T.T. *J. Appl Phys.* **1968,** *39,* 3798.
16. (a) Jerphagnon, J.; Kurtz, S.K. *J. Appl. Phys.* **1970,** *41,* 1667. (b) Jerphagnon, J.; Kurtz, S.K. *Phys. Rev.* **1970,** 57, 1739.
17. Hauchecorne, G.; Kerherve, F.; Mayer, G. *J. Phys.* **1971,** *32,* 47.
18. Levine, B.F. *Chem. Phys. Lea.* **1976,** *37,* 516.
19. Davydov, B.L.; Derkacheva. L.D.; Dunina, V.V.; Zhabotinskii. M.E.; Zolin, V.F.; Koreneva, L.G.; Samokhina, M.A. *JETP Lett. (Engl Transl),* **1970**, *12*, 16 and *Opt. Spectrosc.* **1971,** *30,* 27 *A.*
20. Desiraju, G.R *Crystal Engineering: The Design of Organic Solids* Elsevier, Amsterdam, 1989.
21. Chemla, D.S.; Oudar, J.L.; Jerphagnon, J. *Phys. Rev.* **1975,** *B12.* 4534.
22. (a) Oudar, J.L.; Chemla, D.S. *J. Chem. Phys.* **1977,** *66,* 2664. (b) Oudar, J.L. *J. Chem. Phys.* **1977,** *67,* 446.
23. (a) Singer, K.D.; Garito, A.F. *J. Chem. Phys.* **1981,** *75,* 3572. (b) Ledoux, I.; Zyss, J. *chem. Phys.* **1982,** *73,* 203.
24. Oudar, J.L.; Hierle, R. *J. Appl Phys.* **1977,** *48,* 2699.
25. Levine, B.F.; Bethea, C.G., Thurmond, C.D.; Lynch, R.T.; Bernstein, J.L. *J. Appl. Phys.* **1979,** *50,* 2523.
26. Zyss, J.; Berthier, G. *J. Chem. Phys.* **1982,** *77,* 3635.
27. Zyss, J.; Nicoud, J.F.; Coquillay, M. *J. Chem. Phys.* **1984,** *81*, 4160.

28. Zyss, J.; Oudar, J.L. *Phys. Rev.* **1982,** *A26,* 2028.
29. Badan, J.; Hierle, R.; Perigaud, A.; Vidakovic, P. in Ref.3a, p. 297-356 and references therein.
30. Twieg, R.; Azema, A.; Jain, K.; cheng, Y.Y. *Chem. Phys. Lett.* **1982,** *92,* 209.
31. Green, M.L.H.; Marder, S.R.; Thompson, M.E.; Bandy, J.A.; Bloor, D.; Kolinsky, P.V.; Jones, R.J. *Nature* **1987,** *330,* 360.
32. Marder, S.R.; Perry, J.W.; Schaefer, W.P. *Science,* **1989,** *245,* 626.
33. Kondo, K.; Godo, H.; Takemoto, K.; Aso, H.; Sasaki, T.; Kawakami, K.; Yoshida, H.; Yoshida, K. *J. Mater. Chem.* **1992,** *2,* 1097.
34. Bourhill, G.; Mansour, K.; Perry, K.J.; Khundkar, L.; Sleva, E.T.; Kern, R.; Perry, J.W. *Chem. Mater.* **1993,** *5,* 802.
35. Wong, M.S.; Nicoud, J.F. *J. Chem. Soc, Chem. Commun.* **1994,** 249.
36. Ledoux, I.; Zyss, J.; Siegel, J.; Brienne, J.; Lehn, J.-M. *Chem. Phys. Lett.* **1990**, *172*, 440.
37. Dhenaut, C; Ledoux, I.; Samuel, I.D.W.; Zyss, J.; Bourgault, M.; Le Bozec, H. *Nature* **1995,** *374,* 339.
38. Wijekoon, W.M.K.P.; Zhang, Y.; Karna, S.P.; Prasad, P.N.; Griffin, A.C.; Bhatti, A.M. *J. Opt. Soc. Am. B* **1992,** 9, 1832.
39. Choi, D.H.; Wijekoon, W.M.K.P.; Kim, H.M.; Prasad, P.N. *Chem. Mater.* **1994,** *6,* 234.
40. Hsiue, G.H.; Kuo, J.K.; Jeng, R.J.; Chen, J.I.; Jiang, X.L.; Marturunkakul, S.; Kumar, J.; Tripathy, S.K. *Chem. Mater.* **1994, (5,** 884.

41. Jeng, R.J.; Chen, Y.M.; Jain, A.K.; Kumar, J.; Tripathy, S.K. *Chem. Mater.* **1992,** *4,* 972.
42. Zhang, Y.; Prasad. P.N.; Burzynski, R. *Chem. Mater.* **1992,** *4,* 851.
43. (a) Ashwell, G.J.; Dawnay, E.J.C.; Kuczynski, A.P.; Szablewski, M.; Sandy, I.M. *J. Chem. Soc, Faraday Trans.* **1990,** *86,* 1117. (b) Groh, W.; Lupo, D.; Sixl, H. *Adv. Mater.* **1989,** *28,* 1548.(c) Miller, L.S.; Walton, D.J.; Stone, P.J.W.; McRoberts, A.M.; Sethi, R.S. *J. Mater. Sci., Mater. Elec.* **1994,** 5, 75.
44. Moerner, W.E.; Silence, S.M. *Chem. Rev.* **1994,** *94*, 127.
45. Bredas, J.L.; Adant, C; Tackx, P.; Persoons, A. *Chem. Rev.* **1994,** *94,* 243.
46. Kanis, D.R.; Ratner, M.A.; Marks, T.J. *Chem. Rev.* **1994, *94,*** 195.
47. Bosshard, C; Giinter, P. in *Nonlinear Optics of Organic Molecules and Polymers,* Nalwa, H.S.; Miyata, S.(Eds), CRC Press, New York, 1997, p 391.
48. Onsager, L. *J. Am. Chem. Soc.* **1936,** *58,* 1486.
49. Lorentz, H.A. *The Theory of Electric Polarization,* Elsevier, Amsterdam, 1952.
50. Long, NJ. *Angew. Chem. Int. Ed. Engl.* **1995,** *34,* 21.
51. (a) Verbiest, T.; Clays, K.; Samyn, C.; Wolff, J.; Reinhoudt, D.; Persoons, A. *J. Am. Chem. Soc.* **1994**, *116*, 9320. (b) Ray, P.C.; Das, P.K. *Chem. Phys. Lett.* **1995,** *244,* 153.
52. Bahl, A.; Grahn, W.; Stadler, S.; Feiner, F.; Bourhill, G.; Brauchle, C.; Reisner, A.; Jones, P.G. *Angew. Chem. Int. Ed. Engl.* **1995,** *34,* 1485.

53. Twieg, R.J.; Jain, K.; Cheng, Y.Y.; Crowley, J.I.; Azema, A. *Polym. Prepr., Am. Chem. Soc. Div. Polym. Chem.* **1982,** *23,* 147.
54. Zyss, J.; Berthier, G. *J. Chem. Phys.* **1982,** *77,* 3635.
55. Sarma, J.A.R.P.; Laxmikanth Rao, J.; Bhanuprakash, K. *Chem. Mater.* **1995,** 7, 1843.
56. Sarma, J.A.R.P.; Allen, H.A.; Hoy, V.J.; Howard, J.A.K.; Thaimattam, R.; Biradha, K.; Desiraju, G.R *J. Chem. Soc, Chem. Commun.* **1997,** 101.
57. Burland, D.M.; Miller, R.D.; Walsh, CA. *Chem. Rev.* **1994,** *94,* 31.
58. Lalama, S.J.; Sohn, J.E.; Singer, K.D. *SPIE. Proc.* **1985,** *578,* 168.
59. Barraud, A.; Vandevyver, M. in Ref.3a, p 357-384.
60. Marder, S.R.; Perry, J.W.; Yakymyshyn, C.P. *Chem. Mater.* **1994,** *6,* 1137.
61. (a) Ramamurthy, V.; Eaton, D.F. *Chem. Mater.* **1994,** *6,* 1128. **(b)** Hoss. R.; König, O.; Kramer-Hoss, V.; Berger, U.; Rogin, P.; Hulliger, J. *Angew. Chem. Int. Ed. Engl.* **1996,** 55, 1664.
62. Cox. S.D.; Gier, T.E.; Stucky, G.D. *Chem. Mater.* **1990,** *2,* 609.
63. Tabei, H.; Kurihara, T.; Kaino, T. *Appl. Phys. Lett.* **1987,** *50,* 1855.
64. Marks, T.J.; Ratner, M.A. *Angew. Chem. Int. Ed. Engl.* **1995,** *34,* 55.
65. Kurtz, H.A.; Stewart, J.J.P.; Dieter, K.M. *J. Comput. Chem.* **1990,** *11,* 82.
66. MOPAC93 © Fujitsu Inc.
67. Stewart, J.J.P. *Quantum Chemistry Program Exchange;* Indiana University: Bloomington, Indiana; Program 455, Version 6.0.
68. Jain, M.; Chandrasekhar, J. *J. Phys. Chem.* **1993,** *97,* 4044.

69. Kleinman, D.A. *Phys. Rev.* **1962,** *126*, 1977.

70. (a) Levine, B.F.; Bethea, C.G. *J. Chem. Phys.* **1975,** *63,* 2666. (b) Singer, K.D.; Sohn, J.E.; King, L.A.; Gordon, H.M.; Katz, H.E.; Dirk, C.W. *J. Opt. Soc. Am. B* **1989,** *6,* 1339.

71. Kielich, S.; Lalanne, J.R.; Martin, F.B. *Phys. Rev. Lett.* **1971,** *26,* 1295.

72. Clays, K.; Persoons, A. *Phys. Rev. Lett.* **1991,** *66,* 2980.

73. Clays, K.; Persoons, A. *Rev. Sci. Instrum.* **1992,** *63,* 3285.

74. Ray, P.C.; Das, P.K. *J. Phys. Chem.* **1995,** PP, 17891.

CHAPTER 2

COMPUTATION OF MOLECULAR HYPERPOLARISABILITY AND THE STUDY OF STRUCTURE-PROPERTY RELATIONSHIPS

2.1 BACKGROUND

Evaluation of molecular hyperpolarisabilities is the starting point for a systematic analysis of the bulk second order NLO properties of molecular materials. The relation between the bulk nonlinear susceptibilities and the molecular hyperpolarisabilities provide insight into the intermolecular interactions which affect the local electric fields experienced by the molecular building blocks. These studies are of great value in the design of new structures with enhanced nonlinear responses. In this thesis, we have focused attention on some push-pull diamino substituted dicyanoquinodimethane molecules (Fig. 2.1) based on the prototypical system 1, reported in 1962 by a du Pont group.[1] We have

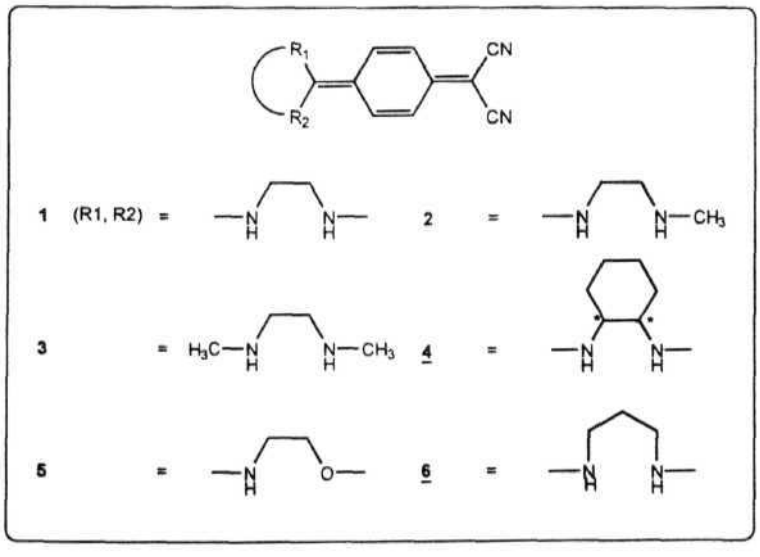

Figure 2.1: (continued on next page)

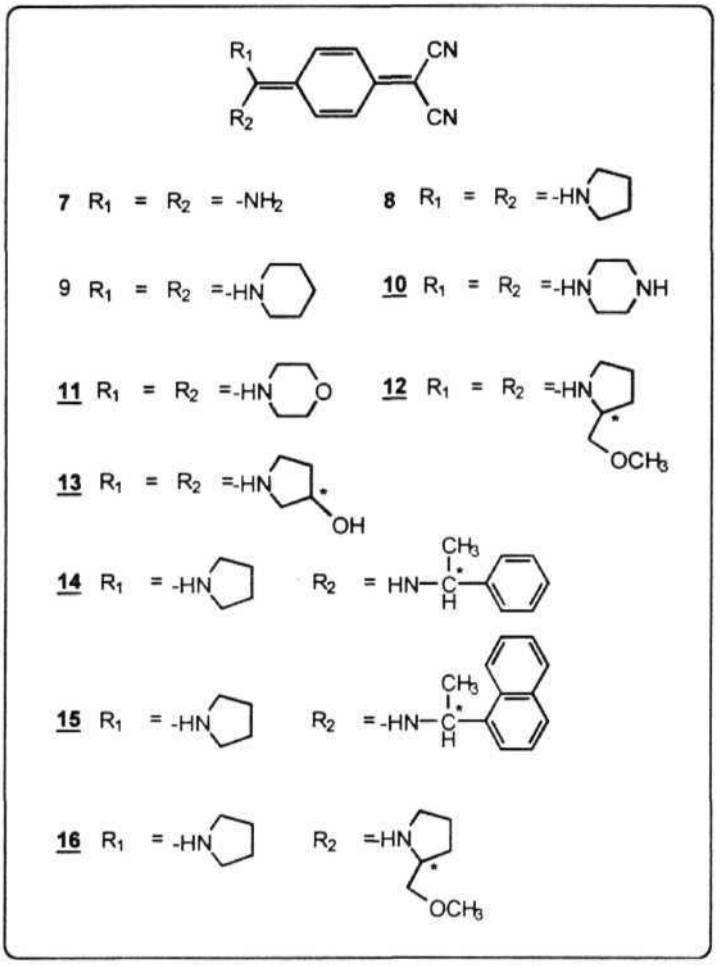

Figure 2.1: *Molecules considered in this study (the new derivatives we have developed are underlined)*

initially carried out systematic computational studies to unravel the hyperpolarisabilities of these molecules. We have also studied in detail the structure-property relationships that affect the hyperpolarisabilities of this class of molecules by carrying out computations on some model systems. This Chapter is devoted to these computational studies and is divided into three Sections: (i) the computation of molecular β of

various molecules considered in this study, (ii) a theoretical analysis of the p's as a function of the quinonoid-benzenoid character which reflects the push-pull nature of the substituents or the electrostatic environment of the molecule; calculations focused on the model system, 7,7-diamino-8,8-dicyanoquinodimethane (DADQ, 7), and (iii) the study of the dependence of (3 on the molecular twist commonly observed in this class of compounds; calculations focused on the model system, 7,7-dipyrrolidino-8,8-dicyanoquinodimethane (DPDQ, 8).

There are several quantum chemical procedures in use today, for the calculation of molecular hyperpolarisabilities, " both at the semiempirical and at the *ab initio* levels; for example, the sum-over-states (SOS), finite field (FF), correction vector (CV) and time - dependent Hartree-Fock (TDHF) methods have been applied along with semiempirical computational schemes, and the latter coupled HF method has been included in *ab initio* programmes as well. In this work we have used mainly the SOS and TDHF methods in conjunction with the semiempirical AM1 procedure for geometry optimisation. These methods have already been described in detail in Sec. 1.5. The computations presented in Sec. 2.2 and 2.4 were carried out using the MOPAC93 program.[4] Molecular structure optimisations were carried out using the AM1 method[5] with the PRECISE keyword which enhances the stringency of the criteria for self consistency and geometry optimisation. Full geometry relaxation was usually allowed and constraints imposed, if any, are discussed at the appropriate places. For calculations involving the excited state (for excitation energy, transition dipole, dipole moment changes etc.) the corresponding

ground state optimised geometry was used and a configuration interaction (CI) scheme involving all single and pair excitations within a manifold of ten molecular orbitals (five HOMO's and five LUMO's) was employed, invoking the keyword MICROS and reading in the 76 microstates generated. Molecular hyperpolarisabilities, β were calculated using the TDHF method[6] implemented in MOPAC93. We have found that these computed values are in very good agreement with the values obtained from MOPAC 6.0, which employs the finite field (FF) method.[7,8] The value of the static hyperpolarisabilities, P(0) we report in this work are the magnitude of the average β vector, scaled by a factor of 0.5 to make it comparable to experimental data (this is an aspect clarified in the MOPAC 6.0 programme but not explicitly stated in MOPAC93).

In Sec.2.3 we were interested in analysing the contribution of various excited states to the large β of the push-pull quinonoid molecules. Therefore we have used an SOS algorithm implemented in the SCAMP programme [a] (which is a modified version of the VAMP programme[9b]) for the β calculations. Geometry optimisations were again carried out using the AM 1 method and the p were computed using the SOS involving all single and pair excitations typically within a manifold of 12 molecular orbitals (6 HOMO's and 6 LUMO's).

We note that the hyperpolarisabilities of the molecules we study are all negative. This arises from the decrease in dipole moment on excitation of these zwitterionic molecules, which we have verified experimentally by the observation of negative solvatochromism

(discussed in Sec.4.3). To estimate the inherent (nonresonant) hyperpolarisability we have computed, the static p (also denoted as (3(0)) throughout this study.

The computations reported here were carried out either on a MicroVax 3300 Computer or on a Sun Sparc 10 Work Station.

2.2 COMPUTATION OF MOLECULAR HYPERPOLARISABILITIES

The hyperpolarisabilities we present here, based on the calculations carried out using the MOPAC93 program, are the average β (sometimes referred as β_{vec} in literature) defined as follows :

$$\beta = \left(\sum_{i=1}^{3} \beta_i^2 \right)^{1/2} \qquad \textbf{(2.1)}$$

where

$$\beta_i = \beta_{iii} + \frac{1}{3} \sum_{i=1}^{3} \left(\beta_{ijj} + 2\beta_{jji} \right) \qquad \textbf{(2.2)}$$

and β_{iii} *etc.* are the components of the hyperpolarisability tensor. As in other donor-acceptor substituted systems, β_{xxx} (by convention, x is chosen as the direction of the dipole axis) is the dominant component in these push-pull quinonoid compounds, since the maximum polarisation occurs along the dipole direction as a result of the charge transfer interaction between the dicyanomethylene and diaminomethylene unit.

The computational results for all the quinonoid molecules we have studied are provided in Table 2.1. The calculated ground state dipole moments are also presented. These push-pull quinonoid molecules have a characteristic twist between the diaminomethylene plane and the quinonoid ring; we denote this twist angle as 9. This twist has been observed in all the crystallographically determined molecular structures (described in Chapters 5 and 6) as well as in the computed geometries. The 9 values obtained from AM1 optimised geometries are provided in Table 2.1.

The hyperpolarisabilities have been calculated at the AM1 optimised geometries for all molecules. The value of p(0) calculated for most of the compounds are fairly large considering the relatively short conjugation lengths they have (we consider the exceptional cases below). Usually the nonlinear coefficients of conjugated molecules are found to increase with increasing length of the π-electron conjugation pathways since the excited states come closer to the ground state. For molecules with shorter conjugation lengths the β values are small, for example, p-nitroaniline has a P(0) of -9.1 x 10^{-} esu. The push-pull quinonoid compounds we have investigated here also have short conjugation paths and consequently relatively large energies of excitation. Therefore, the large values of β in these compounds appears to arise from the large Δu associated with the excited states, several of which have large transition dipoles with the ground state.[11] This aspect is analysed in greater detail in the next Section where we look at an SOS picture of β and the contribution from various excited states.

Table 2.1: *The computed ground state dipole moments, μ_g, twist angle (dihedral angle shown in Fig. 2.5), 0, and hyperpolarisability calculated at excitation energy of 0 eV, $\beta(0)$*

Molecule	μ_g (D)	Twist angle, θ (°)	$-\beta(0)$ (10^{-30} esu)
1	14.8	0.0	3.2
2	14.4	12.2	5.6
3	13.3	18.1	12.1
4	12.3	0.0	4.1
5	12.5	1.7	0.7
6	15.4	0.0	11.1
7	14.5	0.0	8.0
8	14.1	59.3	39.5
9	15.0	38.9	19.8
10	12.2	38.9	16.6
11	12.5	34.0	11.9
12	11.4	50.8	35.8
13	16.9	56.4	30.4
14	12.5	45.5	27.6
15	12.9	24.8	1.2
16	14.3	57.9	38.7

The ground state dipole moments of these compounds are found to be quite large. These arise from the zwitterionic nature due to the intramolecular charge transfer from the diaminomethylene end to the dicyanomethylene end. The large dipole moments are responsible for

strong intermolecular electrostatic forces in the crystal lattice which appears to be the reason for the relatively large melting and decomposition temperatures observed in these materials (discussed in later chapters).

The calculated twist angle, 0 is quite small or zero in several cases such as 1, 4, 5, 7 *etc*.. This is because of the fact that both amino substituents in these cases are derived from primary amines and in these compounds, both the amino N atoms have secondary amine character. Consequently the steric repulsion which occurs between the H atoms on these N atoms and the *ortho*-H atoms on the benzene ring are weak. In the other compounds, one or both the amino N atoms have tertiary amine character and the steric repulsion between the CH_n group attached to the amino N and the benzene ring *ortho*-H atoms are stronger. Hence large twist angles ranging from about 25° to 50° are calculated. The reasons for the exceptional nature of 15 are not known. It is interesting to note that the $\beta(0)$ values have some correlation with the twist angles. In general we find that when the θ values are small, the hyperpolarisabilities are also relatively small though some exceptions do exist. The calculated dihedral angle θ are generally in fair agreement with those observed in crystals. The agreement between computed and experimental values of θ are discussed further in Secs.2.4, 5.2 and 6.4.

The twist angle, θ, the electron donor-acceptor groups, as well as the polar environment in the crystal lattice are expected to influence the

molecular hyperpolarisabilities. The latter two effects will be reflected in the quinonoid-benzenoid nature of the conjugation unit in the diaminodicyanoquinodimethane molecules. Dependence of J3 on the quinonoid-benzenoid character and molecular twist are investigated in detail, in the forthcoming Sections.

2.3 DEPENDENCE OF HYPERPOLARISABILITY ON THE QUINONOID-BENZENOID CHARACTER

In the previous Section we have observed that the substituted diaminodicyanoquinodimethane molecules have unexpectedly large β values. Since we were interested in synthesising and investigating the NLO properties of this class of molecules, we carried out a detailed analysis of the large hyperpolarisabilities of these systems. We have chosen the simplest molecule, 7,7-diamino-8,8-dicyanoquinodimethane (DADQ, 7) as a model system to carry out this theoretical investigation.[11] Similar to the study of β variation in polyenes as a function of bond length alternation[12], we present a theoretical analysis of the P's as a function of the quinonoid-benzenoid character of this push-pull quinone. We present below, a definition of the quinonoid-benzenoid character, which we call QBC, based on the bond lengths in the six-member ring conjugation unit. As per this definition, the most quinonoid form of DADQ has a QBC of 0.088 and the most benzenoid form has the value of 0.790. This study provides insight into the effect of substitutions at the donor and acceptor end (or alternately, the effect of electrostatic environment), on the excitation energy,

hyperpolarisability *etc*.. We find that the (5 values are particularly large for the more benzenoid structures; and is found to peak at a QBC of about 0.592. Since two low-lying excited states with notable oscillator strength ($\approx$ 0.6 - 1.0) are observed in these systems we decided to have a closer look at their contributions. Our analysis based on the SOS method, indicates that unlike in many known systems, two-level or three-level approximations are inadequate to explain quantitatively the large β in these quinonoid systems, although qualitative trends can be understood. We indicate briefly, where some of the systems we have experimentally investigated, fit into the theoretical picture.

We have employed the AM1 semiempirical procedure for all geometry optimisations. The structure of DADQ was optimised under a C_{2v} symmetry constraint with different static external fields applied along the long axis of the molecule. The latter was done by placing point positive and negative charges along the long axis at equal distances from the centre of the ring. We calculate the field produced at the centre and assign the sign as positive or negative depending on whether the positive charge is kept at the diamino end or the dicyano end. As the field decreases from the highest positive value (6 x 10^7 V/cm) to the lowest negative one (-8 x 10 V/cm) we have employed, the structure smoothly varies from the quinonoid extreme to the benzenoid one. Higher applied fields of either sign were seen to affect only negligible further changes and sometimes led to unphysical distortions of the molecule.

We define the quinonoid-benzenoid character (QBC) based on the magnitude of the deviations of the ring bonds (Fig.2.2) from a standard value of 1.400 A assumed for benzene. This definition was

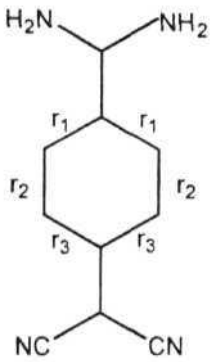

Figure 2.2: *Molecular skeleton of DADQ showing the atom labelling for defining QBC; the double bonds are not shown*

$$QBC = 1 - 6\sum_{1}^{3}|1.400 - r_i| \qquad \textbf{(2.3)}$$

chosen so that the value of QBC approaches 0 at the quinonoid limit and 1 at the benzenoid limit. Table 2.2 presents the various applied external fields and the corresponding optimised bond lengths, r_i as well as the calculated QBC. It also provides the net charges on the amine end, q^+, and the cyano end, q^-, calculated by adding all the atomic charges on the relevant CX_2 (X = NH_2 or CN) group.

Transition dipoles, dipole moment changes on excitation, energies of excitation and associated oscillator strengths and β were

Table 2.2: *Optimised bond lengths r_1, r_2 and r_3 of DADQ subjected to different applied fields and the computed quinonoid - benzenoid character (QBC) and charges on the donor (q^+) and acceptor (q-) moiety for each of the structures ($^{\dagger}In$ units of 10^7 V/cm; see text for the sign convention)*

Field†	r_1(Å)	r_2(Å)	r_3(Å)	QBC	q^+	q^-
6	1.450	1.348	1.450	0.088	0.103	0.033
4	1.448	1.351	1.450	0.118	0.231	0.106
2	1.442	1.354	1.447	0.190	0.374	0.248
1	1.439	1.356	1.445	0.232	0.442	0.319
0	1.435	1.358	1.442	0.286	0.507	0.360
-1	1.431	1.362	1.438	0.358	0.570	0.461
-2	1.426	1.366	1.434	0.436	0.632	0.536
-4	1.417	1.375	1.426	0.592	0.742	0.684
-6	1.410	1.381	1.416	0.730	0.827	0.796
-8	1.405	1.378	1.408	0.790	0.874	0.861

calculated using the SCAMP routine. This program reproduces accurately the experimental β values in a number of test cases[10,1] including the prototypical system, 2-(4-tetrahydro-1H-2-imidazolyliden-2,5-cyclohexadienyliden)malononitrile (1) experimentally investigated by Lalama *et al.*[14] The hyperpolarisabilites are reported as the average (3 defined in the previous Section. We note once again, that the hyperpolarisabilities that we present are the static values.

β_{2level} is obtained using the expression[2] (which is a simplification of Eqn.1.16 for the case of zero excitation energy).

$$\beta_{2level} = 6\left[\frac{\mu_{0i}^{2}\Delta\mu_{0i}}{\Delta E_{0i}^{2}}\right] \qquad \textbf{(2.4)}$$

where i is either of the two low-lying excited states, 1 or 2, which have appreciable oscillator strengths. μ_{0i} is the transition dipole between the ground and the ith state, $\Delta\mu_{0i}$ the change in dipole moment on excitation from the ground to the excited state, i and ΔE_{0i} the energy of this excitation. The β_{3level} involving the two states 1 and 2 is easily derived in a similar way, from the usual SOS expression for β_{ijk} as follows.

$$\beta_{3level} = 6\left[\frac{2\mu_{01}\mu_{02}\mu_{12}}{\Delta E_{01}\Delta E_{02}} + \sum_{i=1}^{2}\frac{\mu_{0i}^{2}\Delta\mu_{0i}}{\Delta E_{0i}^{2}}\right] \qquad \textbf{(2.5)}$$

The hyperpolarisability calculations were carried out under three different conditions. In Method A, the geometries optimised in presence of the different external fields were used, and the external point charges removed during the p calculation. In Method B, the gas phase structure (optimised under zero external field) was used with different external fields described above being imposed using the point charges during the P calculation. In Method C, the structures optimised under different external fields were used along with the external point charges being present during the p calculation. In the terminology of Gorman and Marder[15], the three methods correspond respectively to nonequilibrium electronic-equilibrium nuclear configurations, nonequilibrium nuclear-

equilibrium electronic configurations, and equilibrium electronic-equilibrium nuclear configurations.

Inspection of Table 2.2 indicates that the variation of r_1, r_2 and r_3 are as expected. The r_1 and r_3 values change from approximately 1.45 to 1.41 A on going from the quinonoid limit to the benzenoid limit. r_2 in the quinonoid limit is close to a normal double bond value of 1.35 A and approaches 1.38 A as the benzenoid extreme is reached. The symmetry is close to D_{2h} at the two extremes. Verification of these structural features at the benzenoid limit comes from our experimental systems (with $r_1 \approx r_3 \approx 1.40$ and $r_2 \approx 1.38$ A) as noted below. The quinonoid limit could be related to the case of 7,7,8,8-tetracyanoquinodimethane (with $r_1 \approx r_3 \approx 1.45$ and $r_2 \approx 1.35$ A). The group charges, q^+ and q'' values, increase as expected with the quinonoid to benzenoid transformation. q'' values, in particular, parallel the QBC's. It is noteworthy that the charges do not approach too closely 0 and 1 in the quinonoid and benzenoid forms respectively. This is likely due to the charge transfer from the donor group to the acceptor group in the former case and from the ionized acceptor to the ionized donor in the latter, in spite of the the static external field. The zero applied field structure corresponds to the optimised structure of DADQ. The QBC assigned to the structure is 0.286, and the extent of charge transfer corresponds to approximately 40 - 50%.

Methods A and B involve situations with nonequilibrium electronic and nuclear configurations, respectively, and hence the results are of interest only as control cases. The variations of p with QBC in

method A and with the applied field, F, in method B are plotted in Fig.2.3. It is seen that when the electronic configuration is in a nonequilibrium state, the β continuously increases with QBC indicating the largest values at the benzenoid limit. On the other hand, if the equilibrium nuclear configuration is ignored, the β is found to peak at an external field of about -2 x 10 V/cm corresponding to an electronic configuration intermediate between the quinonoid and benzenoid limits. The overall observation is that, there is a trend towards larger (3 values as one goes from the quinonoid end to the benzenoid end whether one considers the related nuclear or electronic configuration changes; however, the imposition of the strong field at either end (in method B) tends to reduce the β values. The detailed results of the calculations using the most appropriate[1] procedure (method C) which considers equilibrium electronic and nuclear configuration are as follows.

Table 2.3 presents the dipole moment, excitation energy and hyperpolarisability for structures with different quinonoid-benzenoid character, calculated in method C. The ground state dipole moments are very large throughout due to the presence of the external charges; the only relevant quantity is that for the case of zero applied field when QBC = 0.286. The dipole moment changes associated with the excitation as well as the excitation energies and oscillator strengths (proportional to μ_{01}^2) are provided for the two excited states, 1 and 2.

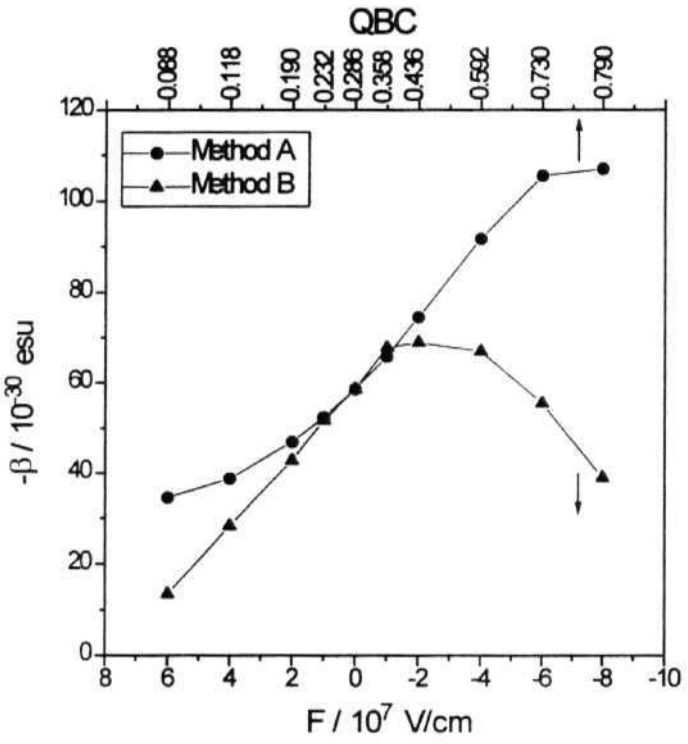

Figure 2.3: *Variation of the static β with QBC and applied field, F (QBC is defined in Eqn.2.3); the line is only a guide to the eye*

The $\Delta\mu$ are always negative and large indicating reverse charge transfer on excitation. We have examined the β_{2level} ($\beta_2(0)$) using either of the two states and the results are provided in Table 2.3. We have also listed the β_{3level} ($\beta_3(0)$) utilising both these excited states. Finally the table also presents the β value calculated utilising all the excited states (p(0)). The β_{2level} values for excited states 1 and 2 are strongly influenced by the trends of μ_{0i} (or f) and $\Delta\mu$ values. For the excited state 1, these values go through a maximum near the QBC value of 0.600.

Table 2.3: *Calculated ground state dipole moment (μ_0),dipole moment change on excitation ($\Delta\mu_{0i}$), excitation energy (ΔE_{0i}) with oscillator strength (f) and static folevel ($\beta_2(0)$) for excited states 1 and 2, β_{3level} (03(0)) and $\beta(0)$ forDADQ structures with different quinonoid - benzenoid character (QBC) calculated using method C. (All ft's are in 10^{-30} esu. †The entries in the first and second row are for the excited states 1 and 2, respectively)*

QBC	μ_0(D)	$\Delta\mu_{0i}$(D)†	ΔE_{0i}(eV) [f]†	$-\beta_2(0)$†	$-\beta_3(0)$	$-\beta(0)$
0.088	67.6	-2.1	2.83[0.006]	0.1	3.7	9.7
		-0.9	3.42[1.130]	2.7		
0.118	86.6	-5.5	2.80[0.044]	1.1	13.6	18.5
		-3.6	3.39[1.065]	10.1		
0.190	124.9	-10.6	2.77[0.195]	9.9	25.9	35.4
		-5.6	3.44[0.841]	12.7		
0.232	174.9	-12.8	2.71[0.264]	17.4	34.2	46.2
		-8.0	3.50[0.718]	13.9		
0.286	14.5	-14.7	2.66[0.326]	26.0	42.5	58.6
		-10.2	3.59[0.599]	13.6		
0.358	146.4	-16.6	2.65[0.390]	35.8	50.4	75.4
		-12.4	3.72[0.471]	11.6		
0.436	96.0	-18.1	2.67[0.457]	44.5	45.6	86.5
		-8.9	3.75[0.032]	0.6		
0.592	56.9	-20.4	2.87[0.583]	51.4	52.9	94.0
		-11.0	3.71[0.050]	1.1		
0.730	38.0	-20.7	3.17[0.571]	37.9	37.9	67.4
		-12.0	3.75[0.000]	0.0		
0.790	28.3	-19.0	3.37[0.479]	24.4	24.4	47.7
		-12.8	3.78[0.000]	0.0		

The contribution from the excited state 2 is negligible after the QBC value of 0.400 because of the nearly vanishing oscillator strengths.

Fig. 2.4 depicts the variation of the full β with the QBC and the contribution of β_{2level} from the first and the second excited state as well as that of the β_{3level}. The negative sign of the β values is a consequence of the negative $\Delta\mu$ as stated earlier. It is seen that the β increases steadily from the quinonoid end and peaks at the QBC of 0.592, then is suppressed to about half the peak value at the benzenoid end. The values except at the quinonoid end are quite large. The β_{2level} using the first excited state is negligible at very low QBC values, but reproduces about 40 - 50% of full β later; the β_{2level} from the second excited state contributes about 30% at low QBC and has nearly zero contribution at higher ranges. The β_{3level} is mostly seen to be an additive contribution of the two β_{2level} terms, with the cross term contributing very little. The β_{3level} is a fair approximation for p at QBC below 0.232, whereas it reproduces only about 50% of β in the more benzenoid structures.

The calculations reveal that the traditional pictures based on a single charge transfer excitation are grossly inadequate to describe the β, except at low QBC values. At the higher QBC's at least 50% of the p is made up of contributions from the higher excited states. Since individual contributions from these states would be smaller than that from states with lower AE's, it is inferred that several of them contribute. The analysis also indicates that the increased polarisation of charges on a quinonoid framework substituted with donor-acceptor groups, leads to very large p values, though the extreme fields at the

benzenoid zwitterionic limit tends to suppress it to some extent. The high p values imply that the individual contributions from each of the large number of excited states should be appreciable. The excited states

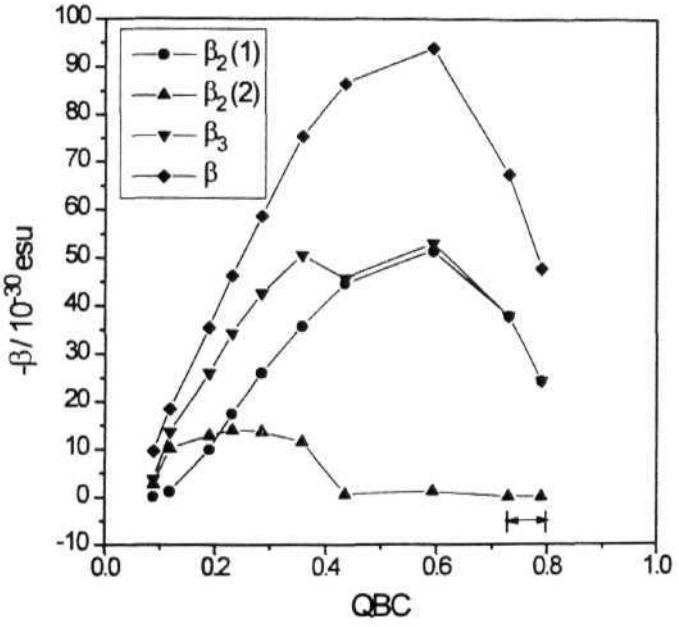

Figure 2.4: *Variation of the static fclevel (excited state J), folevel (excited state 2), foievel and fullft'with the QBC in DADQ calculated using Method C; the lines are only a guide to the eye.* \↔| *indicates the range of QBC values of our experimental systems 8-11*

in most cases are associated with decreased net charges at each end, and consequently a lower dipole moment. The large and negative Δu associated with these states enhance their contributions to p. An

associated practical problem is the large ground state dipole moment of these molecules which could encourage centrosymmetric crystal lattice formation.

Absorption in the UV region (corresponding to the excited state 2) is quite strong for QBC values upto 0.358. The absorption in the visible range (excited state 1) picks up oscillator strength after a QBC of 0.190; however, at high QBC values (> 0.592), this absorption goes to higher energies, *ie.* into the UV region. Thus the systems towards the benzenoid extreme do not absorb in the visible range and are expected to be useful for applications involving visible light even though they do not have the maximum β values.

Strong donors and acceptors can be utilised to push the QBC to values larger than that found in DADQ. Such substitutions effectively replace the negative external field used in our model study, by appropriate internal fields. In Fig. 2.4 we have indicated the range of QBC values covered by four typical molecules we have synthesised. The details of these systems will be presented in Chapter 5. Average values of the bond lengths r_1, r_2 and r_3 from single crystal x-ray structure analysis[17] have been used to assign their QBC values which are found to fall in the range 0.739 to 0.811. It is interesting to note that experimentally easily accessible systems have approximately 50% of the maximum β value attainable in the full QBC range. Reducing the donor/acceptor strength may push QBC towards the values corresponding to maximum β values. The experimental (acetonitrile solution) absorption maxima of our molecules fall in the 350 - 420 nm

range in good accord with the calculation above and the solids are colourless to light yellow. The appreciable transparency of these materials in most of the visible range makes them practically interesting.

2.4 DEPENDENCE OF HYPERPOLARISABILITY ON THE MOLECULAR TWIST

In all the molecular structures we have investigated in the class of diamino substituted dicyanoquinodimethanes, the diaminomethylene group is twisted out of the plane containing the quinonoid ring and the dicyanomethylene unit. This appears to arise from strong steric interactions between groups attached to the amino N atoms and the *ortho* H atoms on the benzenoid ring. To gain some insight into this aspect, we have initially carried out some computations on the prototypical molecule, 1 and its N-methylated derivatives 2 and 3 (Fig.2.1). As stated earlier, a careful observation of the molecular structures obtained from crystal structure analysis and semiempirical AM1 geometry optimisation on several compounds and the computed hyperpolarisabilities, reveals a strong correlation between β and this molecular twist. This prompted us to probe this aspect more systematically. We present in this Section, the results of theoretical studies on the model system, 7,7-dipyrrolidino-8,8-dicyanoquinodimethane, DPDQ (Fig.2.1, 8); DPDQ was chosen, because the chiral compounds we have investigated (Chapter 6), which showed appreciable solid state SHG capability were all based on this basic framework. The surprising observation is that the β as a function

of the twist angle reaches a maximum at the geometry obtained from full AM1 geometry optimisation, which in turn has a close correspondence to the molecular structure obtained from the crystal analysis. On the basis of the well known two state model [18], we discuss the factors that lead to the maximisation of β at the optimal geometry.

To analyse the origin of the molecular twist, we have first optimised (using the AM1 method) the geometries of 1, 2 and 3 imposing a C_2 symmetry constraint with the C_2 axis along the 7, 8 carbons. Table 2.4 provides the ΔH_f and β values calculated at various twisting angles, 0 (dihedral angle shown in Fig.2.5). It is seen that the

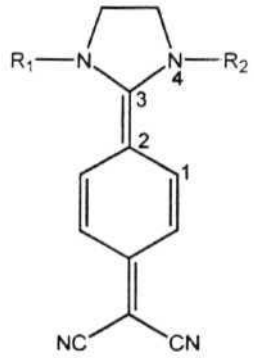

θ = dihedral angle 1-2-3-4

1 : $R_1 = R_2 = H$

2 : $R_1 = CH_3$, $R_2 = H$

3 : $R_1 = R_2 = CH_3$

Figure 2.5: *Molecular structure of **1**, 2 and 3 showing the definition of the twist angle, 6*

heat of formation goes through a minimum at twist angles of 0, 10 and 20° in 1, 2 and 3 respectively (see Table 2.1 for the twist angles in the fully optimised geometries). This shift of the minimum arises due to the introduction of the methyl groups on the N atoms, which gives rise to increased steric hindrance with the *ortho* hydrogen atoms on the benzenoid ring. It is interesting to note that in all the three molecules, the trends of (3 are similar and a maximum is observed at θ = 70°. As a

Table 2.4: *The heat of format ion (AHf in kcal/mol) and static hyperpolarisability (β(0) in 10^{-30} esu) at various twist angles (6) for molecules 1, 2 and 3*

Twist angle, θ	1		2		3	
(°)	ΔH_f	$-\beta(0)$	ΔH_f	$-\beta(0)$	ΔH_f	$-\beta(0)$
0	**135.1**	**1.6**	143.0	0.5	150.0	0.3
10	135.4	2.1	**142.1**	**2.2**	148.3	2.0
20	136.4	4.7	142.4	6.4	**147.8**	**7.0**
30	137.8	9.4	143.8	12.7	148.7	15.2
40	139.9	16.8	145.7	26.5	150.3	27.7
50	142.5	27.5	147.1	31.1	151.6	33.5
60	145.3	40.1	149.3	41.4	153.4	41.5
70	147.6	44.2	151.5	43.7	155.4	43.0
80	149.2	30.8	152.9	27.1	156.7	27.3
90	149.7	16.7	153.5	16.1	157.2	15.2

result of these factors the magnitude of β at the optimal geometry of 1, 2 and 3 is found to increase from 1.6 to 2.2 to 7.0. We explore below, this correlation between β and θ by considering further observations from experimental data and computational studies.

Table 2.5 presents the value of twist angle, θ obtained from crystal structure analysis as well as by full AM1 optimisation of the geometry on seven molecules (see Fig.2.1 for the molecular structures). It is immediately obvious that the 0(CS) and θ(AM1) show poor

Table 2.5: *The twisting angles, θ from crystal structure (CS) and optimised AM1 geometries, corresponding static fi values, the ratio of twisting angles (θ_{AM1}/θ_{CS}) and the ratio of β values (β_{AM1}/β_{CS}) for the seven diamino-substituted dicyanoquinodimethanes whose crystal structures have been investigated (see Chapters 5 and 6)*

	Twist angle θ (°)		-β(0) (10^{-30} esu)		$\frac{\theta_{AM1}}{\theta_{CS}}$	$\frac{\beta_{AM1}}{\beta_{CS}}$
	CS	AM1	CS	AM1		
11	48.7	34.0	54.3	11.9	0.700	0.219
9	46.8	38.6	54.9	19.8	0.825	0.361
10	43.0	38.9	53.9	16.6	0.905	0.308
14	49.8	45.5	51.0	27.6	0.912	0.541
12	54.0	50.8	50.2	35.8	0.937	0.713
16	58.2	57.9	51.4	38.7	0.995	0.753
8	56.2	59.3	52.6	39.5	1.055	0.751

agreement in the case of the three molecules involving saturated six-membered ring heterocycles for the amino moiety. This may be attributed to the fact that the bulkier and conformationally more flexible six-member rings have quite different steric interactions in the gas phase (simulated by the calculations) and the crystalline phase. In the case of the other four molecules the agreement of the two 0 values is much better. Table 2.5 also contains the p values calculated for the two geometries of each of the molecules. The P(AM1) are found to be smaller than the p(CS) in all cases. The smaller value of P(AM1) relative to p(CS) throughout the series arises mainly due to the difference in the bond lengths in the quinonoid framework in the CS and AM1 geometries. An insight into this may be gained by quantifying the quinonoid-benzenoid character of these geometries, using the parameter QBC defined by us in the previous Section. The CS geometries are more benzenoid than the AM1 geometries, since the former are the optimal geometries of those molecules in a strongly polar crystal environment; hence the CS geometries have larger QBC values than the AM1 geometries. We have shown above, using model calculations on DADQ. that the p values decrease monotonically with the QBC values, when the p calculations are carried out without the presence of **a** simulated external field. The p values reported in Table 2.5 are calculated in the same fashion, hence the lower β for the AM1 structures having smaller QBC values.

The interesting aspect that emerges from a careful analysis of **the** θ **and** β **values** discussed **above** is the correlation between $\theta(AM1)/\theta(CS)$ **and** P(AMl)/p(CS) **also** presented in Table 2.5. A minor

variation of 0 from AM1 to CS geometry is associated with a small variation of p between these geometries and a larger variation of θ is associated with a relatively larger change in p. This trend is followed through the series except for a minor discrepancy. This suggested to us that within a molecule, the hyperpolarisability would have a strong dependence on the molecular twist angle, θ. Our calculations of β on molecules, 1, 2 and 3 presented above, as well as overall observations of 0 and β in these push-pull quinonoid molecules presented in Table 2.1 also suggested such a correlation. We have carried out the following detailed computational study on the molecule, DPDQ to analyse this correlation.

The molecular framework indicating the relevant atom labelling is shown in Fig.2.6. The AM1 optimised geometry of DPDQ is very close to the one obtained from the crystal structure analysis, especially

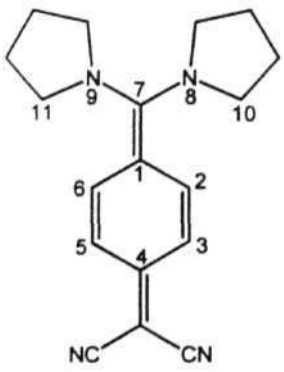

Figure 2.6: *Molecular structure of DPDQ showing the atom labelling for defining relevant dihedral angles*

with regard to the twist angle (Table 2.5). Starting from the crystal structure geometry having nearly C_2 point group symmetry, the twist angle. θ (dihedral angle 8-7-1-2 or 9-7-1-6; see Fig.2.6) was varied in 3° intervals to 0° on one side and 90° on the other and geometry optimisation carried out at each point imposing a C_2 symmetry constraint. The point closest to the crystal structure geometry has G = 57°. We note that each θ point optimisation was carried out using the optimised geometry at the previous point as the starting structure to ensure smooth geometry changes. The imposition of C_2 symmetry does not cause any marked changes in the heat of formation of the optimised structures; it helps to make the geometry changes more controlled and smooth and suppresses unrealistic spikes that otherwise arise in the curve owing to the conformational flexibility associated with the pyrrolidine ring. Table 2.6 presents the calculated heats of formation and the p at 9° intervals, and the variation of ΔH_f and p with the angle θ is plotted in Fig. 2.7 using the full calculated data set. From $\theta = 60^o$, a value close to the one found in the crystal structure geometry (56.2°), the heat of formation rises by about 1.3 kcal/mol at 90° twist and by nearly 4.3 kcal/mol at the planar geometry. There is a small discontinuity at about 27°. Inspection of the optimised geometries reveals that when G = 0°, the dihedral angle, 10-8-7-1 (τ) is ~ 80° *ie.*, the pyrrolidine rings are nearly perpendicular to the plane of the diaminomethylene moiety whereas when θ = 90°, x ~ 0° . The slow rotation of the pyrrolidine ring with respect to the diaminomethylene unit when 0 varies from 0^o to 90^o, takes a sudden jump at 0 = 27° and this appears to be the cause of the discrepancy in the monotonous fall of AHf noticed at this point. The value of p is also found to go through a

small anomaly as a consequence of this; initially it decreases slightly from the planar geometry and then rises smoothly till θ = 57°, followed by a decline to the perpendicular geometry. The most significant observation here is that the β value goes through a maximum close to the θ corresponding to the optimised geometry of the molecule. This is rather unusual and in contrast to the behaviour observed in other systems investigated previously,[19] where β was found to decrease monotonously

Table 2.6: *The heat of formation (ΔH_f) and static hyperpolarisability ($\beta(0)$) at various twist angles (6) for DPDQ along with the square of the transition moment (μ^2), dipole moment change ($\Delta\mu$) and energy difference (AE) between the ground and first excited state*

θ (°)	ΔH_f (kcal/mol)	$-\beta(0)$ (10^{-30} esu)	μ^2 (esu^2)	$-\Delta\mu$ (D)	ΔE (eV)
0	133.920	9.29	0.8770	0.63	2.992
9	133.410	8.65	1.5688	0.50	2.811
18	133.103	3.83	1.8093	0.52	2.600
27	132.867	4.48	2.0034	1.16	2.393
36	131.635	23.28	2.1715	3.47	2.170
45	130.455	33.19	2.0828	5.32	2.150
54	129.740	38.91	1.7806	7.45	2.146
57	129.641	39.59	1.6333	8.14	2.151
63	129.660	38.90	1.2873	9.46	2.163
72	130.114	31.53	0.6816	11.51	2.206
81	130.682	18.95	0.1644	13.59	2.259
90	130.938	13.53	0.0007	15.45	2.269

with increasing molecular twist. We analyse below, the factors that lead to this interesting effect.

The simple two state model of Oudar,[18] is based on a description of β in terms of the ground state and a single excited state of the molecule and shows that the static hyperpolarisability, $\beta_{2level}(0)$ depends on the square of the transition dipole moment, μ (directly proportional

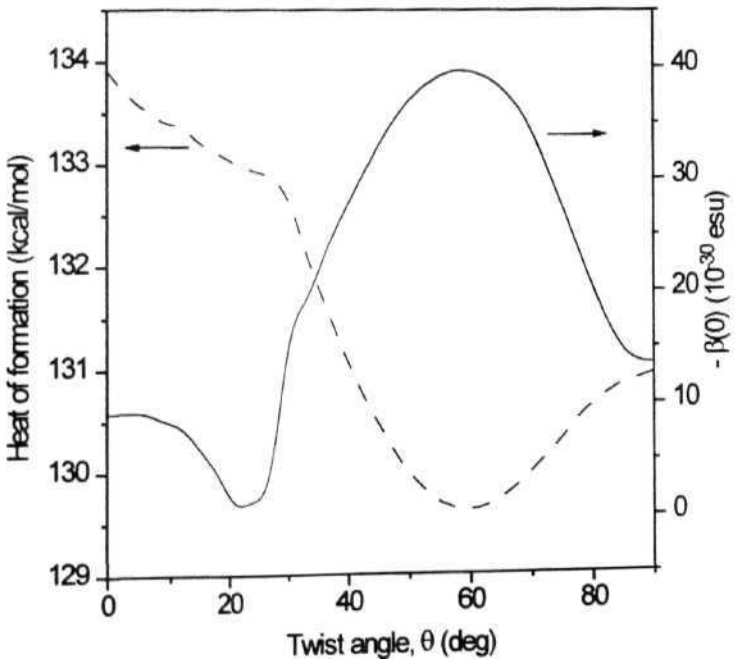

Figure 2.7: *The plot of the heat of formation, ΔH_f (– – –) and the static hyperpolarisability, -β(0) (——) versus twist angle, θ for DPDQ*

to the oscillator strength) and energy of this excitation, AE, as well as the change in dipole moment, Au between the ground and the excited state (Eqn.2.4). In Sec.2.3 we have shown that the two-state picture fails to predict quantitatively the hyperpolarisabilities of this class of molecules, however, the qualitative trends are reproduced well. Therefore we have estimated, using semiempirical AM1 /CI computations, the values of μ^2, Au and AE in DPDQ at various twist

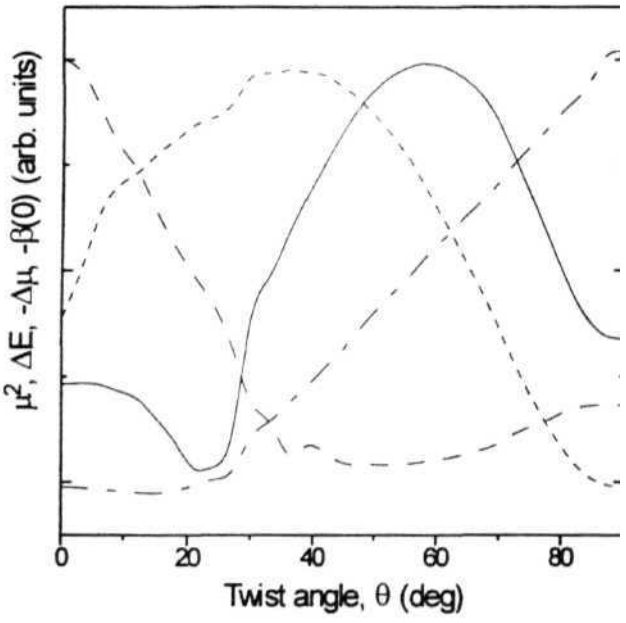

Figure 2.8: *The plot of the square of the transition moment, μ^2 (----), energy difference, ΔE (– – –) and the dipole moment change, $-\Delta\mu$ (— — — –) between the ground and excited state and the static hyperpolarisability, $-\beta(0)$ (——) versus the twist angle, θ for DPDQ*

angles using the geometries optimised above (Table 2.6). The variation of -P(0), u^2, -A|i and AE with θ is depicted in Fig.2.8 (note that the absolute values of the y-axis variables are not indicated in the figure to make the comparison of trends easier, however the relative values are to scale). It is seen that the μ^2 rises initially upto 9 ~ 40° and then decreases continuously to 90°. The $-\Delta\mu$ shows a small decline from 0^o to 15^o followed by a gradual rise to 30° and a stronger and nearly linear increase subsequently. This arises from the strong increase in the ground state dipole moment and a small decrease of the excited state dipole moment on going from the planar (μ_g = 11.46 D, μ_e = 10.83 D) to the orthogonal (μ_g = 21.58 D, μ_e = 6.13 D) geometry. It is noteworthy that the change in dipole moment on excitation is very large even at the optimised geometry and as stated earlier, this is probably one of the important factors that contributes to the large (3 of this class of molecules. The AE decreases continuously from 0° to about 50° and then registers a gradual increase to 90°. Leaving aside the anomalous behaviour of the various quantities in the range 15° to 30° which arises from the rotation of the pyrrolidine ring as discussed earlier and is irrelevant to the focus of our analysis here, the trends of the three quantities noted above influence the β as follows. The maximum in μ^2 and the minimum in AE are expected to lead to a maximum in p at some value of θ between 40° and 50°. The strong rise of $\Delta\mu$, however, shifts this maximum to an angle closer to 60°. Thus we find that the hyperpolarisability goes through a maximum at a twist angle close to that found in the optimal structure.

2.5 CONCLUSION

In this Chapter, we have carried out computational studies of the hyperpolarisabilities of the novel push-pull quinonoid molecules. It is found that this class of molecules possess unexpectedly large β values. The calculations also reveal that they are strongly zwitterionic systems; the associated large ground state dipole moments could be detrimental to the formation of noncentric crystal lattices of interest in quadratic NLO applications.

We have carried out theoretical analysis of p as a function of the quinonoid - benzenoid character. The calculations on DADQ reveal that the traditional pictures based on a single charge transfer excitation are grossly inadequate to describe the p, except at low QBC values. At the higher QBC's at least 50% of the p is made up of contributions from the higher excited states. The experimental systems possess large QBC values at which the p has declined below its maximum possible value. The current analysis indicates that slightly poorer donor or acceptor groups can lead to enhanced β values. However, in terms of the transparency window, the present experimental systems appear to possess the appropriate range of QBC.

We have also analysed in detail the close correlation between the strong molecular twist observed in the series of diamino-substituted dicyanoquinodimethanes and their hyperpolarisabilities. The significant result from the semiempirical computational study is that the β as a function of the twist, 0, goes through a maximum at the angle

corresponding to the optimal geometry. The factors that contribute to this are analysed in terms of the two state model. The fact that these molecules manifest their highest possible values of β at the 9 observed in their crystals is very encouraging for the development of these molecular materials.

REFERENCES

1. Heitler, L.R.; Hartzler, H.D.; Acker, D.S.; Benson, R.E. *J. Am. Chem. Soc.* **1962,** *84,* 3387.
2. Kanis, D.R.; Ratner, M.A.; Marks, T.J. *Chem. Rev.* **1994,** *94,* 195.
3. Shuai, Z.; Ramasesha, S.; Bredas, J.L. *Chem. Phys. Lett.* **1996,** *250,* 14.
4. MOPAC93 © Fujitsu Inc.
5. Dewar, M.J.S.; Zoebisch, E.G.; Healy, E.F.; Stewart, J.J.P. *J.Am. Chem. Soc.* **1985,** *107,* 3902.
6. Dupuis, M.; Karna, S../. *Comp. Chem.* **1991,** *12,* **487.**
7. Stewart, J.J.P. *Quantum Chemistry Program Exchange;* Indiana University: Bloomington, Indiana; Program 455, Version 6.0.
8. Kurtz, H.A.; Stewart, J.J.P.; Dieter, K.M. *J. Comp. Chem.* **1990**, *11*, 82.
9. (a) Jain, M; Chandrasekhar, J. *J. Phys. Chem.* **1993,** *97,* 4044. (b) Rauhut, G.; Alex, A.; Chandrasekhar, J.; Steinke, T.; Clark, T. Universität Erlangen-Niirnberg, 1993.
10. Clark, T.; Chandrasekhar, J. *Isr. J. Chem.* **1993,** *33B,* 435.
11. Ravi, M.; Radhakrishnan. T.P. *J. Phys. Chem.* **1995,** *99,* 17624.
12. (a) Bourhill, G.; Bredas, J.L.; Cheng, L.T.; Marder, S.R.; Meyers, F.; Perry, J.W.; Tiemann, B.G. *J. Am. Chem. Soc.* **1994,** *116,* 2619. (b) Meyers, F.; Marder, S.R.; Pierce, B.M.; Bredas, J.L. *J. Am. Chem. Soc.* **1994**, *116*, 10703.
13. Whitaker, C.M.; Patterson, E.V.; Kott, K.L.; McMahon, R.J. *J Am. Chem. Soc.* **1996,** *118*, 9966.

14. Lalama, S.J.; Singer, K.D.; Garito, A.F.; Desai, K.N. *Appl. Phys. Lett.* **1981,** *39,* 940.
15. Gorman, C.B.; Marder, S.R. *Chem. Mater.* **1995,** 7, 215.
16. Long, R.E.; Sparks, R.A.; Trueblood, K.N. *Acta Crystallogr.* **1965,***18,* 932.
17. Ravi, M; Cohen, S.; Agranat, I.; Radhakrishnan, T.P. *Struct. Chem.* **1996,** 7, 225.
18. Oudar, J.L. *J. Chem. Phys.* 1977, *67,* 446.
19. (a) Lequan, M.; Lequan, R.M.; Chane-Ching, K.; Barzoukas, M.; Fort, A.; Bravic, G.; Chasseau, D.; Barrans, Y.; Huche, M. *Chem. Phys. Lett.* **1993,** *21* J, 71.(b) Lequan, M.; Lequan, R.M.; Chane-Ching, K.; Bassoul, P.; Bravic, G.; Barrans, Y.; Chasseau, D. *J. Mater. Chem.* **1996,** 6, 5.

CHAPTER 3

SYNTHESIS AND CHARACTERISATION

3.1 BACKGROUND

In the previous chapter we have shown that diamino substituted dicyanoquinodimethane molecules (Fig.2.1) are interesting candidates for the development of a new class of molecular second order nonlinear optical materials, because of the appreciable hyperpolarisabilities and transparency windows they possess. The computational studies we have carried out, also indicated possible ways of fine tuning the β of these molecules through the control of electronic and molecular structure. The prototypical molecules in this class were synthesised by a du Pont group[1] in 1962, by the direct reaction between amines and 7,7,8,8-tetracyanoquinodimethane (TCNQ). Later Gomper *et al* have reported the synthesis of some more derivatives and the kinetics of the reactions of long chain alkylamines with TCNQ was studied in various organic solvents by Seoud *et al*[3] One of the most attractive features of these molecules is the extremely simple synthetic protocol involved. The reactions for their synthesis are mostly single-step and the conditions required are extremely mild. Atmospheric oxygen and moisture do not hamper the reaction in most cases, so special care with regard to these are obviated. The synthesis is very versatile and the flexibility to introduce a wide variety of substituent groups exists. In many cases, the products can be grown into reasonably large single crystals. All these factors prompted us to take up the synthesis of several derivatives and investigate their potential for optical second harmonic generation.

We note that there are some brief reports of NLO studies on these molecules. As mentioned earlier, Lalama *et at* have carried out EFISHG studies on the prototypical system, 1 and reported extremely large hyperpolarisability in this molecule. Nicoud and coworkers ' have prepared some chiral derivatives and measured their powder SHG. However the SHG obtained were all rather weak and no further systematic investigations were carried out. Recently, Szablewski *et al* have prepared some closely related zwitterionic systems; however no solid state NLO properties have been investigated in these crystalline materials. We present in this Chapter, the details of the preparation of the compounds indicated in Fig.2.1 and their characterisation. Molecular and crystal structures of selected compounds have been determined and their SHG capabilities investigated. These will be presented in the following Chapters.

We have prepared compounds 1-16 following the procedure reported by Heitler *et al.* In Sec.3.1 the preparation procedures are described for 1 (representing 1 - 6), 11 (representing 7 - 13) and 16 (representing 14 - 16). The derivatives 1 - 3, 5, and 7 - 9 have been synthesised and characterised by earlier workers ' as well. Therefore we provide in Sec.3.2, the characterisation details (melting point, IR, UV-Vis and mass spectral data, optical rotation for chiral compounds and elemental analysis) for the compounds 4, 6 and 10-16 which are the novel systems we have prepared during our investigations. Even though 8 has been reported earlier, we have carried out extensive studies of some novel NLO

features in this compound; hence we present the characterisation details of this compound as well.

3.2 SYNTHESIS

The chemicals used in the following preparations are TCNQ and a variety of amines. TCNQ and the chiral amines used were procured from Aldrich Chemical Co. and the other amines were obtained from E-Merck (India). TCNQ was recrystallised from acetonitrile and the amines were usually purified by distillation.

The general course of reactions of amines with TCNQ can be described as follows. Addition of an aliphatic amine to a TCNQ solution results in the instantaneous production of an intense green colour, which then changes to purple brown. In the presence of excess amine the solution turns yellow. These changes can be represented as follows.

$$RNH_2 + TCNQ \longrightarrow (RNH_2^{+\cdot})\,TCNQ^{-\cdot} \xrightarrow{-HCN}$$

$$\text{Type 1 compound (purple-brown)} \xrightarrow[-HCN]{+RNH_2} \text{Type 2 compound (yellow)}$$

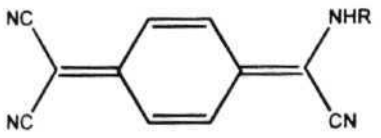

Type 1 compound

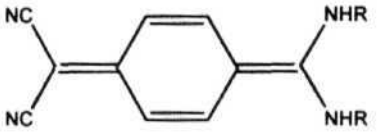

Type 2 compound

The formation of a charge transfer complex between the amine and TCNQ most certainly precedes the electron transfer step which leads to the production of $TCNQ^{\cdot}$ having the intense green colour. This is followed by the internal proton transfer leading to the formation of the intermediate $(CN)_2CHC_6H_4$-p-$C(CN)_2NHR$ which then loses HCN rapidly to give the Type 1 product. The formation of Type 2 product proceeds in an analogous fashion.

Preparation of 1 - 6 exemplified** by **the** procedure for **J.

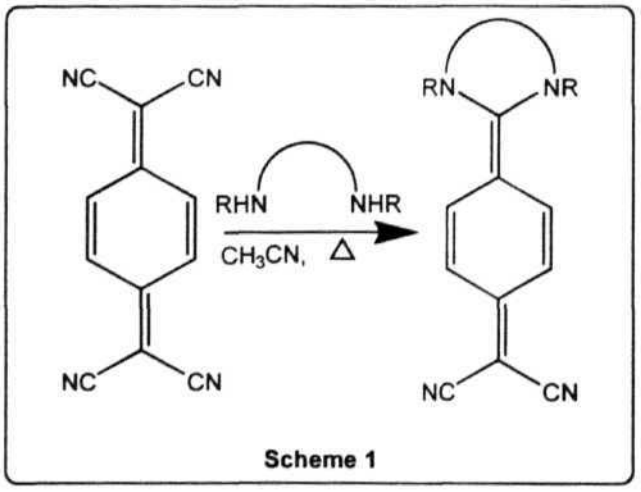

Scheme 1

The procedure adopted for the preparation of 1 - 6 is shown in Scheme 1. To a warm solution of 0.10 g (0.49 mmol) of 7,7,8,8-tetracyanoquinodimethane (TCNQ) in 60 ml of acetonitrile (distilled and dried over P_2O_5) 0.04 g (0.66 mmol) of ethylenediamine was added. A green colour appeared immediately and a light-coloured precipitate began to form. After 1.5 hours at room temperature, filtration gave 0.09 g (90% yield) of a yellow-green solid. Recrystallisation from acetonitrile gave 0.04 g of 1 as a yellow powder. Attempts to grow crystals of 2-(4-tetrahydro-1H-2-imidazolyliden-2,5-cyclohexadienyliden)malononitrile, 1 and the related compounds 2 - 6 were unsuccessful though a variety of solvents were tried.

*Preparation **of** 7 - 13 exemplified by the procedure **for** 11.*

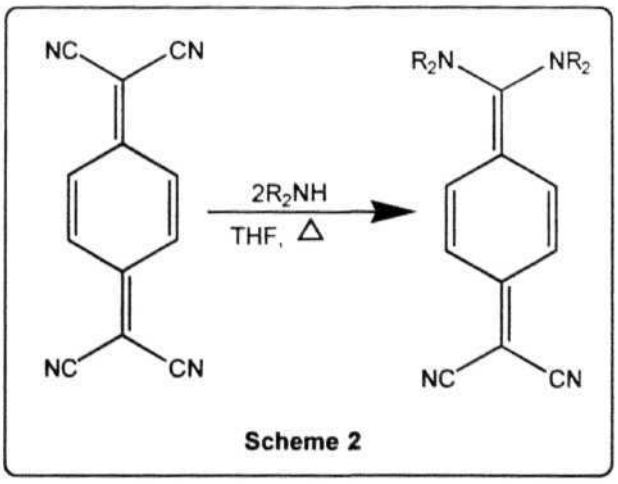

Scheme 2

Scheme 2 was used for these preparations. To a warm solution **of** 0.10 g (0.49 mmol) of TCNQ in 20 ml of tetrahydrofuran (freshly distilled and dried over sodium), 0.17 g (2.07 mmol) of piperazine dissolved in 5 **ml** of THF was added. A dark green colour developed immediately. The solution was heated at 50°C and stirred for ~2 min when the colour faded slowly and a yellow crystalline compound began to precipitate. After standing for 5 hrs. at about 30°C, the solution was cooled to about 10°C and the precipitate was filtered out. The filter cake was washed first with cold tetrahydrofuran and then with ether to give 0.11 g (70% yield) of the crystalline compound 11. Recrystallisation from acetonitrile gave transparent needle-like crystals. Several other compounds in this class also could be grown as single crystals.

Preparation of 14 *- 16 exemplified by the procedure* ***for*** *16.*

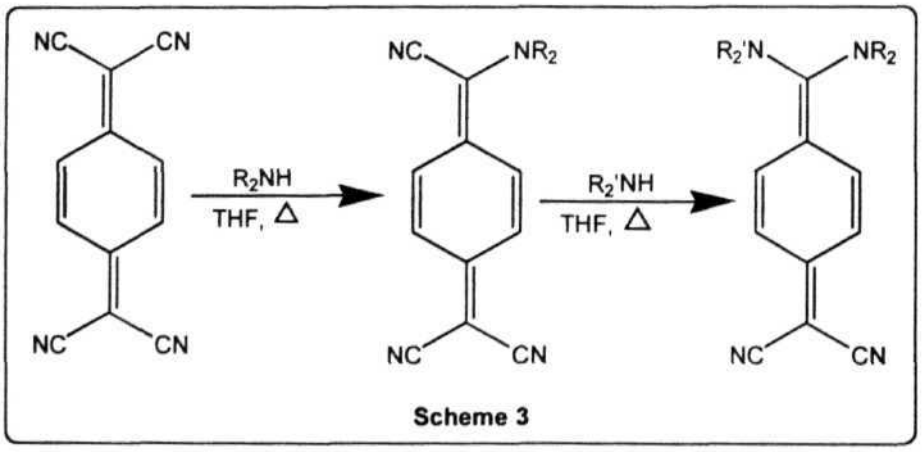

Scheme 3

These compounds were prepared following Scheme 3, with R_1NH being pyrrolidine. 7-pyrrolidino-7,8,8-tricyanoquinodimethane (PTQ) was prepared using the reported procedure[1] as follows. To a warm solution of 0.20 g (0.98 mmol) of TCNQ in 20 ml. of tetrahydrofuran (freshly distilled and dried over sodium) was added 0.042 g (0.6 mmol) of pyrrolidine. It is important to add slightly less than one equivalent of pyrrolidine to avoid the formation of the disubstituted product. The solution turned green immediately, but subsequently it changed to a gray-purple colour. After standing for 17 hours at about 30°C. the solution was cooled in an ice-bath and filtered to give 0.205 g (84% yield) of a purple solid. Recrystallisation from acetonitrile gave PTQ as fine purple needles. To a warm solution of 0.10 g (0.4 mmol) of PTQ in 20 ml of tetrahydrofuran, 0.037 g (0.32 mmol) of S-(+)-2-methoxymethylpyrrolidine was added and the solution was stirred at 50°C for 10 min. After standing for 5 hours at 30°C, the solution was cooled to 10°C and filtered to obtain 0.167 g (90% yield) of the light green compound 16, which was recrystallised from acetonitrile to give pale yellow crystals.

3.3 CHARACTERISATION

The IR and UV-Vis Spectra were recorded on a Jasco-5300 FTIR Spectrometer and Jasco-7800 Spectrophotometer respectively. Optical rotations were measured on a Jasco Digital Polarimeter (Model DIP-370). Elemental analysis was carried out on a Perkin Elmer CHN Analyser

(Model 240C). We provide below, the characterisation details of the new compounds we have synthesised in this series, several of which have been investigated in detail as discussed in Chapters 5 and 6. We do not present detailed characterisation of those derivatives which have been reported by earlier workers. However, we present the details of characterisation of 8 (though it has been reported in the first paper from du Pont), since we have investigated some novel NLO phenomenon in this material.

2-{4-[(3aR, 7aR)perhydrobenzo[l]imidazol-2- yliden]-2,5-cyclohexadienyliden}malononitrile (4)

4 was recrystallised from acetonitrile. Melting point: >340°C. FTIR (KBr wafer) $\bar{\nu}$/cm^{-1}: 3179 (N-H stretch); 2185 and 2141 (conjugated nitrile stretch). UV-Vis (acetonitrile solution) λ_{max}/nm : 407. Optical rotation $[\alpha]_D^{25}$ (c = 0.02, MeOH)) : +80°. Elemental analysis : % found (% calculated for $C_{16}H_{16}N_4$) - C, 72.69 (72.73); H, 6.15 (6.06); N, 20.76 (21.21).

2-(4-hexahydropyrimidinyliden-2,5-cyclohexadienyliden)malononitrile *(6)*

6 was recrystallised from acetonitrile. Melting point: >340°C. FTIR (KBr wafer) $\bar{\nu}$/cm^{-1}: 3250 (N-H stretch); 2190 and 2140 (conjugated nitrile stretch). UV-Vis (acetonitrile solution) λ_{max}/nm : 385. Elemental

analysis : % found (% calculated for $C_{13}H_{12}N_4$) - C, 68.27 (69.64); H, 5.41 (5.36); N, 24.75 (25.00).

7,7-dipyrrolidino-8,8-dicyanoquinodimethane *(DPDQ, 8)*

8 was recrystallised from acetonitrile. Melting point: 290°C (dec). FTIR (KBr wafer) ν/cm^{-1}: 2168 and 2128 (conjugated nitrile stretch). UV-Vis (acetonitrile solution) λ_{max}/nm : 375. Elemental analysis : % found (% calculated for $C_{18}H_{20}N_4 . 0.4H_2O$) - C, 72.42 (72.19); H, 6.85 (6.95); N, 18.29 (18.72) for the acetonitrile recrystallised product and for the chloroform recrystallised product it gave (% calculated for $C_{18}H_{20}N_4$) - C, 74.35 (73.97); H, 6.82 (6.85); N, 18.72 (19.19). MS(EI): m/z - 292 (100), 180 (22), 222 (27). 91 (34), 70 (12).

7,7-dimorpholino-8,8-dicyanoquinodimethane(DMDQ, *10)*

10 was recrystallised from acetonitrile. Melting point: >340°C. FTIR (KBr wafer) ν/cm^{-1}: 2170 and 2130 (conjugated nitrile stretch). UV-Vis (acetonitrile solution) λ_{max}/nm : 420. Elemental analysis : % found (% calculated for $C_{18}H_{20}N_4O_2$) - C, 66.65 (66.66); H, 6.28 (6.17); N, 16.57 (17.28).

7,7-dipiperazino-8,8-dicyanoquinodimethane (DPZDQ, 11)

11 was recrystallised from acetonitrile. Melting point : 300°C (dec). FTIR (KBr wafer) $\bar{\nu}$/cm^{-1} : 3150 (N-H stretch); 2180, 2140 (conjugated nitrile stretch). UV-Vis (acetonitrile solution) λ_{max}/nm : 415. Elemental analysis : % found (% calculated for $C_{18}H_{22}N_6$) - C, 66.31 (67.08), H, 6.82 (6.83); N, 25.39 (26.08).

7,7-di[S(+)-2-methoxymethylpyrrolidino]-8,8-dicyanoquinodimethane (DMPDQ, 12)

12 was recrystallised from acetonitrile. Melting point: 250°C (dec). FTIR (KBr wafer) $\bar{\nu}$/cm^{-1} : 2172, 2133 (conjugated nitrile stretch);1450 (CH_2-O-CH_3 stretch). UV-Vis (acetonitrile solution) λ_{max}/nm: 406. Optical rotation, $[\alpha]_D^{25}$ (c = 0.04, MeOH) : +485°. Elemental analysis : % found (% calculated for $C_{22}N_4O_2H_{28}$) - C, 70.06 (69.47); H, 7.83 (7.37), N, 14.43 (14.74). MS(EI): m/z - 380 (85), 83 (6), 70 (22), 69 (22), 45 (23), 40 (100).

7,7-di[R(-)-3-hydroxypyrrolidino]-8,8-dicyanoquinodimethane (DHPDQ, 13)

13 was recrystallised from methanol. Melting point : 260°C (dec); FTIR (KBr wafer) $\bar{\nu}$/cm^{-1} : 3375 (O-H stretch); 2184, 2137 (conjugated nitrile stretch). UV-Vis (acetonitrile solution) λ_{max}/nm : 388. Optical

rotation, $[\alpha]_D^{25}$ (c = 0.03, MeOH) : -175°. Elemental analysis : % found (% calculated for $C_{18}H_{20}N_4O_2$) - C, 66.90 (66.66); H, 6.16 (6.17); N, 17.44 (17.28).

7,7-di[(±)-3-hydroxypyrrolidino]-8,8-dicyanoquinodimethane (13-RS)

13-RS, the compound from the racemic 3-hydroxypyrrolidine, was recrystallised from methanol. Melting point: 265°C (dec); FTIR (KBr wafer) $\bar{\nu}$/cm^{-1}: 3375 (O-H stretch); 2174, 2131 (conjugated nitrile stretch). UV-Vis (acetonitrile solution) λ_{max}/nm : 393. Optical rotation, $[\alpha]_D^{25}$ (c = 0.03, MeOH) : 0°. Elemental analysis : % found (% calculated for $C_{18}H_{20}N_4O_2$) - C, 66.86 (66.66); H, 6.28 (6.17); N, 16.51 (17.28).

7-[(S)-α-methylbenzylamino]-7-pyrrolidino-8,8-dicyanoquinodimethane (MBPDQ, 14)

14 was recrystallised from acetonitrile. Melting point: 245°C (dec); FTIR (KBr wafer) $\bar{\nu}$/cm^{-1}: 3387 (N-H stretch); 2174, 2128 (conjugated nitrile stretch). UV-Vis (acetonitrile solution) λ_{max}/nm : 368. Optical rotation, $[\alpha]_D^{25}$ (c = 0.04, MeOH) : -395°. The product recrystallised from acetonitrile contained the solvent of crystallisation which was partially lost on exposure, hence it was recrystallised from dichloromethane and subjected to elemental analysis: % found (% calculated for $C_{22}H_{22}N_4.H_2O$):

C, 73.13 (73.33); H, 6.22 (6.66); N, 15.26 (15.55). MS(EI): m/z - 342 (4), 327 (4), 105 (76), 91 (76), 77 (30), 70 (100).

7-[(R)-α-methylbenzylamino]-7-pyrrolidino-8,8-dicyanoquinodimethane (MBPDQ-R, 14-R)

14-R was recrystallised from acetonitrile. Melting point: 245°C (dec). FTIR (KBr wafer) P/cm"[1]: 3390 (N-H stretch); 2173, 2128 (conjugated nitrile stretch). UV-Vis (acetonitrile solution) λ_{max}/nm : 368. Optical rotation, $[\alpha]_D^{25}$ (c = 0.05, MeOH) : +240°. Elemental analysis: % found (% calculated for $C_{22}H_{22}N_4$): C, 77.60 (77.19); H, 6.85 (6.43), N, 15.54 (16.37). MS(EI): m/z - 342 (14), 327 (17), 105 (52), 91 (61), 77 (23), 70(100).

7-[(S)-naphthylethylamino]-7-pyrrolidino-8,8-dicyanoquinodimethane (NEPDQ, 15)

15 was recrystallised from acetonitrile. Melting point: 270°C (dec). FTIR (KBr wafer) $\bar{\nu}$/cm^{-1}: 3350 (N-H stretch); 2172, 2131 (conjugated nitrile stretch). UV-Vis (acetonitrile solution) λ_{max}/nm : 370. Optical rotation, $[\alpha]_D^{25}$ (c = 0.05, MeOH) : +69°. Elemental analysis : % found (% calculated for $C_{26}H_{24}N_4$): C, 79.60 (79.59); H, 6.42 (6.12); N, 13.85 (14.29). MS(EI): m/z - 392 (16), 377 (16), 222 (8), 155 (64), 141 (81), 97 (14), 70 (100).

7-[(S)-methoxymethylpyrrolidino]-7-pyrrolidino-8,8-dicyanoquino-dimethane (PMPDQ, 16)

16 was recrystallised from acetonitrile. Melting point: 290°C (dec). FTIR (KBr wafer) P/cm"[1]: 2170, 2129 (conjugated nitrile stretch); 1448 (CH_2-O-CH_3 stretch). UV-Vis (acetonitrile solution) λ_{max}/nm : 398. Optical rotation, $[\alpha]_D^{25}$ (c =0.08, $CHCl_3$) : +1687°. Elemental analysis: % found (% calculated for $C_{20}H_{24}N_4O$) - C, 71.34 (71.43); H, 7.41 (7.14); N, 16.65 (16.67). MS(EI):m/z-336(100),222(8), 181 (8), 167 (13), 71 (24).

3.4 CONCLUSION

In addition to the systems described in this Chapter, we have synthesised several more derivatives. Either they did not show any appreciable solid state SHG or were not amenable to crystal structure studies. Hence they were not of either direct or indirect interest in our investigations of materials for SHG. Hence we have not pursued their characterisations and structural studies. All the systems we have presented here were obtained by variation of the donor group alone. Keeping the simplicity of this synthetic approach the acceptor group cannot be varied, hence we have not made any attempts in that direction. However, we have considered the variation of the conjugation unit. For example, the tetracyano derivative of anthraquinone (TCNQ analogue with anthracene

instead of benzene framework) has been reported.[8] We have attempted similar reactions as above to replace two of the cyano groups by amino groups. Though the reaction appears to work, the products were invariably complex and clean samples of the push-pull anthraquinonoid system could not be isolated. However, we believe that this approach has interesting potential for future work.

REFERENCES

1. Hertler, L.R.; Hartzler, H.D.; Acker, D.S.; Benson, R.E. *J. Am. Chem. Soc.* **1962,** *84,* 3387.

2. Gomper, R.; Wagner, H.; Kutter, E. *Chem. Ber.* **1968,***101,* 4144.

3. El Seoud, O.A.; Ribeiro, F.P.; Martins, A.; Brotero, P.P. *J. Org. Chem.* **1985,** *50,* 5099.

4 Lalama, S.J.; Singer, K.D.; Garito, A.F.; Desai, K.N. *Appl. Phys. Lett.* 1981,39,940.

5. (a) Nicoud, J.-F.; Twieg, R.J. in *Nonlinear Optical Properties of Organic Molecules and Crystals;* Chemla, D.S.; Zyss, J. (Eds), Academic Press, New York, 1987, Vol.1, p. 227. (b) *Nonlinear Optical Properties of Organic Molecules and Crystals,* Chemla, D.S.; Zyss. J.(Eds), Academic Press, New York, 1987, Vol. 2, p. 221.

6. Nicoud, J.-F. *Mol. Cryst. Liq. Cryst.* **1988**, *156*, 257.

7. (a) Szablewski, M. *J. Org. Chem.* **1994,** *59,* 954. (b) Szablewski, M.; Thomas, P.R.; Thornton, A.; Bloor, D.; Cross, G.H.; Cole, J.M.; Howard, J.A.K.; Malagoli, M; Meyers, F.; Bredas, J-L.; Wenseleers, W.; Goovaerts, E. *J. Am. Chem. Soc.* **1997**, *119*, 3144.

8. Kini, A.M.; Cowan, D.O.; Gerson, F.; Mockel, R. *J. Am. Chem. Soc.* **1985**, *107*, 556.

CHAPTER 4

EXPERIMENTAL DETERMINATION OF MOLECULAR HYPERPOLARISABILITY

4.1 BACKGROUND

The popular experimental techniques to measure molecular hyperpolarisabilities are electric field induced second harmonic generation (EFISHG) and hyper Rayleigh scattering (HRS). Both techniques require coherent light sources and relatively expensive and sophisticated equipment for data collection. A simpler method to estimate the β values using the well known two-level approximation was first reported by Oudar,[1] this procedure requires only measurement of absorption spectra and estimation of the dipole moment change between the ground and the first excited state ($\Delta\mu = \mu_e - \mu_g$). Studies of excited state dipole moments which has been important in a variety of photochemical and Photophysical problems, has thus become important in the design of molecular NLO materials as well. In Sec.4.2, we present a simple procedure that we have developed for the solvatochromic determination of $\Delta\mu$ of donor-acceptor substituted organic molecules. Utilising this method we have determined the 2-level hyperpolarisabilities of several test systems based on coumarin dyes as well as push-pull diaminodicyanoquinodimethanes that we have developed. These results combined with the reported EFISHG β of the coumarins, allow us to estimate the hyperpolarisabilities of the push-pull quinonoid systems. These results are presented in Sec.4.3. We have also fabricated the set up required to carry out EFISHG studies. Measurement on a prototypical push-pull quinonoid system is presented in Sec.4.4. This study provides a verification of the estimates of β of this class of compounds that we have obtained through computations

presented in Sec.2.2 as well as simple solvatochromic methods presented in Sec.4.3.

The absorption and fluorescence studies reported here were carried out on a Perkin Elmer spectrophotometer (Model Lambda 3B) or Jasco Spectrophotometer (Model 7800) and a Hitachi spectroflourimeter (Model 3010) or Jasco spectrofluorimeter (Model FP-777) respectively. Chemicals of high purity were used directly (Kodak laser grade coumarins studied in Sec.4.3) or purified by usual recrystallisation procedures. The solvents were purified using standard protocols and the purity checked using their E_T values.

4.2 DETERMINATION OF EXCITED STATE DIPOLE MOMENTS USING A SIMPLE SOLVATOCHROMIC METHOD

Even though the more equipment-intensive methods like fluorescence polarisation, electric dichroism, Stark splitting of rotational levels and microwave conductivity are the more accurate methods for the experimental determination of excited state dipole moments, the most popular method is based on the analysis of the solvatochromism of absorption and/or fluorescence maxima. In the later procedure, based on the early experiments of Lippert and Mataga , one normally follows the variations of absorption maxima, fluorescence maxima or the Stokes shift with solvent polarity. Several formulations of this linear relation are known; the review of Koutek[9] has an

exhaustive compilation of the various equations in use. Only some of these formulations show good correlation between experimental and theoretical solvatochromic data, and when they do, it is only under optimal conditions in terms of the number and the choice of solvents. We note that, all these models utilise bulk solvent properties like dielectric constant and refractive index to represent the solvent polarity functions. Though the choice of the correct Onsager cavity radius is admittedly a serious problem, the former may further impair the efficacy of the solvatochromism method for the evaluation of excited state dipole moments.

During the course of our investigation of the molecules of interest in the design of nonlinear optical materials, we have observed that the Stokes shift data of several molecules showed excellent correlation with the popular solvent polarity measure, E_T (or equivalently, $E_T(30)$) proposed by Reichardt, and defined as :

$$E_T(30) / (\text{kcal mole}^{-1}) = 2.8591 \times 10^{-3} \ \bar{\nu} / \text{cm}^{-1}$$

$$E_T^N = \frac{E_T(Solvent) - E_T(TMS)}{E_T(Water) - E_T(TMS)}$$

where ν is the wavenumber corresponding to the absorption peak of an N-phenoxide betaine dye in the relevant solvent and TMS is tetramethylsilane. Though such correlations have been noted previously,[11] no detailed analysis has been reported. In this Section we first delineate the theoretical basis for the correlation of solvatochromic

Stokes shift data with the E_T^N parameter. The expressions derived, facilitate the direct determination of the change in dipole moment on excitation. Subsequently we present an appraisal of the quality of the excited state dipole moments derived from these correlations and the relevance of this approach from an experimental point of view in terms of the use of mixed solvents. The efficacy of the whole procedure is demonstrated by a detailed study of the $\Delta\mu$ of N,N-dimethylaminobenzonitrile (DMABN) a system that has attracted a lot of attention in connection with the interesting phenomenon of dual fluorescence.

Following the formulation of Koutek,[9] the linear relation between the Stokes shift of a molecule (m) in solvent (s) represented by Y(m,s) and the solvent polarity function, X(s) is given by,

$$Y(m,s) = B(m)X(s) + Y(m,g) \qquad (4.1)$$

where B(m) is the regression coefficient and is related to Au. We take Y(m,s) as (ν_a- ν_f) (ν_a = wavenumber of absorption, ν_f - wavenumber of fluorescence; one of these may be solvent independent in some cases) and Y (m,g) is a constant independent of the solvent, sometimes related to the gas phase properties of the compound. B(m), the regression coefficient and a commonly used X(s) are given by,

$$B(m) = \frac{2(\Delta\mu)^2}{hca^3} \qquad \textbf{(4.2)}$$

$$X(s) = \left[\frac{(D-1)}{(D+2)} - \frac{(n^2-1)}{(n^2+2)}\right]\left[\frac{(2n^2+1)}{(n^2+2)}\right] \qquad (4.3)$$

where $\Delta\mu = \mu_e - \mu_g$, h is the Planck's constant, c, the velocity of light, D and n the dielectric constant and refractive index of the solvent respectively and a, the Onsager radius of the solute molecule. If now we consider, X(s) = E_T , the B(m) can be obtained as described below.

Consider the application of Eqn.4.1 to the solvatochromic absorption data of the pyridinium N-phenoxide betaine dye proposed originally by Reichardt *et al.* as a measure of the solvent polarity and which has now become the basis of the $E_T(30)$ scale. The dye is not at all fluorescent, and hence one can only follow the shift of absorption maximum with change in solvent polarity. Since the μ_e (= 6 D) of the dye is considerably smaller than μ_g (= 15 D), we can make the safe assumption that, the solvatochromic shift of the fluorescence peak, if any, will be negligible compared to the shift of the absorption peak. Hence, Y(m,s) = ν_a - constant. Therefore, we can rewrite Eqn.4.1 for the Stokes shifts of the dye, using the common formulation of B(m) (Eqn.4.2), but without specifying the nature of X(s) as,

$$\bar{\nu}_a = \left[\frac{2(\mu_D)^2}{hca_D^3}\right]X(s) + Y(m,g) \qquad (4.4)$$

where $\Delta\mu$ = 9 D, the change in dipole moment on excitation of the dye and a_D is its Onsager radius. Y(m,g) is a modified constant. Using the definition of $E_T(30)$ in terms of ν_a, Eqn.4.4 can be transformed to,

$$X(s) = 349\left[\frac{hca_D^3}{2(\Delta\mu_D)^2}\right]E_T(30) + Y'(m,g) \qquad \textbf{(4.5)}$$

To avoid dimensionality problems, the normalised value of $E_T(30)$, namely E_T may be employed, so that,

$$X(s) = 11307.6\left[\frac{hca_D^3}{2(\Delta\mu_D)^2}\right]E_T^N + Y''(m,g) \qquad (4.6)$$

This treatment of solvatochromism of the dye, has thus led to an expression for X(s) which may be substituted back into Eqn.4.1, so that we arrive at the following working expression,

$$Y(m,s)/cm^{-1} = 11307.6\left(\frac{\Delta\mu}{\Delta\mu_D}\right)^2\left(\frac{a_D}{a}\right)^3 E_T^N + Y^*(m,g) \qquad \textbf{(4.7)}$$

Eqn.4.7 clearly illustrates that the Stokes shifts will have a linear dependence on the E_T^N values of the solvent. It also shows that, $\Delta\mu$ of the molecules of interest can be extracted from the slopes if a standard value for $\Delta\mu_D$ and a_D are available, and an estimate of a for the solute is known. It is also significant to note that since a ratio of a/a_D is involved, errors involved in the estimation of Onsager radius may be obviated to some extent.

We have analysed the solvatochromic changes of Stokes shifts of several molecules from reported data and our own experiments in terms of a variety of solvent polarity functions. Table 4.1 provides the

correlation coefficients for several systems for the following solvent functions, X(s): (i) the E_T^N values, (ii) the function, $F_2(D,n)$ recommended by Koutek[9] on the basis of a detailed statistical analysis of sixteen different model equations and (iii) the functions used in the original papers dealing with the solvatochromic studies on these molecules. In the statistical analysis, we have excluded those solvents which may have specific local interactions with the probe molecules.

Table 4.1: *Correlation coefficients for the fit of the Stokes shifts with the solvent polarity functions E_T^N,$F_2(D,n)$ and $F_x(D,n)$ for different compounds. N is the number of solvents used in each case*

Compound	E_T^N	$F_2(D,n)$	$F_x(D,n)$	N[b]	Ref.
4-(dimethylamino)-4'-nitrostilbene	0.984	0.843	0.852	13	12
hexamethylbenzene-tetrchloro-phthalic anhydride (CT complex)	0.925	0.784	0.790	8	12
4-amino-4'-nitrostilbene	0.968	0.921	0.919	14	13
1-dicyanovinylnaphthalene	0.904	0.815	0.774	8	14a
9-dicyanovinylphenanthrene	0.861	0.746	0.705	8	14a
9-dicyanovinylanthracene	0.674	0.703	0.696	8	14a
1-dicyanovinylpyrene	0.935	0.863	0.818	8	14a
6-propionyl(dimethylamino) naphthalene	0.965	0.943	0.933	8	14b
4-(dimethylamino)phthalimide	0.895	0.840	0.826	11	14b
4-aminophthalimide	0.977	0.970	0.962	8	14b

It is seen that, the Stokes shift data correlates a lot better with the E_T values of the solvent, rather than the other bulk solvent polarity functions used by the original authors or the one recommended by Koutek. An example is illustrated graphically in Fig.4.1 which compares the plots of experimental Stokes shifts of 4-dimethylamino-4'-nitrostilbene (DNS) versus those estimated using E_T^N values as well as the $F_2(D,n)$ function.

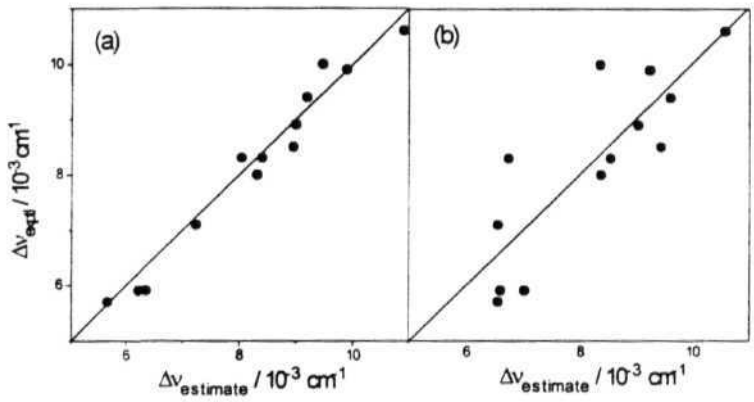

Figure 4.1: *Plots of experimental Stokes shift data of DSS versus the Stokes shifts estimated from the fit of the experimental values against the solvent polarity measures: (a) E_T^N and (b) $F_2(D,n)$*

Now we turn to the question of extracting the excited state dipole moments from the slopes obtained in the Stokes shift versus E_T^N plots. These experiments yield directly, the $\Delta\mu$ values. Hence, the μ_e values can be estimated provided the ground state dipole moments are already known. We have used the ground state dipole moments obtained from literature. From Eqn.4.7 it is clear that the quality of $\Delta\mu$ obtained will

depend on the accuracy of the Onsager radius for the molecule and the dye. As is well known, choice of the Onsager radius is a difficult problem in any solvatochromic method and this remains so in our procedure as well. However as noted earlier, partial amelioration of this problem occurs in our procedure since ratios of two Onsager radii are being used. We compare μ_e obtained from the present analysis with the previous estimates for several molecules in Table 4.2. The Onsager radius used for each molecule was taken from the original literature. The value of a_D was determined through a least square fit analysis of the experimental values of $\Delta\mu$ of the molecules, presented in Table 4.2 (electrooptical measurements, where available, and previous solvatochromic data) against that calculated using the slope from Eqn.4.7. 4-(dimethylamino)benzonitrile (DMABN) was not included in this statistical analysis, and its $\Delta\mu$ given in Table 4.2 is the one predicted by our procedure as discussed below. The value obtained for a_D, *6.2k* (r = 0.977) is intuitively meaningful, since it agrees fairly well with the separation of the centres of maximum charge, namely the N and O atoms in the dye (5.8A from a molecular mechanics optimisation). We note here, that even though the original betaine dye as well as its t-butyl substituted derivative have been used to prepare the $E_T(30)$ scale, since the strong dipole associated with the pyridinium N-phenoxide group is unaffected by the substitution, we assume a single Onsager radius and the excellence of the correlation bears out the validity of this assumption. Table 4.2 shows that the comparison of the μ_e from previous literature and from the present analysis, using Eqn.4.7 and a_D = 6.2A is good. Since the spread in μ_e from different experiments is very large,

Table 4.2: *Comparison of μ_e obtained from the present analysis with previous reported values for the following compounds : 4-(dimethyl-amino)-4 '-nitrostilbene (A), hexamethylbenzene-tetrachlorophthalic anhydride (CT complex) (B), 4-amino-4 '-nitrostilbene (C), 4-amino-phthalimide (D), 1-dicyanovinylnaphthalene (E), 9-dicyanovinyl-phenanthrene (F), 9-dicyanovinylanthracene (G), 1-dicyanovinylpyrene (H), 4-(dimethylamino)benzonitrile (I) (†based on the present analysis of the data in Ref 23 using the propionitrile-octane mixed solvent system)*

	a (Å)	μ_g (D)	μ_e(D)		
			Solvatochromic Methods		Other Methods (Ref)
			Present Work	Previous Work (Ref)	
A	8.0	7.6	23.3	25.0 (12) 32.0 (16)	21.9 (3) 23.0 (4)
B	4.5	3.6	10.5	9.6 (12) 14.0 (16)	10.0 (3)
C	7.2	6.5	20.0	21.0 (13)	21.0 (17) 22.0 (18)
D	3.5	3.5	5.8	6.7 (19)	9 ± 1 (20)
E	3.7	4.7	8.6	7.9 (14a)	-
F	4.4	4.7	10.3	9.8 (14a)	-
G	4.0	4.3	7.4	7.0 (14a)	-
H	4.7	4.8	9.9	10.8 (14a)	-
I	5.0	6.6	12.3 13.0†	16.1 (9)	13 ± 2 (21a) 12.5 (21b) 13.0 (22)

we suggest that the value we obtain here from the analysis which shows excellent correlation of experimental data should be treated as one of the most reliable.

A further test of the above result is provided by an independent study, we carried out on the molecule, DMABN. This experiment was designed to test two aspects of the present analysis. First we wanted to check the ability of this procedure to predict excited state dipole moments, which in turn tests the meaningfulness of the slope of the linear regression as well as the choice of the Onsager radius for the dye. Secondly, we wanted to explore the practical utility of the method in terms of using mixed solvents. From the experimental point of view, solvatochromism studies often become difficult, if the molecule of interest has acceptable solubility only in a very limited number of solvents. The statistical analysis becomes less reliable when the number of data points are few. When mixed solvents are used to overcome this problem, traditional solvent polarity functions have to be obtained either through detailed experiments on each mixture to determine its dielectric constants, refractive index *etc*., or these values have to be approximated from empirical rules. Further, for some pairs of solvents these functions may not be very sensitive to small changes in composition. E_T on the other hand is very sensitive to composition changes and can be easily measured experimentally using the absorption of the betaine dye. It may also be noted that extra precautions to purify the solvents can be relaxed, since the solvent polarity function is being experimentally determined and used. Of course, impurities that may cause undesirable specific

interactions with the probe molecule should be excluded; also high percentages of solvents with specific interactions may be undesirable.

We have studied the Stokes shift data of DMABN in benzene - acetonitrile mixtures of several compositions. Due to specific π-interactions, nonlinearities arise at high percentages of benzene. Hence we have excluded compositions of < 10% acetonitrile. The E_T values of these compositions were determined separately and are presented in Table 4.3. The solvatochromism of the twisted intramolecular charge transfer (TICT)[24] emission of DMABN was studied in these mixed solvents and the results are plotted against the E_T values in Fig.4.2. The linearity of the plot is excellent (r = 0.995). The intramolecular (ICT) and TICT emissions of DMABN do overlap slightly. However for the solvent compositions we have used, standard deconvolution procedures indicate that the λ_{max} of the TICT emission is unaffected by

Table 4.3: *E_T^N values measured for benzene-acetonitrile mixtures of different compositions*

vol% of acetonitrile	E_T^N	vol% of acetonitrile	E_T^N
20	0.286	70	0.397
30	0.312	80	0.410
40	0.349	90	0.420
50	0.360	100	0.454
60	0.379		

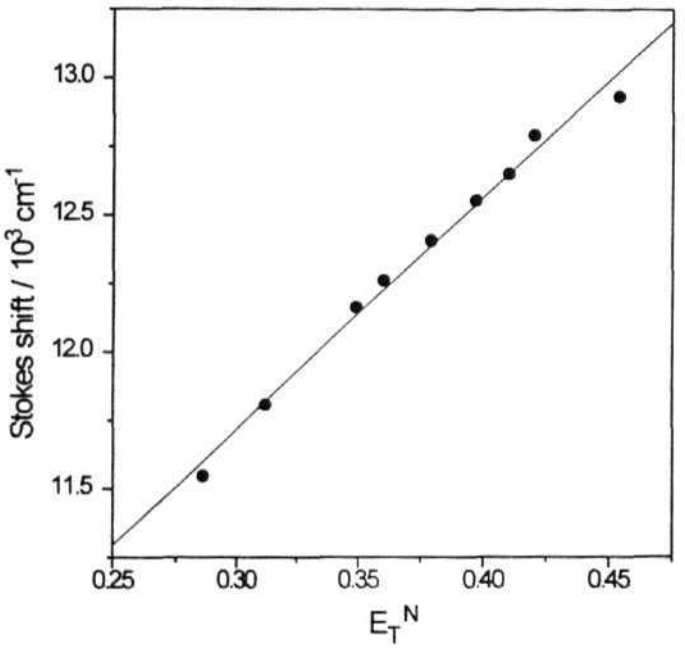

Figure 4.2: *Plot of Stokes shifts of DMABN versus E_T^N value of the solvent mixtures. The straight line represents the least-square fit*

the ICT emission band. This confirms that we are following the emission from the pure TICT state. The μ_e evaluated from the slope of the plot is compared in the last row of Table 4.2, with the values from other studies. The agreement is again quite good.

Thus we find that the solvatochromic procedure we have developed for the estimation of dipole moment changes on excitation is a

practically convenient method which also affords excellent correlation of experimental data with theoretical formulations.

4.3 ESTIMATION OF HYPERPOLARISABILITIES USING EXTRAPOLATION FROM THE TWO-LEVEL MODEL

We have discussed in the previous Section a simple solvatochromic procedure for the determination of $\Delta\mu$ of organic molecules. The change in dipole moment on excitation together with electronic absorption data, provides a ready access to the estimation of the 2-level hyperpolarisability of molecules of interest in NLO studies. Harris and coworkers[25] and Qin *et al*[26] have demonstrated that the β's of various organic molecules determined using this simple technique compared very well with the results from other methods. They have made a case for the utilisation of this simple method in routine work on NLO systems. In this Section, we present our experimental determination of the two-level hyperpolarisabilities, β_{2level} of several diamino substituted dicyanoquinodimethane molecules (Fig.2.1) using the solvatochromic determination of $\Delta\mu$ developed in the previous Section; as we noted earlier, β_{2level} mav also be referred to as β_{ct}, to highlight the fact that the only excited state considered for the evaluation of hyperpolarisability is the intramolecular charge transfer (CT) state.

We have next carried out the following novel exercise to estimate the actual hyperpolarisability, p of these molecules by extrapolation of their β_{2level} values. A set of coumarin dye molecules (**C102, C151,**

C152, and C153; see Fig. 4.3) widely used as laser dyes was chosen and their β_{2level} was determined as above. Their hyperpolarisabilites, β have been reported recently using EFISHG experiments.[27] The theoretical

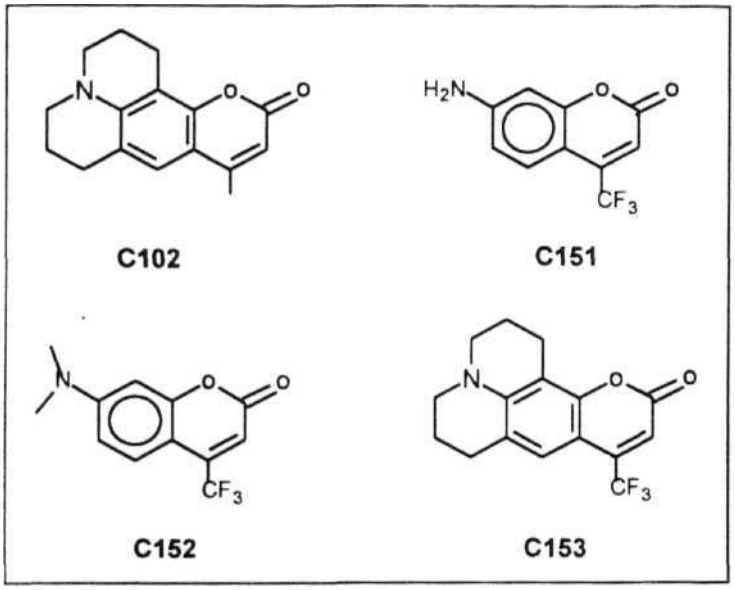

Figure 4.3: *Molecular structures of the coumarins considered in this study*

hyperpolarisability, β and the 2-level approximation to it, β_{2level} for the quinonoid systems and the coumarins were estimated by computational methods. This allowed us to obtain a scaling between the β_2 and β in these systems. With the additional information on the EFISHG determined β values of the coumarins, we are able to make semiquantitative predictions for the actual hyperpolarisabilities of the push-pull quinonoid systems.

From Eqn. 1.16 it is seen that we need to measure (i) the energy gap AE, (ii) the oscillator strength, f and (iii) the dipole moment change, $\Delta\mu$ for the lowest excitation (charge transfer excitation) to estimate experimentally, the β_{2level}. The AE and f were determined from the electronic absorption spectra. The absorption band shape is very close to Gaussian for all the molecules. The energy of the transition, AE was taken as the maximum of the UV-Vis absorption band (λ_{max}). The oscillator strength, f of the transition was determined from the area under the band by means of Eqn.4.8.

$$\mathcal{A} = \int \varepsilon(\nu)\, d\nu$$

$$f = 1.44 \times 10^{-19} \times \mathcal{A}\ (M^{-1}\ cm^{-1}\ sec^{-1}) \qquad \textbf{(4.8)}$$

$\mathcal{A}$ is the integral absorption coefficient, e(v) is the molar extinction coefficient at frequency, v (v(Hz) = AE / hc) and the integral is over the entire absorption band. The extinction coefficient ε_{max} (at λ_{max}) and the integral absorption coefficient, $\mathcal{A}$ (from which the oscillator strength was calculated) for the molecules 8, 9, 11, 12, 14 and 16 and the coumarin dyes are presented in Table 4.4.

The $\Delta\mu$ were determined using the solvatochromic method described in Sec.4.2 using benzene-acetonitrile mixtures of typically about nine compositions. Fig. 4.4 shows the plot of the Stokes shifts *vs*

Table 4.4: *Extinction coefficient at maximum absorption (ε_{max}) and integral absorption coefficient ($\mathcal{A}$) measured for molecules 8, 9,* ***11,*** *12,* ***14, 16*** *(Fig. 2.1) and the coumarm dyes* ***C102, C151, C152, C153*** *(Fig. 4.3)*

Molecule	ε_{max} / $M^{-1}cm^{-1}$	$\mathcal{A}/10^{15}$ $M^{-1}cm^{-1}s^{-1}$
8	18436	2674
9	26987	2922
11	24612	3212
12	23142	2619
14	15012	2690
16	23856	2905
C102	25117	3074
C151	23014	3325
C152	22401	3074
C153	33470	4304

the E_T^N polarity parameter at compositions ranging from 20% to 100% of acetonitrile for the molecule 12; the correlation is found to be good (r - 0.946). Similar correlations were obtained for the other molecules as **well.** The $\Delta\mu$'s **of** the quinonoid molecules are large and negative and indicates a benzenoid zwitterionic ground state going over to a quinonoid excited state. The Au's of the coumarins are small and positive and are associated with an intramolecular charge transfer. The AE, f, Au determined as described above for the coumarin dyes and for the molecules, 8, **9, 11, 12, 14** and 16 are collected in Tables 4.5 and 4.6

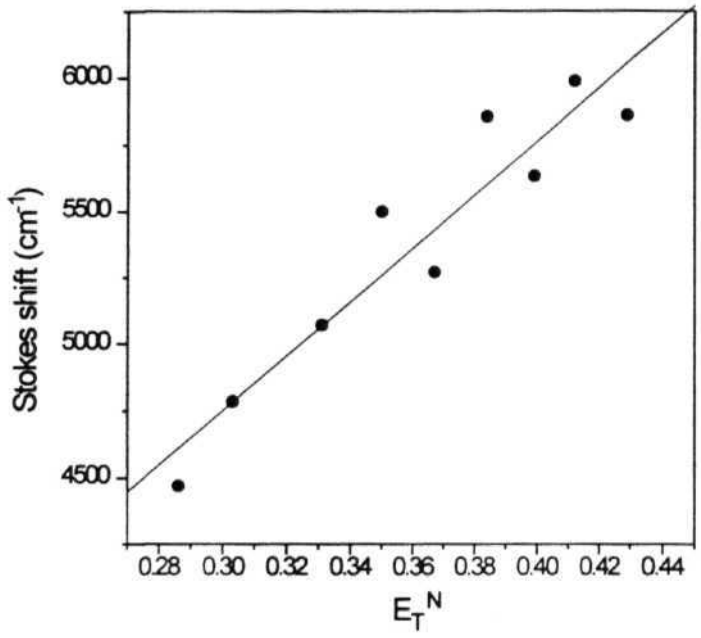

Figure 4.4: *Plot of Stokes shift vs E_T^N in benzene-acetonitrile mixtures of nine different compositions for molecule 12. The line is obtained from least square fitting*

respectively. These tables also provide the computed values of hyperpolarisabilities. We have used the AM1 optimised geometries for the coumarin dyes and crystal structure geometries for the quinonoid molecules in the computations. The AE, f and $\Delta\mu$ for the lowest excitation, required to estimate β_2 were calculated using the AM1 method[29] (MOPAC93)[30] invoking a configuration interaction (CI) scheme involving all single and pair excitations within a manifold of 10 molecular orbitals (5 HOMO's and 5 LUMO's). Since the 2-level approximation as well as EFISHG measurements relate to the strongest

Table 4.5: *The experimental energy (AE), the dipole moment change ($\Delta\mu$) and the oscillator strength (f) for the lowest excitation, the experimental and the theoretical two-level hyperpolarisability (β_{2level}) and ft from EFISHG (from Ref. 2 7) and from semiempirical computation, for the coumarin dyes C102,* ***C151, C152*** *and* ***C153*** *(Fig.4.3); all pare at $\hbar\omega$ = 0 eV and are in units of 10^{-30} esu.*

Molecule	ΔE (eV)	Δμ (D)	f	β_{2level} (exp)	β (exp)	β_{2level} (calc)	β (calc)
C102	3.24	2.11	0.443	4.5	12.4	1.3	6.0
C151	3.38	1.58	0.479	3.2	9.0	1.3	5.0
C152	3.15	2.16	0.443	5.0	10.6	2.2	8.3
C153	2.95	2.22	0.620	8.8	15.8	2.4	9.4

component of the p along the dipole vector direction (by convention chosen as x) we have computed the component, β_x (defined in Sec.2.2).

In Table 4.5 it is seen that the experimental β_{2level} are approximately 3 - 4 times that of the computed β_{2level} values. In the case of β, this ratio is roughly about 1.5 to 2. In Table 4.6, we find that the experimental β_{2level} is again 1.5 to 2 times larger than the theoretical β_{2level}. This trend of higher values of experimental β with respect to theoretical values is in accordance with the earlier reports.[31] This overestimation in the experimental values could be due to the effect of solvent dielectric environment and local field factors on β. [32]

Table 4.6: *The experimental energy (AE), the dipole moment change ($\Delta\mu$) and the oscillator strength (f) for the lowest excitation, the experimental and theoretical two-level hyperpolarisability, ft?level and β from semiempirical computation, for the molecules 8, 9, 11, 12, 14* and *16 (Fig.2.1); all flare at $\hbar\omega$ = 0 eV and in units of 10^{-30} esu.*

Molecule	ΔE (eV)	Δμ (D)	f	β_{2level} (exp)	β_{2level} (calc)	β (calc)
8	2.99	-9.4	0.385	-22.1	-11.5	-52.6
9	2.74	-8.2	0.421	-27.4	-13.5	-54.9
11	2.69	-8.1	0.462	-31.4	-11.7	-54.3
12	2.86	-9.5	0.377	-25.1	-16.9	-50.2
14	3.12	-10.0	0.387	-20.8	-14.7	-51.0
16	2.89	-8.7	0.418	-24.6	-14.5	-51.4

What is more pertinent here is the comparison of β_{2level} values to the β values, either from experiment or from theory. In Table 4.5, it seen that the theoretical β to β_{2level} ratio is about 4, and the experimental p to β_{2level} ratio is roughly 2 - 3. For the quinonoid molecules the theoretical P to β_{2level} ratio is again about 4 (Table 4.6) consistent with the case of coumarins. Significantly, these observations allow us to make an estimate of the experimental (EFISHG) hyperpolarisabilities expected for the quinonoid systems. Based on the transferability of the β_{2level} / P ratios between coumarins and the quinonoids, the EFISHG p values of the quinonoids would be expected to be 2 - 3 times their experimental β_{2level} values *ie.* about -50 to -60 x 10^{-30} esu (at $\hbar\omega$ = 0 eV).

The present analysis again shows that the push-pull quinonoid systems have potentially large β values as seen from the 2-level approximation, theoretical estimates or the projected EFISHG values. They are inherently negative values, which is consistent with the negative solvatochromism arising from the decrease in the dipole moment on excitation. The static (3 (or β_{2level}) values in these molecules are very similar irrespective of the donor groups. From the computed values of β (Sec.2.2) as well as the experimental 2-level estimates and the projected values obtained above for the push-pull quinonoid systems, it is clear that these molecules possess nearly similar hyperpolarisabilities irrespective of the donor groups. This is understandable in view of the similar NLO active chromophoric group they possess. Thus we have carried out in the following Section, an EFISHG study of a representative push-pull quinonoid molecule to check the veracity of the results obtained in the present analysis.

The investigations presented in this Section show that the simple solvatochromic method of estimating 2-level hyperpolarisabilities can be a convenient procedure to screen molecules for NLO applications. The experimental requirements are trivial compared to the EFISHG or even HRS techniques. When combined with computational studies and data on other systems for the purpose of calibration, this method can have very useful predictive value.

4.4 DETERMINATION OF HYPERPOLARISABILITY USING EFISHG TECHNIQUE

The semiemipirical quantum chemical studies presented in Chapter 2 and the experimental studies based on the solvatochromic measurements presented in the previous Section show that the push-pull quinonoid systems possess fairly large molecular hyperpolarisabilities which makes them interesting candidates for the fabrication of NLO materials. To confirm these results we have determined the β's of a representative system, 9 using the electric field induced second harmonic generation (EFISHG) technique. In this Section we present the basic concepts involved in the experiment and the details of the setup we have fabricated. We describe the simple and convenient cell design we have developed for the EFISHG experiment. Experimental details and analysis of the data involved in the determination of β are also described. The theoretical background of the EFISHG is already described in Sec. 1.6.

The experimental setup is shown in Fig.4.5. The source of the fundamental beam is a Q-switched Nd:YAG laser (Continuum, Model 660B-10) operating at 1.064 μm with pulse width of 6 ns and repetition rate of 10 Hz. The beam is split and filtered (to remove green light at 532 nm). One portion is focused on to the sample cell and the other on to a reference solid sample (usually urea or one of our compounds, DMPDQ which shows strong solid state SHG) to monitor the pulse-to-pulse fluctuations of I_ω. A high voltage pulse (100 μs wide) of upto 5 kV (from a Velonex Model 345 High Voltage Pulser), synchronised with

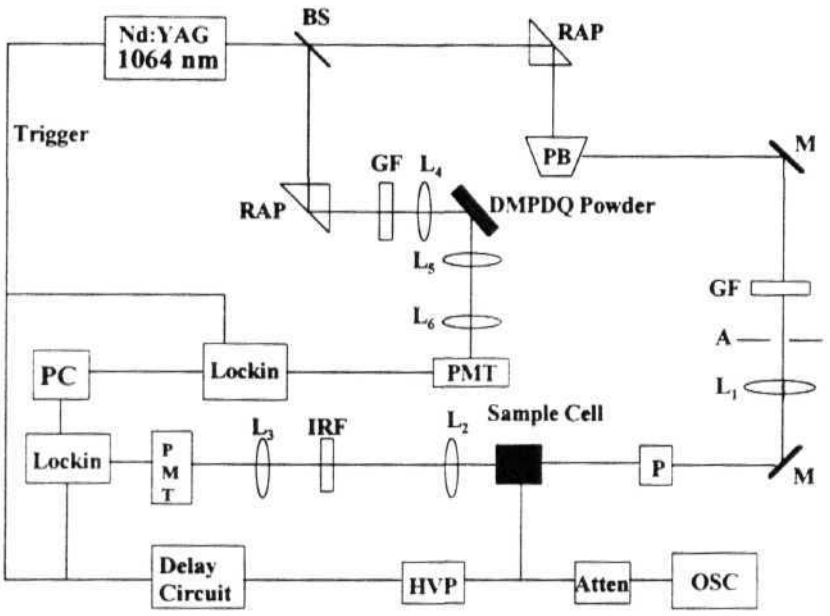

Figure 4.5: *Experimental setup for EFISHG measurements. (BS, beam splitter; RAP, right angle prism; PB, Pellin-Broca prism; M mirror; GF, interference filter for 532 nm; IRF, interference filter for 1 064 nm; A, aperture; L, lense; P, polariser; HVP, high voltage pulser; PMT, photomultiplier tube)*

the laser pulse using a delay circuit, is applied across the electrodes in the sample cell. The second harmonic light generated is filtered (to remove the ir), collected and analysed using appropriate optics (high gain photomultiplier tube (Hamamatsu) and an oscilloscope (Tektronix, 2465B, 400 MHz) or lock-in amplifier (SRS, Model SR830) were used together with a personal computer.

The sample cell used for the experiment is shown in Fig.4.6(a). The cross sectional view is shown in Fig.4.6(b). Two polished BK-7 glass plates, SG (one straight and one wedge-shaped) of thickness 2.5 mm are held tightly between optically polished stainless steel electrodes, SS, so that the spacing between electrodes is maintained as 2.5 mm and the empty space between the glass plates is 2 mm at the bottom and 1 mm at the top. The edges of the electrodes were given a gentle smoothening to avoid charge accumulation. Further protection against discharge was provided by thin glass plates, PG, placed on the sides of

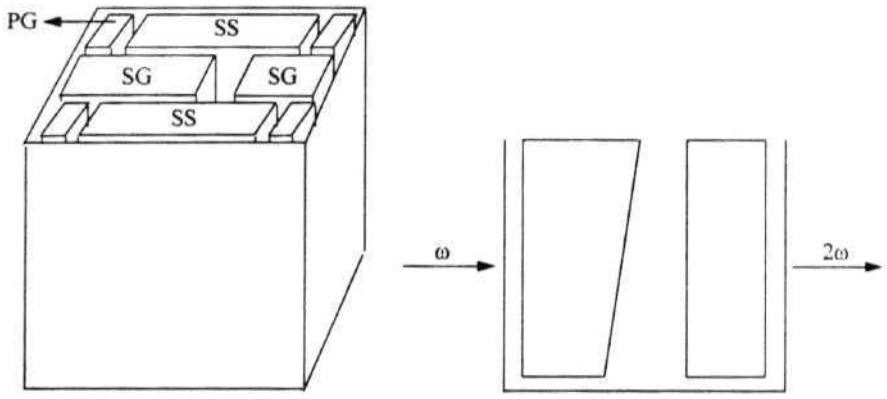

Figure 4.6: *(a) Schematic diagram of the sample cell used in the EFISHG experiment (SS : stainless steel electrode, SG : spacer glass plate, PG : protector glass plate) (b) cross-sectional view of the cell*

the electrodes. The whole assembly of glass plates and electrodes is placed in a 1 x 1 x 4.5 cm glass cuvette.

The cell assembly is mounted on a platform which could be translated vertically using microprocessor controlled motors. The wedge shaped glass spacers allow the path length of the beam in the solution to be varied from 1 mm to 2 mm. The interface with the personal computer allows easy recording of the $I_{2\omega}$ data as a function of the cell translation to produce the Maker fringe pattern.[33]

Dimethylsulphoxide (DMSO) was used as the solvent in the experiments as well as the reference to normalise the SHG intensity from the sample. The Maker fringe pattern of $I_{2\omega}/I_{\omega}$ recorded for the molecule, 9, is shown in Fig.4.7. The spacing between the two maxima on the fringe pattern is the coherence length, l_c (defined as $\lambda/4(n_{2\omega}-n_{\omega})$ where n_{ω} and $n_{2\omega}$ are the refractive indices at the fundamental and second harmonic frequencies). This data was analysed using a least square fit to the function

$$\frac{I_{2\omega}}{I_{\omega}} = A_1 \sin^2\left(\frac{\pi d}{2A_3} + A_4\right) + A_2 \qquad (4.9)$$

The fitting parameters A_3 is related to l_c, A_4 is a phase correction factor and A_1 and A_2 together define the amplitude of the second harmonic generation as follows :

$$A^{2\omega} = \frac{A_1}{2} + A_2$$

The amplitudes of the SHG obtained for the solution is denoted as $A_s^{2\omega}$ and that for the pure solvent (DMSO) as $A_l^{2\omega}$. Since the absorption of

the compound at 2© is negligible (e = 1.0 $M^{-1}cm^{-1}$) the ratio of these amplitudes can be directly related to the macroscopic susceptibilities as given below.

$$\frac{A_s^{2\omega}}{A_l^{2\omega}} = \left(\frac{\chi_s}{\chi_l}\right)^2 \qquad \text{(s = solution, l = solvent)} \qquad (4.10)$$

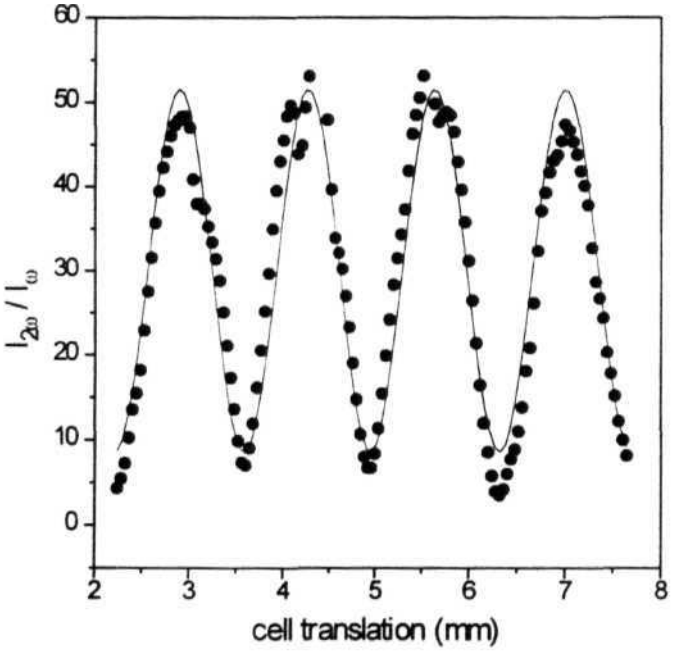

Figure 4.7: *Maker fringe pattern recorded for 9 at a concentration of 2 x 10-3 Min DMSO (solid line shows the fitting to Eqn. 4.9)*

From Eqn. 1.22, we can write,

$$\chi = \frac{NE_0 f\mu\beta}{5kT} \qquad \textbf{(4.11)}$$

Combining 4.10 and 4.11, and assuming that the local field factors for the solvent and solution are same, we obtain,

$$\left(\frac{A_s^{2\omega}}{A_l^{2\omega}}\right)^{1/2} = \frac{\chi_l + \chi_{solute}}{\chi_l}$$

$$= 1 + \frac{N_{solute}\mu_{solute}\beta_{solute}}{N_l\mu_l\beta_l}$$

$$= 1 + \frac{N_A\mu_{solute}\beta_{solute}}{N_l\mu_l\beta_l}c \qquad (4.12)$$

where N_A is the Avogadro number, c is the concentration of the solute in mols/litre, N_l is the number density (molecules per litre) of the solvent and β and μ are the hyperpolarisability and ground state dipole moment. We have measured the amplitudes A_s^{ω} at various concentrations in the range 0.8 x 10^{-3} to 4 x 10^{-3} M of the sample and plotted the square root of the ratio of the amplitudes in Eqn.4.12 *vs* c. From the slope of this plot and using the reported experimental values of μ_{DMSO} (4 D)[35] and β_{DMSO} (-007 x 10^{-30} esu)[35] and the calculated (AM1) value of μ_{solute} (15 D), the β of the solute was determined to be (-72 ± 15) x 10^{-30} esu. This β is the hyperpolarisabiltiy at 1064 nm excitation. Using the simple two state model[1] one can estimate the static hyperpolarisability, $\beta(0)$ as follows:

$$\beta(0) = \beta(\omega)\left(1 - \frac{\lambda_{max}^2}{\lambda^2}\right)\left(1 - 4\frac{\lambda_{max}^2}{\lambda^2}\right) \qquad \textbf{(4.13)}$$

where λ and λ_{max} are the exciting wavelengths and the wavelength of maximum absorption for the compound. Using the λ_{max} of 9 (415 nm), the (5(0) is found to be -24 x 10^{-} esu. From AM1 computations we have found that the p(0) is -19.8 x 10^{-30} esu for the AM1 optimised geometry (Table 2.1) and -54.9 x 10* esu for the molecular geometry from crystal structure analysis (Table 2.6); as pointed out earlier, the crystal structure molecular geometries are more benzenoid than the gas phase optimised structures and have larger β values. Thus we find that the experimentally determined static hyperpolarisability is in very good agreement with the value calculated for the gas phase structure. This is as expected since the solution structure would resemble more closely the gas phase structure rather than the molecular structure in the crystal.

4.5 CONCLUSION

In this Chapter, we have shown that, the use of E_T' as the solvent polarity function for solvatochromism studies of Stokes shifts can be an efficient procedure to determine excited state dipole moments of organic molecules. The high degree of correlation obtained, points to the efficacy of E_T^N as a descriptor of the microscopic environment of the molecular dipoles in solution. The reformulation of earlier equations which relate absorption and/or fluorescence solvatochromism with solvent polarity function, in terms of E_T^N values reveals the basis for the good correlation and provides a simple expression for the gradient of A ν versus E_T^N plots, from which μ_e can be determined. The ability of the method to employ mixed solvents for solvatochromism studies and to

ultimately determine two-level hyperpolarisabilities of organic molecules is expected to be of considerable practical utility.

The comparison of β_{2level} to P from theory and experiment on a set of coumarin dyes and similar comparisons in the quinonoid systems has enabled us to estimate the experimental molecular β's of several representative members of the new class of the push-pull quinonoid systems. The EFISHG experiment on a typical member of this class is consistent with the theoretical and experimental analysis we have carried out on the hyperpolarisability of these novel NLO molecules. All the results indicate that these molecules have potentially large P's. Since our primary goal in this thesis work is to develop a new class of quadratic NLO materials, we have not spent further effort on studies such as EFISHG determination of molecular hyperpolarisabilities. We have concentrated more on the solid state aspects, as discussed in the next two Chapters.

REFERENCES

1. Oudar, J.L. *J. Chem. Phys.* ***1971,*** *67,*446.
2. *Nonlinear Optical Properties of Organic Molecules and Crystals,* Chemla, D.S.; Zyss, J. (Eds), Academic Press, New York, 1987, Vols.l and 2.
3. Czekalla, J. Z *Electrochem.* **1960,** *64,* 1221.
4. Czekalla, J. *Chimia.* **1961,***15,* 26.
5. (a) Lombardi, J.R. *J. Chem. Phys.* **1969,** *50,* 3780. (b) Lombardi, J.R. *J. Am. Chem. Soc.* **1970,** *92,* 1831.
6. Haas, M.P.; Warman, J.M. *Chem. Phys.* **1982,** *73,* 35.
7. Lippert, E. Z *Naturforsch.* **1955,** *Wa,* 541.
8. Mataga, N.; Kaifu,Y.; Koizumi, M. *Bull. Chem. Soc. Jap.* 1956, *29,* 465.
9. Koutek, B. *Coll. Czeck. Chem. Commun.* **1978,** *43,* 2368.
10. Reichardt,C. *Solvents and Solvent Effects in Organic Chemistry,* VCH, Weinheim, 1988.
11. (a) Cox, G.C.; Hauptman, P.J.; Turro, N. J. *Photochem. Photobio.* **1984,** *39,* 597. (b) Nagarajan,V.; Brearly, A.M.; Kang, T.; Barbara, P.F. *J. Chem Phys.* **1987,** *86,* 3183.
12. Bilot, v.L.; Kawaski, A. Z *Naturforsch.* **1962**, *17a*, 621.
13. Bartoszewicz, B.; Kawaski, A. *Bull. Acad. Pol. Sci. Ser.* **1971,** *19,* 249.
14. (a) Katritzky, A.R.; Zhu, D.; Schanze, K.S. *J. Phys. Chem.* **1991,** *95,* 5737. (b) Soujanya, T. *Ph.D. Dissertation,* University of Hyderabad, 1996.

15. (a) Dimorth, K.; Reichardt, C; Siepman,T.; Bohlman, F. *Liebigs. Ann. Chem.* **1963,** 7, 661. (b) Reichardt, C; Harbusch-Gornert,E. *Liebigs. Ann. Chem.* **1983,** 721. (c) Spange, S.; Lanterboch, M.; Gyra, A.K.; Reichardt, C. *Liebigs. Ann. Chem.* **1991,** 323.
16. Lippert, E. Z *Electrochem.* 1957, *61,* 962.
17. Weber,G. *J. Chem. Phys.* 1965, *43,* 521.
18. Labhart, H. *Optische Anergung Organischer Systeme*, Verlag Chemie, Gmbh, 1966, S.160.
19. Suppan, P. *J. Chem. Soc. Faraday Trans.* **1987**, *183*, 495.
20. Hagan,T.;Pilloud, D.; Suppan, P. *Chem. Phys. Lett.* **1987**, *139*, 499.
21. (a) Czekalla, J.; Liptay, W.; Meyer, K.O. *Ber. Bunsenges. Phys. Chem.* **1963,** *67,* 465. (b) Labhart, H. *Adv. Chem. Phys.* **1967**, *13*, 179.
22. Jonker, S.A.; Warman, J.M. *Chem. Phys. Lett.* **1991**, *183*, 36.
23. Nag, A.; Kundu, T.; Bhattacharya, K. *Chem. Phys. Lett.* **1989,** *160,* 257.
24. Rettig, W. *Ang. Chem. Int. Edn. Engl.* **1986,** *25,* 971.
25. Paley, M.S.; Harris, J.M.; Looser, H.; Baumert, J.C.; Bjorklund, G.C.; Jundt, D.; Twieg, R.J. *J.Org. Chem.* **1989,** *54*, 3774.
26 Qin, J.; Wu, X.; Zhang, X.; Zhan, C; Liu, D. *Syn. Met.* **1995,** *71,* 1711.
27. Moylan, C.R. *J. Phys. Chem.* **1994,** *98,* 13513.
28. Atkins, P.W. *Physical Chemistry,* ELBS, Oxford, 1990, p 503.
29. Dewar, M.J.S.; Zoebisch, E.G.; Healy, E.F.; Stewart, J.J.P. *J. Am. Chem. Soc.* **1985**, *107*, 3902.
30. MOPAC93 © Fujitsu Inc.

31. Dehu, C; Meyers, F.; Bredas, J.L. *J. Am. Chem. Soc.* 1993,*115,* 6198.
32. Willetts, A.; Rice, J.E.;.Burland, D.M; Shelton, D.P. *J. Chem. Phys.* **1992,** *97,* 7590.
33. Maker, P.D.; Terhune, R.W.; Nisenhoff, M.; Savage, CM. *Phys. Rev. Lett.* **1962**, *8*, 21.
34. Singer, K.D.; Cai, Y.M.; Garito, A.F. *J. Opt. Soc. Am. B* **1991,** *8,* 2132.
35. Singer, K.D.; Garito, A.F. *J. Chem. Phys.* **1981,** *75,* 3572.

CHAPTER 5

MATERIALS FROM ACHIRAL MOLECULES : CRYSTAL STRUCTURES AND POWDER SHG STUDIES

5.1 BACKGROUND

In the previous Chapters, we have presented the computational studies of several diamino substituted dicyanoquinodimethane systems (Chapter 2), the synthesis and characterisation of these compounds (Chapter 3) and experimental exploration of their molecular hyperpolarisabilities (Chapter 4). The theoretical and experimental studies on these systems have revealed that they possess large molecular hyperpolarisabilities and hence are of potential interest in the development of novel NLO materials. As can be seen from Fig.2.1 and Chapter 3, we have synthesised both achiral and chiral molecule-based materials. For the sake of convenience, we divide these materials into two classes, one based on achiral molecules and the other based on chiral molecules and present detailed structural and NLO studies on selected candidates of each class in this Chapter and the next one.

In Sec.5.2, we present the crystal structure details of the compounds 9, 10 and 11 in which the donor amino groups are derived respectively from the six-member saturated ring systems, piperidine, piperazine and morpholine. These molecules have large ground state dipole moments and crystallise in centrosymmetric crystal lattices. Nevertheless these systems warranted careful study as models based on which modifications to obtain noncentrosymmetric materials could be attempted. The details of the molecular and crystal structure analysis is presented along with the discussion of relevant molecular structure characteristics in this Section. In Sec.5.3, we present a novel phenomenon of solvate switching of powder second harmonic generation

in one of the polymorphic forms of 8 (DPDQ). DPDQ is an achiral molecule and crystals grown from acetonitrile do not show any SHG. However, the flaky powder of DPDQ obtained by recrystallisation from chloroform shows strong SHG. Further, the SHG observed in the latter polymorph could be switched on and off by exposure to chloroform vapour and subsequent drying. The crystal structure details of both the polymorphic forms are presented and an explanation is provided for the novel phenomenon.

For all crystal structure determinations presented in this thesis, the x-ray intensity data were collected on an ENRAF-NONIUS CAD4 computer-controlled diffractometer. CuK_α (X = 1.54178 A) radiation with a graphite crystal monochromator in the incident beam was used. The standard CAD4 centering, indexing and data collection programs were used. The unit cell dimensions were obtained by a least square fit of 24 centered reflections in the range of $21 < 6 < 30°$.

The powder SHG measurements were carried out using the Kurtz-Perry method discussed in detail in Sec. 1.6. The fundamental wavelength (1064 nm) of a Q-switched Nd:YAG laser (Continuum, Model 660B-10) was used. The detection system consisted of the photomultiplier tube (Hamamatsu) and oscilloscope (Tektronix, Model 2465B, 400MHz) or lock-in amplifier (SRS, Model SR830). Powder samples were sandwiched between glass plates with the thickness of the sample controlled by uniform teflon sheets. Powder sizes were graded using standard sieves. Urea of particle size 100 - 150 u was used as the standard since at these particle sizes, the powder SHG of urea saturates

at its maximum value. As is often the practice, the powder SHG capability of all the compounds are expressed in terms of the unit, U (SHG of urea = 1 U). The quinonoid materials we have investigated have all shown very good stability under laser irradiation and no sign of decomposition even on continued irradiation with a laser power of 1 GW/cm^2 (6 ns, 10 Hz) was detected.

5.2 CRYSTAL STRUCTURES OF DPIDQ (9), DPZDQ (10) AND DMDQ (11)

Quantum chemical calculations presented in Chapter 2 had revealed some important aspects of the molecular structure of the push-pull quinonoid molecules. For example the optimised geometries of several systems showed strong twist of the diaminomethylene unit with respect to the benzenoid plane. We have discussed the influence of this structural feature on the optical absorption energies and molecular hyperpolarisabilities. The calculations also indicated that these molecules are likely to be strongly zwitterionic. The experimentally found melting points imply strong electrostatic binding forces in the crystal.

In an effort to gain direct insight into the molecular and crystal structure of the diamino substituted dicyanoquinodimethanes, we initially attempted to grow crystals of several easily synthesised derivatives. The molecules obtained from the reaction of primary amines with TCNQ were in general not amenable to good crystal

growth. In this initial exploratory study, the molecules which gave good quality single crystals were those prepared using simple and easily available achiral, secondary amines such as pyrrolidine, piperidine, piperazine and morpholine; the resulting compounds are respectively 8, 9, 10 and 11. Since no deliberate design of noncentrosymmetric crystal lattices was involved and these molecules have strong ground state dipole moments, it would not be surprising if these achiral compounds produced only centrosymmetric crystals. This was borne out in all the cases. However, 8 recrystallised from chloroform manifested some unexpected and interesting features; this is discussed in detail in the next Section.

The space groups, unit cell details and features of the x-ray analysis of 9, 10 and **11** are collected in Table 5.1 (fractional coordinates for the asymmetric unit are provided in Tables A-1.1 to A-3.2). It is seen that all the three compounds belong to centrosymmetric space groups. Based on a statistical analysis, it has been argued[1] that there is no strong correlation between large ground state dipole moments of molecules and the tendency to form centrosymmetric crystal structures. However, strong ground state dipole moment does often encourage a centrosymmetric arrangement of molecules in the crystal lattice; our systems are typical examples of this.

The molecular structure and stereoviews of the unit cells of 9, 10 and **11** are presented in Figs. 5.1, 5.2 and 5.3 respectively. The significant bond lengths in the three compounds are collected in Table

5.2 (the atom labellings are as shown in Figs. 5.1 (a), 5.2(a) and 5.3(a) respectively). In all the three molecules, the bonds in the unsaturated

Table 5.1: *Crystallographic data for compounds 9, 10 and* ***11.***

Compound	**9**	**10**	**11**
molecular formula	$C_{20}H_{24}N_4$	$C_{18}H_{22}N_6$	$C_{18}H_{20}N_40_2$
morphology	cubes	plates	needles
crystal system	triclinic	triclinic	monoclinic
space group	$P\bar{1}$	$P\bar{1}$	$P2_1/n$
a, Å	13.540(1)	13.372(1)	12.695(1)
b, Å	16.239(1)	15.614(1)	15.355(1)
c, Å	8.771(1)	8.756(1)	8.756(1)
α, deg.	101.78(1)	99.31(1)	90.0
β, deg.	104.79(1)	105.63(1)	106.44(1)
γ, deg.	95.61(1)	97.06(1)	90.0
V, $Å^3$	1802.4(5)	1710.5(6)	1656.0(4)
Z	4	4	4
ρ_{calcd}, g cm^{-3}	1.18	1.25	1.30
$\mu(CuK_\alpha)$, cm^{-1}	5.24	5.91	6.71
no. of unique reflections	5260	5073	2404
no. of reflections with $I \geq 3\sigma_I$	4635	4591	2171
R	0.034	0.034	0.032
R_w	0.062	0.061	0.056

(a)

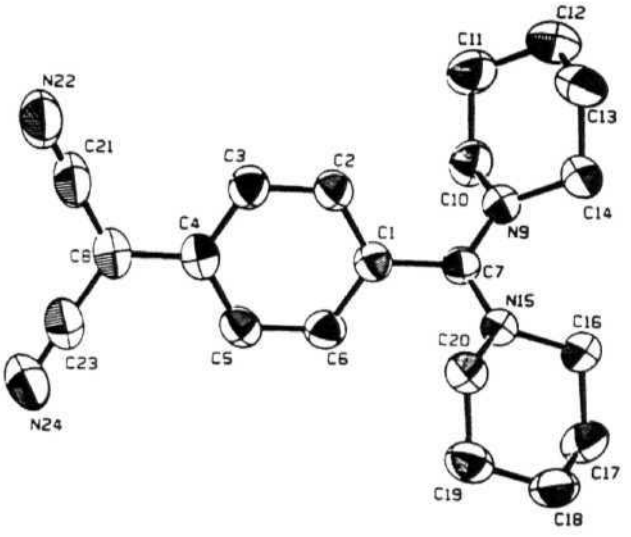

(b)

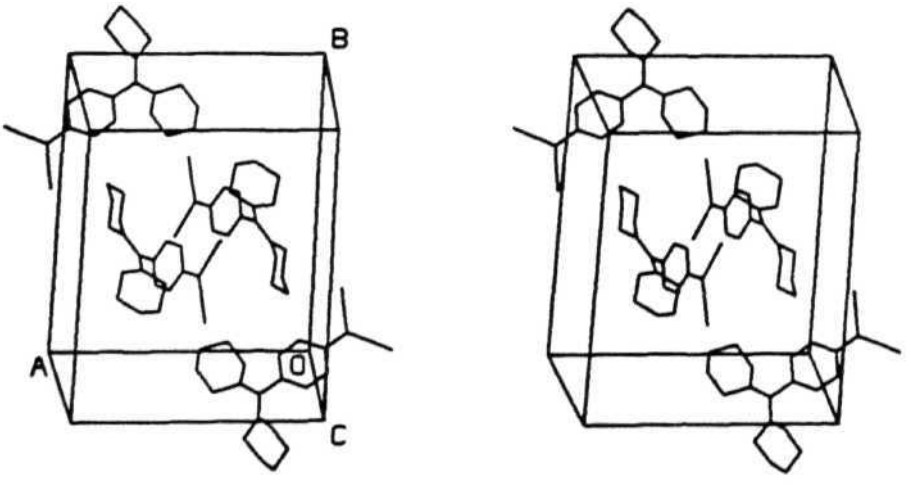

Figure 5.1: *(a) The molecular structure and (b) stereoview of the unit cell along the c axis of 9 (the H atoms are omitted for clarity)*

(a)

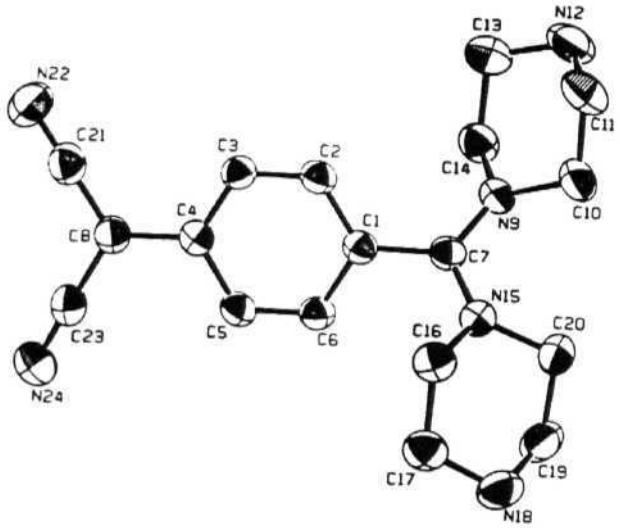

(b)

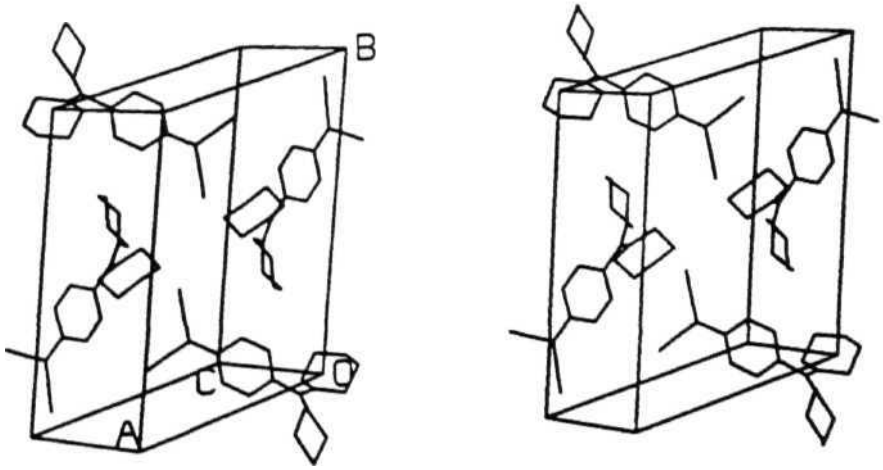

Figure 5.2: *(a) The molecular structure and (b) stereoview of the unit cell along the a axis of 10 (the H atoms are* ***omitted*** *for clarity)*

(a)

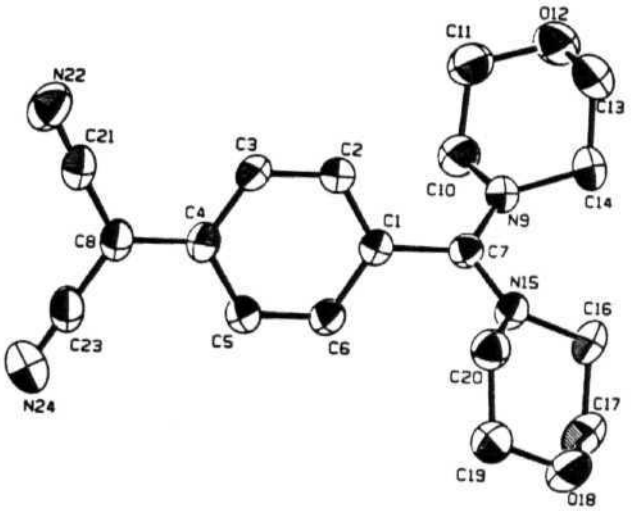

(b)

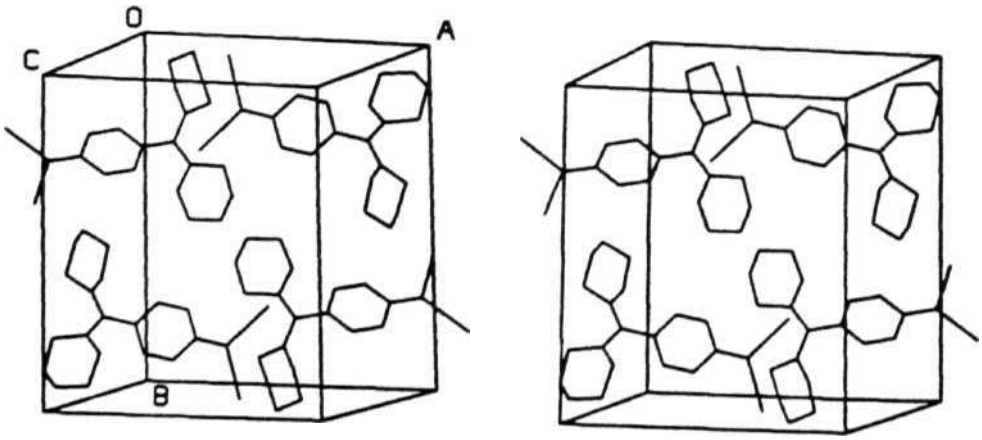

Figure 5.3: ***(a)*** *The molecular structure and (b)* ***stereoview*** *of the* ***unit*** *cell along the* ***c*** *axis of 11 (the* ***H atoms*** *are omitted for clarity)*

six-membered ring that serves as the 'conjugation unit' in the push-pull system are found to be nearly benzenoid in character, not quinonoid. The lengths of the exocyclic bonds as well as the N-C bonds at the amino end and C-N bonds at the cyano end also reflect the dominance of the zwitterionic resonance form with strong positive charge on the diaminomethylene unit and negative charge on the dicyanomethylene unit. Our theoretical analysis[2] of the parent system 7,7'-diamino-8,8'-dicyanoquinodimethane (Sec.2.3) with structural changes induced by the influence of varying external fields, indicated a peaking of the β at structures intermediate between the benzenoid and quinonoid extremes but closer to the benzenoid end. This implies that the large hyperpolarisabilities of these strongly benzenoid zwitterionic molecules we have synthesised could still be improved by slightly decreasing the zwitterionic nature by appropriate chemical modifications.

The molecular structures of 9, 10 and 11 reveal normal bond angles within the benzenoid ring, the exocyclic bonds and the heterocyclic substituents. The unsaturated rings are quite planar in all the structures. Table 5.2 also provides two important dihedral angles θ_1 and θ_2 in these structures. θ_1 is the dihedral angle between the average planes of the diaminomethylene unit and the benzenoid ring and θ_2 the similar angle between the dicyanomethylene unit and the benzenoid ring. The θ_2 values indicate that the dicyanoquinodimethane moiety is almost coplanar with the benzenoid ring as it is in TCNQ.

Table 5.2: *Important bond lengths in A and dihedral angles (see text for definition) in degrees in 9, 10 and 11 (see Figs. 5.1 (a), 5.2(a) and 5.3 (a) for atom labelling)*

	9	10	11
C(7) - N(9)	1.333	1.336	1.333
C(7) - N(15)	1.335	1.335	1.337
C(1) - C(7)	1.467	1.465	1.466
C(1) - C(2)	1.394	1.392	1.396
C(1) - C(6)	1.395	1.396	1.397
C(2) - C(3)	1.370	1.373	1.371
C(5) - C(6)	1.369	1.372	1.372
C(3) - C(4)	1.406	1.403	1.405
C(4) - C(5)	1.405	1.404	1.407
C(4) - C(8)	1.438	1.436	1.440
C(8) - C(21)	1.399	1.404	1.407
C(8) - C(23)	1.405	1.407	1.404
θ_1	46.8	43.0	48.7
θ_2	5.0	6.6	1.4

The large values of θ_1 (43° - 49°) indicate that a strong out-of-**plane** twisting of the diaminomethylene unit occurs in these molecules. **We note** that the computed values of these twists presented in Table 2.1 are smaller. As discussed earlier (Sec.2.4), this may be arising from the high conformational flexibility of the six-member heterocyclic rings which takes up equilibrium geometries in the solid state which are quite different from that optimised for the gas phase structure. The analogy of

this twisted geometry to the well known twisted intramolecular charge transfer (TICT) systems is not out of place; the important contrast with conventional TICT systems is that the twisting in our systems is a ground state phenomenon. The twisting arises from the overcrowding due to the steric repulsion between the *ortho*-H atoms on the benzenoid ring and those on the neighbouring carbons of the nitrogens of the heterocyclics as illustrated by our theoretical study in Sec. 2.4 The twisting is further facilitated by the zwitterionic nature of the molecules with the consequent weakening of the C1-C7 bond (Table 5.2). An important consequence of this molecular twist is the chirality that it induces in the molecule. If one ignores the detailed structure of the amino moieties, the twisted molecule is nearly C_2 symmetric. In principle, this could lead to isolable chiral molecular structures and should provide a route to induce noncentrosymmetric lattices. However, the activation energy for interchange between the M and P forms of this chiral structure is expected to be very small. The computational study of the twisting in DPDQ carried out in Sec. 2.4 indicates that this barrier is of the order of 1 kcal/mol. Hence these chiral structures are likely to exist as racemates in solution and finally provide only centrosymmetric structures as has been observed.

We find that the three crystal structures irrespective of the donor amino group are rather similar. Since the steric effect due to the six-member rings are similar and the electronic nature of the amines are practically identical, this is not surprising. The possibility of H-bonding through the piperazine unit in **11** does not appear to have developed any novel features in the crystal packing. However if one examines the

molecular dipole arrangements in the *ac* plane projections (in all the unit cells the longest axis is the *b* axis) in 9, 10 and **11** the following subtle differences in the packing of dipoles can be observed. In 9, the dipoles are arranged antiparallel to form two distinct dimer units which form a centric array roughly perpendicular to the *b* axis. In 11, parallel head-to-tail arrangement of the dipoles form a noncentric array in the *ac* plane. However the adjacent plane has opposite orientation leading to an overall centrosymmetric structure. In 10, the arrangement is more complex; the molecules form zig-zag head-to-tail chains approximately in the [101] direction, with adjacent chains out of phase with each other. The effectively noncentric array together with the neighbouring arrays of opposite orientation again leads to a centrosymmetric lattice. If by inclusion of solvent molecules or cocrystallising with weak dipolar molecules, the interaction between the noncentric arrays in 10 or 11 could be diminished, there is a possibility of fabricating noncentrosymmetric lattices.

5.3 SOLVATE SWITCHABLE POWDER SHG IN DPDQ (8)

DPDQ is one of the compounds reported in the first paper from du Pont on the diamino substituted dicyanoquinodimethanes.[4] We have also synthesised this compound during the preliminary investigations of this class of push-pull quinonoid compounds. The du Pont group had used methanol for the recrystallisation of DPDQ. However we found that good quality crystals could be grown from acetonitrile. These crystals were found to be centrosymmetric and SHG inactive. We also

have recrystallised this material from a variety of other solvents. The crystals obtained from chloroform are also found to be centrosymmetric; however they lose the solvate molecules even upon a brief exposure of the crystals to air, giving rise to flaky powders. Interestingly we noticed that these powders are capable of strong SHG. The SHG activity can be reversibly switched off and on by exposure to chloroform and subsequent drying. In this Section, we present the structures of the crystals from acetonitrile and chloroform and provide an explanation for this novel phenomenon of solvate switching of the powder SHG in the later.

Several instances of apparently centrosymmetric systems giving rise to SHG have been reported. Weak SHG found[5] in powders of aromatic charge transfer molecules with centrosymmetric crystal structures has been attributed to minor deviations from a strictly centrosymmetric lattice. Strong SHG from LB monolayers of centrosymmetric squarine dyes[6] indicates that these molecules which form centrosymmetric crystals assemble noncentrosymmetrically in the LB film. Occlusion of chiral molecules has been shown to induce noncentrosymmetry in centrosymmetric lattices and lead to strong SHG activity.[7] SHG has been observed in centrosymmetric crystals of racemic mixtures when circularly polarised light was used. All these cases involve induction of noncentrosymmetry in centrosymmetric systems in rather unusual ways. A more obvious though less directed approach has been to search through solvent-based polymorphs. Polar solvents have been reported to encourage noncentrosymmetric crystal structures.[9] Completely SHG inactive and moderately to strongly SHG

active polymorphs have been grown from different solvents.[1] An extreme case of solvent dependent polymorphism has been reported in stilbene and diphenylacetylene derivatives with one derivative having seven polymorphs with SHG activity ranging from 0.15 U to 300 U. The observation mentioned above in the case of DPDQ is very different from all these cases.

DPDQ crystals grown from acetonitrile solution (DPDQ-A) (Sec.3.3) belong to $P2_1/c$ space group (Table 5.3) and contain a water molecule of crystallisation per DPDQ picked up from the solvent, which even upon drying, apparently has retained traces of moisture. Crystals obtained from a chloroform solution (DPDQ-C) (Sec. 3.3) had to be immediately coated with grease to prevent solvent loss and crystal degradation. Structure analysis indicated a $P2_1/n$ space group (Table 5.3) and a solvate molecule of chloroform per DPDQ. The fractional coordinates of the asymmetric unit of DPDQ-A and DPDQ-C are presented in Tables A-4.1 to A-5.2.

The molecular geometry is nearly identical in the two crystals; the molecular structure from DPDQ-C crystal analysis is shown in Fig.5.4(a) and the important bond lengths and dihedrals for both DPDQ-A and DPDQ-C are collected in Table 5.4. The diaminomethylene unit is twisted out of the 6-membered ring plane by *ca.* 56°, a feature common among these molecules (Sec.2.4). The bond lengths in the 6-member ring conjugation unit indicate strong benzenoid character and

Table 5.3: *Crystallographic data for DPDQ-A and DPDQ-C*

Compound	DPDQ-A	DPDQ-C
molecular formula	$C_{18}H_{20}N_4 . H_2O$	$C_{18}H_{20}N_4 . CHCl_3$
crystal system	monoclinic	monoclinic
space group	$P2_1/c$	$P2_1/n$
a, Å	16.473(2)	13.278(1)
b, Å	8.481(1)	17.658(1)
c, Å	25.383(3)	8.907(1)
β, deg.	105.20(1)	103.11(1)
V, $Å^3$	3422.2(6)	2034.0(8)
Z	8	4
ρ_{calcd}, g cm^{-3}	1.21	1.34
$\mu(CuK_\alpha)$, cm^{-1}	5.81	42.40
no. of unique reflections	5492	3071
no. of reflections with $I \geq 3\sigma_I$	4200	2296
R	0.046	0.091

hence the zwitterionic nature of this molecule. The resultant dipole moment of this molecule is expected to be high (AM1 calculation indicated μ = 14.1 D which probably leads to a preference for the centrosymmetric packing in the crystals as in the cases of 9 - 11).

Layers of molecules roughly parallel to the *ac* plane are seen in the DPDQ-C structure. Projection of these layers in the *ab* plane indicates zig-zag chains of molecules running along the *a* axis with the

adjacent dipoles making an angle of *ca.* 30° (Fig.5.4(b)). The centrosymmetrically related layer along the *b* axis (the longest unit cell

Table 5.4: *Important bond lengths in A and dihedral angles (see Sec. 5.2 for definition) in degrees in DPDQ-C (see Fig. 5.4 (a))*

	DPDQ-A	DPDQ-C
C(7) - N(9)	1.321	1.318
C(7) - N(14)	1.330	1.333
C(1) - C(7)	1.472	1.480
C(1) - C(2)	1.401	1.380
C(1) - C(6)	1.390	1.402
C(2) - C(3)	1.363	1.373
C(5) - C(6)	1.367	1.376
C(3) - C(4)	1.405	1.399
C(4) - C(5)	1.399	1.391
C(4) - C(8)	1.446	1.449
C(8) - C(19)	1.394	1.400
C(8) - C(21)	1.400	1.41
θ_1	56.2	56.2
θ_2	5.5	5.4

axis) is well separated from the first one by a layer of chloroform molecules. In DPDQ-A we find a layered structure consisting of stacks of DPDQ, approximately perpendicular to the longest unit cell axis, *c*, however there is no distinct layer of solvate molecules (Fig.5.4(c)). Inspection of interatomic distances indicates that the water molecules of

(a)

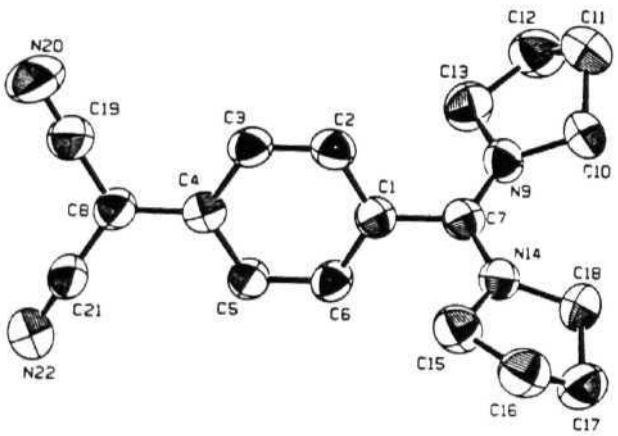

(b)

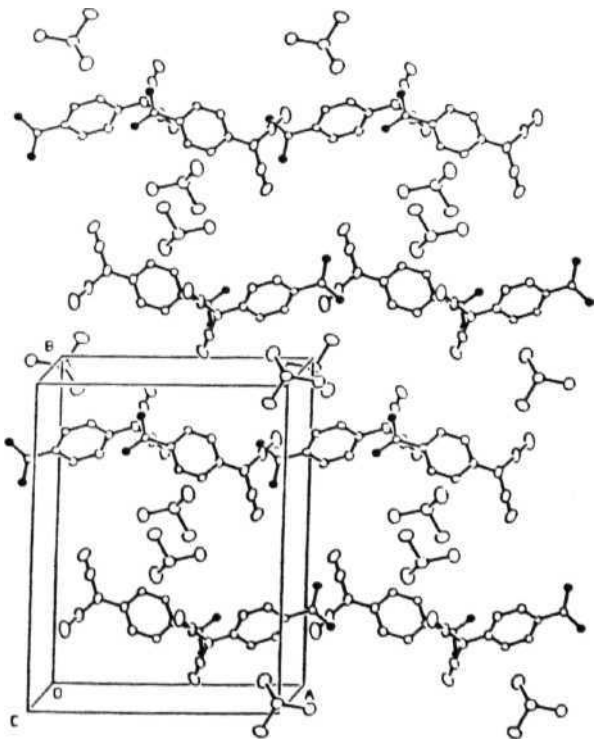

Figure 5.4: (continued on next page)

(c)

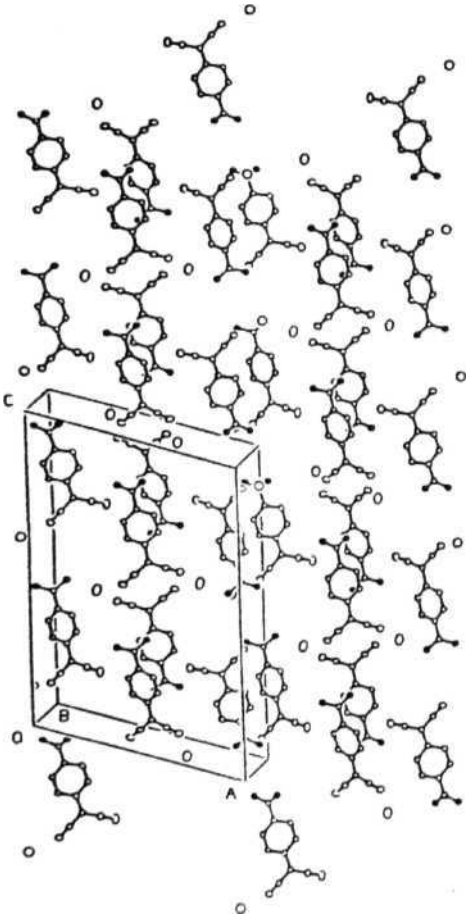

Figure 5.4: *(a) Molecular structure of DPDQ-C; H atoms are omitted for clarity. Unit cell view of(b) DPDQ-C along the c axis and (c) DPDQ-A along the b axis; C atoms of the pyrrolidine rings and all H atoms are omitted for clarity; the N atoms of the pyrrolidine rings are shown as filled circles*

crystallisation are H-bonded to the cyano groups (O-N distances are found to be 2.73Å and 3.10A in the two molecules in the asymmetric unit).

DPDQ recrystallised from acetonitrile, tetrahydrofuran, methanol, ethanol and dichloromethane did not show any SHG either in the crystal or in the dried powders. Freshly recrystallised DPDQ-C suspended in chloroform did not show any SHG. Upon drying, the crystals lost their transparency and formed a flaky powder. In a Kurtz-Perry experiment using 1064 nm radiation from a ns-pulsed Nd:YAG laser, this powder showed a strong SHG of 30 - 40 U. The powder size of the sample was varied and the SHG was found to be nearly constant at particle sizes above 75 u indicating that the material is phase-matchable. This SHG activity is highly reproducible provided the sample has been purified by several recrystallisations. We have monitored a couple of samples for 15 months and found that the SHG activity remained undiminished. This indicates that the SHG is quite genuine and not arising from some spurious effects.

We carried out an experiment in which dry DPDQ-C powder was taken in a narrow glass tube attached through a stopcock to a flask containing chloroform. With the laser beam incident on the sample, while monitoring the SHG activity of the powder the stopcock was opened and the chloroform gently warmed to allow vapours to flow over **the** powder. The green light emitted by the sample diminished considerably and vanished completely when the powder got wetted by traces of condensed chloroform. There was no dissolution since **the**

solubility of DPDQ in chloroform at room temperature is extremely low. After closing the stopcock the sample was dried using a hot air blower whereupon the SHG returned to the original intensity. This experiment could be repeated several times. We have carried out control experiments with other compounds that we have prepared and having similar SHG activity and solubility characteristics as DPDQ (discussed in Chapter 6). However, no reduction of SHG activity on exposure to chloroform vapours or wetting by chloroform could be detected.

The structure of DPDQ-C described above provides an explanation for this interesting phenomenon. The chloroform layer separates layers of DPDQ molecules related by the centre of inversion. Loss of the chloroform layer upon exposure or drying of the crystals (the elemental analysis of dried powders show complete absence of chloroform) results in flaky powders, wherein the original structure has collapsed to intrinsically noncentric layers of DPDQ which are no longer related by a centre of inversion. In DPDQ-A the water molecules could be partially removed by drying under vacuum (elemental analysis indicated 0.4 mols of water of crystallisation) and driven out completely by extended drying under vacuum at 150°C (confirmed by the disappearance of the O-H stretch absorption in the infra red spectrum of such samples). These samples showed no SHG indicating that the type of layer separation seen in DPDQ-C does not occur here. The mechanism of re-entry of chloroform into DPDQ-C is not clear, however it obviously resurrects a centric structure so that the SHG activity is lost. We have attempted to prepare single crystals of DPDQ by solvent-free methods such as sublimation to gain insight into the unsolvated crystal

structure. However, these attempts were unsuccessful since the compound decomposes just before melting at 290°C.

5.4 CONCLUSION

Diaminodicyanoquinodimethane systems provide a novel class of push-pull quinonoid molecules with suitable molecular properties to develop molecular NLO materials. The three molecules 9-11 presented here are typical examples of these easily synthesised compounds. These molecules crystallise quite well; the crystal structure analysis indicated centrosymmetric space groups for all the molecules. The investigations of these crystal structures have revealed important insight into the molecular structure of these compounds, in particular, the benzenoid nature of the conjugation unit and the dihedral twist. It is concluded that though these systems have potentially useful nonlinear optical properties at the molecular level, the high ground state dipole moments are a hurdle to noncentric crystal lattice formation. The tendency towards a centrosymmetric arrangement of the molecules has to be overcome by suitable crystal engineering strategies or poling techniques, so that useful quadratic NLO materials can be fabricated from this class of molecules.

Molecule-based materials for sensor applications is an area of great fascination today, since molecular devices may offer unprecedented active device sizes on the nanometer scale and extremely fast response to the stimuli to be sensed. A variety of electronic, magnetic or optical responses may be exploited in such devices. The

novel phenomenon of reversible SHG activity which is highly sensitive to the presence of solvate molecules observed in DPDQ may be of interest in the context of sensor applications. The introduction of noncentrosymmetry in a centrosymmetric material by the loss of solvate is of fundamental interest in the design of molecular NLO materials since this case is unprecedented and the associated second harmonic generation activity is quite substantial, unlike those found in some earlier systems.

REFERENCES

1. Whitesell, J.K.; Davis, R.E.; Saunders, L.L.; Wilson, R.J.; Feagins, J.P. *J. Am. Chem. Soc.* 1991, *113*, 3267.
2. Ravi, M.; Radhakrishnan, T.P. *J. Phys. Chem.* **1995,** *99,* 17624.
3. Rettig, W. *Angew. Chem. Int. Edn. Engl.* **1986,** *25,* 971.
4. Heitler, L.R.; Hartzler, H.D.; Acker, D.S.; Benson, R.E. *J. Am. Chem. Soc.* **1962,** *84,* 3387.
5. Ledoux, I.; Zyss, J.; Siegel, J.S.; Brienne, J.; Lehn, J.-M. *Chem. Phys. Lett.* **1990**, *1*72,440.
6. Ashwell, G.J.; Jefferies, G.; Hamilton, D.G.; Lynch, D.E.; Roberts, M.P.S.; Bahra, G.S.; Brown, C.R. *Nature* **1995,** *375,* 385.
7. Weissbuch, I.; Lahav, M.; Leiscrowitz, L.; Meredith, L.R.; Vanherzeele, H. *Chem. Mater.* **1989**, *1*, 114.
8. (a)Meijer, E.W.; Havinga, E.E.; Rikken. G.L.J.A. *Phys. Rev. Lett.* **1990,** *65,* 37. (b) Meijer, E.W.; Havinga, E.E *Synth. Metals* **1993,** *55-57*, 4010.
9. Tabei, H.; Kurihara, T.K.; Kaino, T. *Appl Phys. Lett.* **1987,** *50,* 1855.
10. (a) Nogami, T.; Nakano, H.; Shirota, Y.; Umegaki, S.; Shimizu, Y.; Uemiya, T.; Yasuda, N. in *Nonlinear Optics of Organics and Semiconductors,* T.Kobayashi (Ed), Springer Proceedings in Physics, Vol. 36, Springer-Verlag, Berlin, 1989, p 232. (b) Huang, K.; Britton, D.; Etter. M.C.; Byrn, S.R. *J. Mater. Chem.* **1995,** *5,* 379.
11. Wang, Y.; Tarn, W.; Stevenson, S.H.; Clement, R.A.; Calabrese, J. *Chem. Phys. Lett.* **1988**, *148*, 136.
12. Kurtz, S.K.; Perry, T.T. *J. Appl. Phys.* **1968,** *39,* 3798.

CHAPTER 6

MATERIALS FROM CHIRAL MOLECULES : CRYSTAL STRUCTURES AND POWDER SHG STUDIES

6.1 BACKGROUND

In the previous Chapter we have described the crystal structures of some push-pull quinonoid molecules based on achiral substituent groups like pyrrolidine, piperidine *etc*.. We found that all these materials had centrosymmetric space groups. None of these compounds exhibited solid state SHG (except of course, the peculiar case of DPDQ-C described in Sec.5.3). The various other achiral derivatives listed in Fig.2.1 also showed no solid state SHG presumably because of centrosymmetric crystal lattices. The large hyperpolarisabilities of the push-pull quinonoid molecules held out the promise of generating efficient NLO materials if one could induce appropriate alignment of the molecular dipoles in the bulk state. We therefore attempted a wide variety of approaches to obtain noncentrosymmetric materials based on these compounds.

We have tried several strategies like poling of polymers and sol-gel matrices containing these compounds, cocrystallisation of these molecules with urea, p-nitroaniline and tartaric acid, preparation of salts of derivatives such as of DADQ and DPZDQ with counterions such as Cl", $CF_3CO_2^-$ and $CH_3C_6H_4SO_3^-$. But none of these approaches gave any clear indication of successful fabrication of a noncentric bulk system. Along with these strategies, we also investigated the approach of synthesising chiral derivatives of the basic diaminodicyanoquinodimethane framework. As discussed in Sec. 1.4, the molecular chirality guarantees the crystallisation of a pure enantiomer in a noncentric space group; there are several chiral

compounds reported,[1] which have been found to be efficient NLO materials, NPP (Fig. 1.2) being an excellent example. The diaminodicyanoquinodimethane framework allows innumerable variety of chiral groups to be substituted and a very wide choice can be envisioned. The chiral derivatives we have prepared and investigated (12 - 16) are simple extensions of the prototypical system, DPDQ (8) and they all were found to belong to noncentric space groups. A systematic program of molecular engineering involved in the synthesis of these compounds, led to the enhancement of powder SHG from 3 U to 55 U among these derivatives.

In Sec.6.2, we present the crystal structures of 7-*S*(-)-α-methylben2ylamino-7-pyrrolidino-8,8-dicyanoquinodimethane, MBPDQ (14) and 7-*S*(+)-2-methoxymethylpyrrolidino-7-pyrrolidino-8,8-dicyano-quinodimethane, PMPDQ (16) (Fig.2.1). We also describe the powder SHG experiments and the observation of moderate to fairly strong phase-matched SHG in these compounds. The NLO properties of the stereoisomer of 14 (14-/?) and the naphthyl derivative (15) are also presented.

We were interested in investigating the possible role of H-bonding in the crystal lattices of push-pull quinonoid systems. Attempts to prepare prolinol (2-hydroxymethylpyrrolidine) derivatives were unsuccessful. However, the preparation of the 3-hydroxypyrrolidine derivative was successful. In Sec.6.3, we describe the role of H-bonding leading to

moderately large SHG of 13 U in 7,7-bis[*R*(-)-3-hydroxypyrrolidino]-8,8-dicyanoquinodimethane, DHPDQ (13). The molecular chirality has created a noncentric lattice here, as in the previous cases. The H-bonding has a buttressing effect on this molecular packing and hence contributes positively to the bulk SHG. However, we noticed an unusual effect of the intermolecular H-bonding in this crystal in terms of enhancing the molecular twist commonly found in this class of zwitterionic push-pull systems. This molecular structural change leads to an increase in absorption energy and a decrease in the hyperpolarisability, the latter effect leading to a negative impact on the bulk SHG activity whereas the former has a positive influence in terms of enlarging the transparency window of this material. Thus we present in this Section a unique case of the dual role played by H-bonding in deciding the NLO property of a push-pull quinonoid molecular material.

A careful analysis of the crystal structures of MBPDQ and PMPDQ revealed that even though the introduction of chirality led to crystallographic noncentrosymmetry in both cases, the molecular dipole moment vectors (in the following discussion, we define this as the vector from the diaminomethylene carbon to the dicyanomethylene carbon) were still fairly close to an antiparallel arrangement. Therefore it was clear that we were not realising yet, the full potential of these molecular materials in terms of their SHG efficiency. 14-/? showed very similar linear and nonlinear optical properties as 14; therefore the specific choice of the configuration *(R* or *S)* does not appear to be crucial. 15, with a large side group was found to have still lower SHG than 14. In MBPDQ, the

stereogenic centre is on a conformationally flexible side group and in PMPDQ, it is on a relatively more rigid cyclic moiety. This feature has led to larger deviation of dipole vectors from an antiparallel orientation, and consequently an improvement in the SHG capability from MBPDQ (3 U) to PMPDQ (28 U). Thus it appeared to us that the introduction of two stereogenic centres of the more rigid type close to the dipole axis would lead to still higher SHG capability. We discuss in Sec.6.4, the molecular engineering aspects which led to the dramatic improvement of the SHG capability to ~ 55 U in 7,7-bis[*S*(+)-2-methoxymethylpyrrolidino]-8,8-dicyanoquinodimethane, DMPDQ (12); we present also the crystal structure details of this compound. A detailed analysis of the correlation of SHG to the dipole alignment and molecular hyperpolarisability is also discussed.

6.2 CRYSTAL STRUCTURES AND POWDER SHG STUDIES OF MBPDQ (14) AND PMPDQ (16)

The first chiral derivative that we synthesised was MBPDQ utilising the chiral group that has been previously employed[2] in 2-N-(α-methylbenzylamino)-3,5-dinitropyridine (MBADNP) and 2-N-(a-methylbenzylamino)-5-nitropyridine (MBANP). Single crystal X-ray structure analysis of the transparent plate-like crystals of MBPDQ obtained from acetonitrile solution indicated an acentric space group, $P2_1$, with two MBPDQ molecules and two solvent molecules in the unit cell. The

crystallographic data are provided in Table 6.1 (fractional coordinates for the asymmetric unit are provided in Tables A-6.1 to A-6.3). The molecular structure and the unit cell view along the *b* axis are shown in Fig.6.1. The N9-C7-N14 plane on the donor side is twisted out of the quinonoid ring plane by *ca.* 49.8°. The bond lengths (Table 6.2) in the conjugation unit indicate a strongly benzenoid character resulting from the intramolecular charge transfer which is accentuated by the out-of-plane twisting of the donor group. The molecular structure is quite reminiscent of the structures discussed in the Chapter 5. The crucial difference now is the loss of the centre of inversion; however, the molecular alignments in the crystal are nearly head-to-tail, the noncentricity arising from the presence of the chiral carbon atoms alone. The angle between the molecular dipoles (see definition above) is found to be 168^{o}.

We have next prepared, the derivative based on the *R* isomer of N-methylbenzylamine. The product (**14-*R***) appeared very similar to 14. The melting points and electronic absorption were identical. The powder SHG was also nearly the same. We also considered the naphthyl derivative in place of the phenyl derivative. The resulting compound, 15, showed no improvement in SHG; in fact it was only 0.5 U. Since these compounds showed no progress with respect to the solid state SHG, we did not attempt any crystal structure analysis on them.

In view of the nearly optimal dipole alignment present in the well known material, NPP having the chiral prolinol group, it would be

(a)

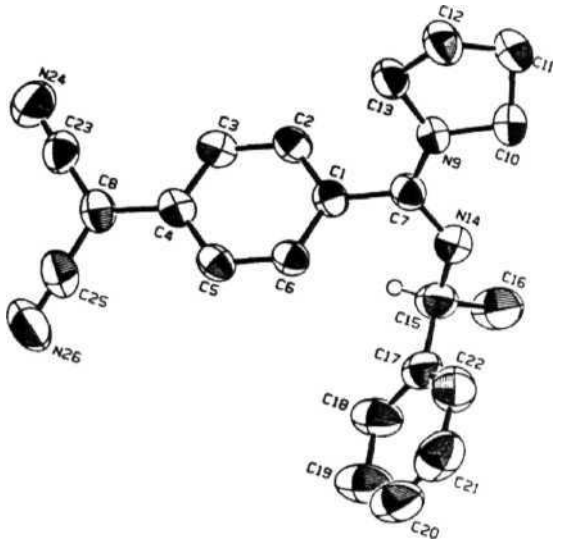

(b)

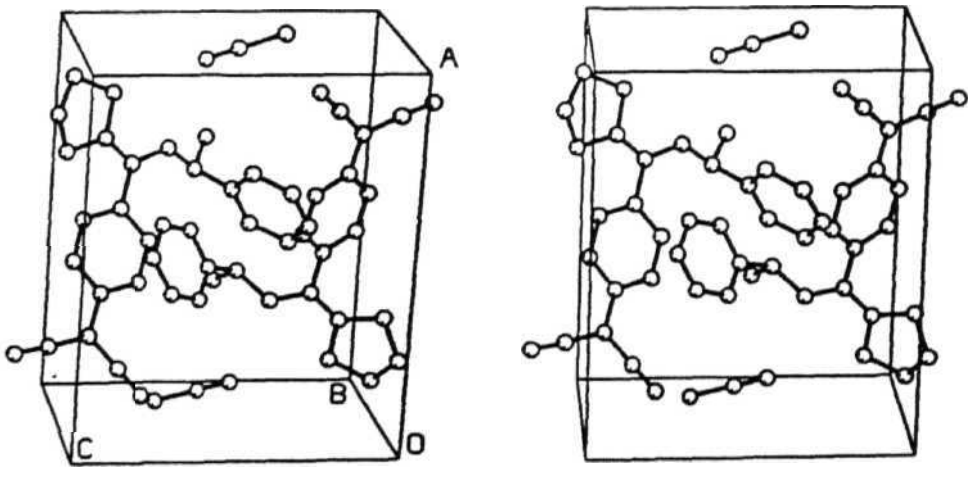

Figure 6.1: *(a) Molecular structure of MBPDQ from single crystal x-ray analysis; H atoms of only the stereogenic centre are shown (b) stereoview of the unit cell along b axis*

Table 6.1: *Crystallographic data for MBPDQ*

molecular formula	$C_{22}H_{22}N_4.CH_3CN$
morphology	plates
crystal system	monoclinic
space group	$P2_1$
a, Å	12.715 (3)
b, Å	8.068 (2)
c, Å	10.422 (2)
β, deg.	91.03(2)
V, $Å^3$	1068.9(5)
Z	2
ρ_{calcd}, g cm^{-3}	1.19
$\mu(CuK_\alpha)$, cm^{-1}	5.36
no. of unique reflections	2182
no. of reflections with $I \geq 2\sigma_I$	2063
R	0.050
R_W	0.076

interesting to consider the prolinol derivative of push-pull quinonoid systems. Therefore, we attempted the introduction of chiral prolinol groups in place of the methylbenzylamino group present in MBPDQ. However, the reaction of the monopyrrolidinotricyanoquinodimethane (PTQ) with

Table 6.2: *Significant bond lengths, bond angles and dihedral angles in MBPDQ from single crystal x-ray analysis; the atom labellings are shown in Fig. 6.1 (a)*

	Distance (Å)		Angle (deg)
C(1) - C(2)	1.393	C(1) - C(7) - N(9)	120.2
C(2) - C(3)	1.383	C(1) - C(7) - N(14)	120.4
C(3) - C(4)	1.400	C(7) - N(9) - C(10)	123.2
C(4) - C(5)	1.406	C(7) - N(9) - C(13)	125.9
C(5) - C(6)	1.378	C(7) - N(14) - C(15)	124.7
C(1) - C(6)	1.398	N(9) - C(7) - N(14)	119.4
C(1) - C(7)	1.467	C(10) - N(9) - C(13)	110.6
C(4) - C(8)	1.447	C(1) - C(7) - N(9) - C(13)	9.9
C(7) - C(9)	1.308	C(1) - C(7) - N(14) - C(15)	17.1
C(7) - N(14)	1.343	C(2) - C(1) - C(7) N(9)	49.7
C(8) - C(23)	1.402	C(3) - C(4) - C(8) - C(23)	8.3
C(8) - C(25)	1.403	C(5) - C(4) - C(8) - C(25)	10.2
C(23) - N(24)	1.146	C(6) - C(1) - C(7) - N(14)	50.0
C(25) - N(26)	1.153		

prolinol led to intractable products. We believe that the hydroxy group of prolinol partially replaces the pyrrolidine group already present in the molecule. Such possibilities have been discussed in the original paper from

du Pont. We also note that Nicoud[4] and Twieg *et al*[5] have prepared compounds by the direct reaction of various chiral aminoalcohols with TCNQ; though they were SHG active no details of synthesis and characterisation has been reported and the SHG observed were not very high. To circumvent the problem associated with the multiple addition of prolinol, we decided to use the methyl ether of prolinol (2-methoxymethylpyrrolidine) and were successful in preparing the compound, PMPDQ. Another motivation for the preparation of this compound is the placement of the stereogenic centre in a rigid ring framework which was expected to lead to improved dipole alignment.

Crystals of PMPDQ were grown from acetonitrile solution as prisms. Preliminary reflection data were indexed to the noncentric orthorhombic space group, $P2_12_12_1$ (Table 6.3) (the fractional coordinates of the asymmetric unit are presented in Tables A-7.1 to A-7.2). However, structure refinement for this crystal was very poor and could not be improved beyond an R value of 0.11 (R_w = 0.15), though data from several crystals were tried. The molecular structure obtained from the analysis indicated unphysical bond lengths in the methoxymethyl side group. It is possible that the free rotation of the methoxymethyl group contributes to this problem. However, low temperature data collection was also unsuccessful in improving the R factor. Even though the molecular structure obtained may not be very reliable, the overall crystal structure and space group are expected to be correct. The unit cell view along the *b* axis

Table 6.3: *Crystallographic data for PMPDQ*

molecular formula	$C_{20}H_{24}N_4O$
morphology	prisms
crystal system	orthorombic
space group	$P2_12_12_1$
a, Å	15.717
b, Å	12.100
c, Å	9.867
$\alpha = \beta = \gamma$, deg.	90.00
V, $Å^3$	1068.9
Z	4
ρ_{calcd}, g cm^{-3}	1.19
$\mu(CuK_\alpha)$, cm^{-1}	5.66
no. of unique reflections	992
R	0.111
R_w	0.149

is presented in Fig.6.2. The molecular dipole vector alignment is considerably improved over MBPDQ. There are two molecules in the asymmetric unit of PMPDQ and the inequivalent interdipole vector angles are 94° and 149°. The idea that the stereogenic centre being on a rigid ring framework would help in improving the dipole alignment appears to be

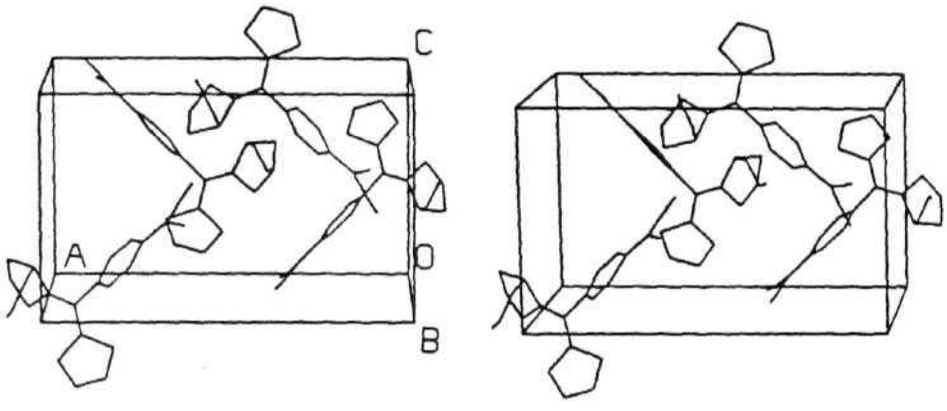

Figure 6.2: *Stereoview of the unit cell along b axis for PMPDQ*

useful. This aspect will be discussed in greater detail in connection with the substitution of two 2-methoxymethylpyrrolidine groups on TCNQ, presented in Sec.6.4.

The powder SHG measurements were carried out as described in the previous Chapter. Powders of MBPDQ with particle size > 150 urn showed a moderate SHG, *ca.* 3 times that of urea. The particle size dependence of the SHG intensity (Fig.6.3) indicates that MBPDQ is a phase-matchable material. In support of this, the SHG of 3 U is obtained in the crystals as well. In the case of PMPDQ, large intensities of *ca.* 25 - 30 U were obtained for powders with particle sizes > 300 urn as well as for crystals; the saturation of the SHG intensity at large particle sizes again indicated phase-matchability (Fig.6.3).

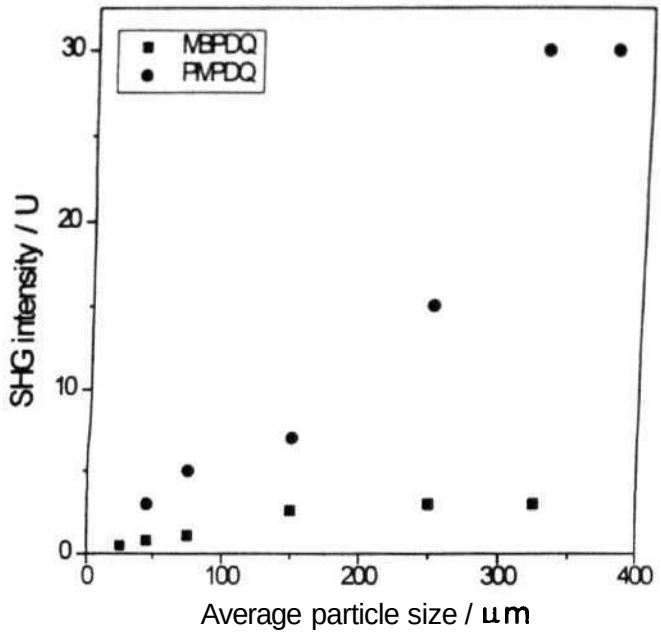

Figure 6.3: *Powder SHG intensity (relative to urea powder with particle size ca. 150 μm) at different particle sizes of MBPDQ and PMPDQ*

6.3 DUAL INFLUENCE OF INTERMOLECULAR H-BONDING ON THE SHG IN DHPDQ (13)

H-bonding is one of the most effective and popular tool for the design of crystal structures. Urea is perhaps the finest example, where the simple and almost trivial molecular structural units have assembled into a three-dimensional crystalline network involving a highly efficient utilisation

of extensive H-bonding. Among the multiple options available which satisfy the strong dipolar forces, the one which simultaneously maximises the H-bonding interactions is naturally selected in the urea crystal.[7] This leads to a concomitant breaking of the centre of symmetry and hence, a strong solid state SHG capability keeping in view the small size and high absorption energy of the urea molecule.

H-bonding has often been utilised in conjunction with other features such as chirality, steric factors etc. to achieve optimal alignment of NLO chromophores, so that high SHG capability is attained in the bulk. One of the most successful cases in question is NPP (Fig. 1.2). Here the chirality in the prolinol unit ensures noncentrosymmetry of the lattice space group, and the extensive H-bonding leads to a crystal packing that provides for close to optimal angles between the molecular dipoles. NPP is one of the best molecular materials for SHG that has been structurally characterised in great detail. Weak to moderate SHG capability have been achieved in crystals having extensive H-bonding with * [1] or without[1] the support from chirality to induce the noncentricity. A well known case of molecular NLO material with intramolecular H-bonding is MAP (Fig.1.2).[13] We note that most of the earlier studies have focused on the influence of H-bonding on the crystal packing. The impact of H-bonding on the molecular structure and hence on the molecular NLO properties that has a direct bearing on the crystal NLO properties, has generally been less significant and less attention has been paid to it. However, a detailed theoretical investigation of the effect of H-

bonding on the hyperpolarisabilities of molecular dimers has been reported.[14]

In an effort to examine, how intermolecular H-bonding would affect the material NLO properties we deliberately included H-bond donor functionalities in the molecular structure. The most convenient approach was to functionalise the amine donor group with hydroxy group. Our initial attempt to use prolinol as the donating amino group was unsuccessful as discussed above. Similar difficulties were encountered with 2-amino alcohols such as valinol. At this point we attempted the preparation of the 3-(*R*)-hydroxypyrrolidino derivative. The crystal structure and solid state SHG of 7,7-bis[*R*(-)-3-hydroxypyrrolidino)-8,8-dicyanoquinodimethane, DHPDQ (13) is presented in this Section. We have studied also the racemate analogue of **13,** namely **13-*RS***; the monosubstituted derivative, namely, 7-[*R*(-)-3-hydroxypyrrolidino)-7-pyrrolidino-8,8-dicyanoquino-dimethane, HPPDQ, has also been prepared in our laboratory. The NLO properties of DHPDQ is compared with the later derivatives.

DHPDQ gave crystals suitable for structure determination from acetonitrile-methanol solvent mixture. X-ray analysis indicated a $P2_1$ space group. Table 6.4 provides the crystal analysis data (the fractional coordinates of the asymmetric unit are provided in Tables A-9.1 to A-9.2). The molecular structure is depicted in Fig.6.4(a). Important bond lengths, angles and dihedrals are collected in Table 6.5. The bond lengths in the benzenoid ring are found to be quite similar to those found in earlier

systems. The most significant feature that this structure showed was the high twist angle, G of ~70° between the benzenoid plane and the plane containing the diaminomethylene unit. We note that the 0 angle in all the crystals in this series that we have examined lie in the range 43 - 58.2° (Table 2.1).

Table 6.4: *Crystallographic data for DHPDQ*

molecular formula	$C_{18}H_{20}N_4O_2$
morphology	plates
crystal system	orthorhombic
space group	$P2_12_12_1$
a, Å	11.761
b, Å	16.888
c, Å	8.537
α, β, γ, deg.	90.0
V, Å^3	1695.6
Z	4
ρ_{calcd}, g cm^{-3}	1.27
$\mu(CuK_\alpha)$, cm^{-1}	6.55
no. of unique reflections	1754
no. of reflections with $I \geq 2\sigma_I$	1584
R	0.037
R_w	0.053

Table 6.5: *Significant bond lengths, bond angles and dihedral angles in DHPDQfrom single crystal x-ray analysis; the atom labellings are shown in Fig. 6.4(a)*

	Distance (Å)		Angle (deg)
C(1) - C(2)	1.383	C(1) - C(7) - N(9)	118.1
C(1) - C(6)	1.389	C(1) - C(7) - N(14)	117.3
C(1) - C(7)	1.485	C(7) - N(9) - C(10)	121.3
C(2) - C(3)	1.380	C(7) - N(9) - C(13)	128.7
C(3) - C(4)	1.411	C(7) - N(14) - C(18)	121.9
C(4) - C(5)	1.395	C(7) - N(14) - C(15)	127.3
C(4) - C(8)	1.444	N(9) - C(7) - N(14)	124.6
C(5) - C(6)	1.376	C(10) - N(9) - C(13)	109.9
C(7) - N(9)	1.321	C(15) - N(14) - C(18)	110.4
C(7) - N(14)	1.322	C(1) - C(7) - N(9) - C(10)	5.6
C(8) - C(19)	1.404	C(1) - C(7) - N(14) - C(18)	12.1
C(8) - C(21)	1.381	C(2) - C(1) - C(7) - N(9)	73.9
C(19) - N(20)	1.148	C(3) - C(4) - C(8) - C(19)	11.9
C(21) - N(22)	1.158	C(5) - C(4) - C(8) - C(21)	17.5
		C(6) - C(1) - C(7) - N(14)	73.7

(a)

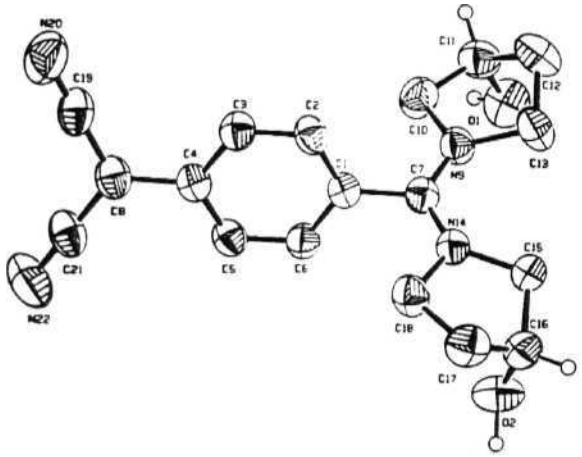

(b)

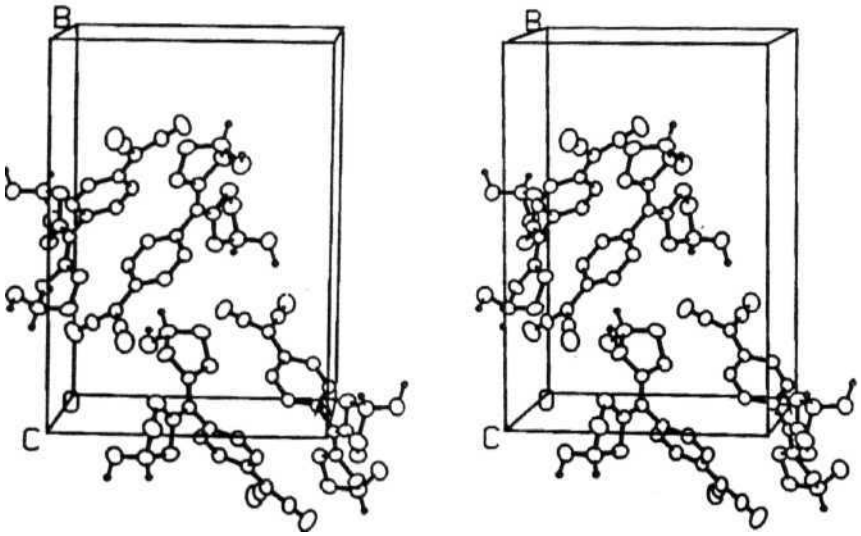

Figure 6.4: *(a) Molecular structure of DHPDQ from single-crystal x-ray analysis;* ***H atoms*** *of only the stereogenic centres and the hydroxy groups are shown (b) stereoview of the unit cell along c axis*

The exceptionally large 9 in the case of DHPDQ is therefore considered very significant and we analyse its origin and implications below.

Fig.6.4(b) shows the stereo view of the unit cell along the *c* axis. The chirality of the molecule has been effective in inducing strong deviation from an antiparallel alignment of the molecular dipoles. There are four molecules in the unit cell and the two independent interdipole vector angles are 126° and 114°. Search for short intermolecular contacts revealed four well defined H-bonds per molecule. One of the hydroxyl groups (O(1)) acts solely as a H-bond donor whereas the other hydroxyl group (O(2)) acts as a H-bond donor as well as a H-bond acceptor. The H-bond donation by O(1) is to the 0(2) of a neighbour molecule and the H-bond acceptance by 0(2) is with 0(1) of a different neighbour. This H-bonded zig-zag chain extends roughly along the *a* direction as shown in Fig.6.5(a). When O(2) acts as a H-bond donor, the acceptor is the N atom of one of the cyano groups (N(22)), and this leads to a zig-zag H-bonded chain extending roughly along the *b* axis (Fig.6.5(b)). These H-bonding pathways thus lead to an extended network in the *ab* plane.

The DHPDQ molecule, is thus tied down by four H-bonds, three on the diaminomethylene moiety and one on the dicyanomethylene moiety. It appears that these four relatively strong and highly directional interactions in the solid state are accommodated at the cost of increased dihedral twist, 9 of the molecule. We believe this to be the case since, 9 is at least 10 - 20° lower in all the non H-bonded systems of this series we have

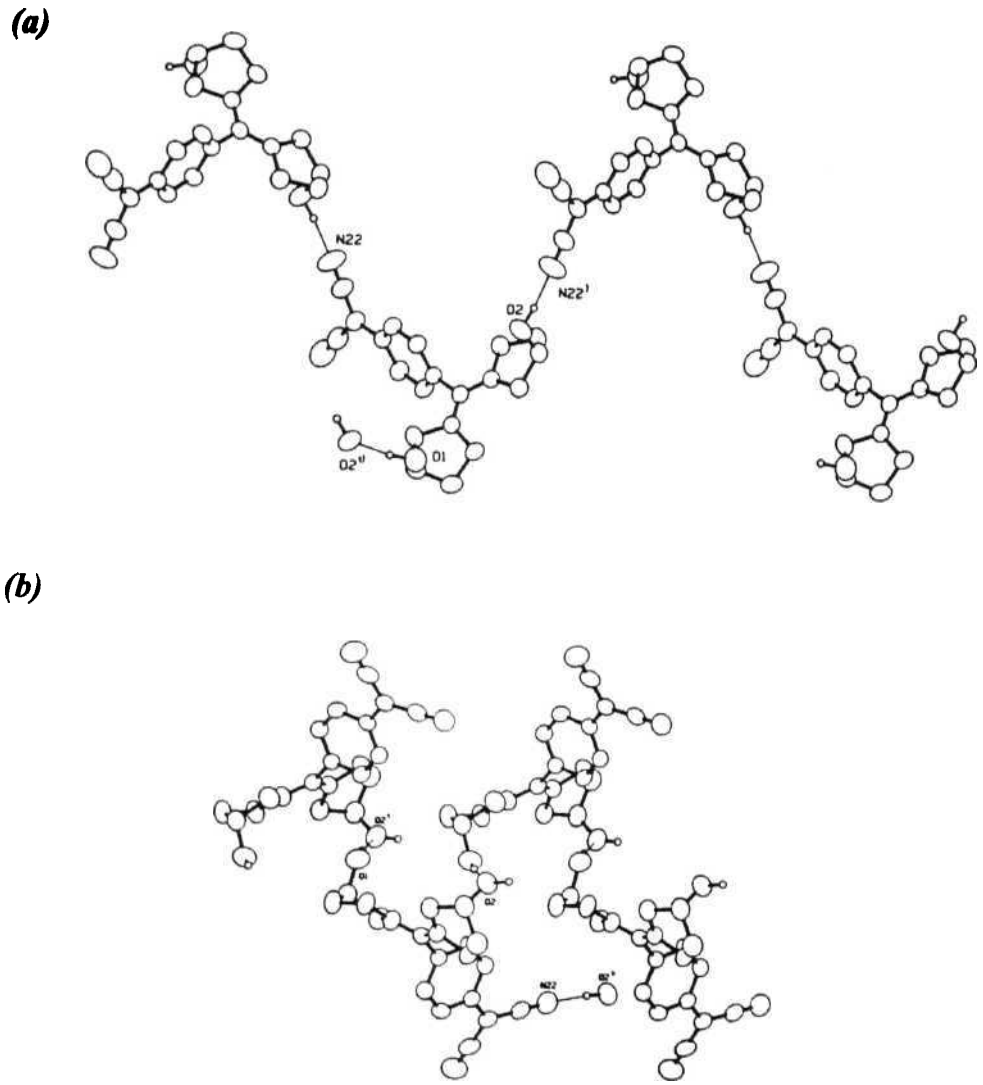

Figure 6.5: *H-bonded chains in DHPDQ (a) along a axis and (b) along b axis; the H-bonds are shown using thin lines*

investigated. Further, semiempirical AM1 calculations (Table 2.1) have predicted the twist angles in these substituted diaminodicyano-quinodimethanes to be in the range 40 - 58°; in the case of DHPDQ, the AM1 calculations indicated a dihedral twist of 56.4°.

In the computational study of DPDQ (Sec.2.4) we have observed that the lowest absorption energy, AE is strongly influenced by the value of the twist angle 0. It was seen that AE goes through a minimum at 0 ~ 54°. Experimentally we find that the solution absorption spectrum of DHPDQ and other systems are very similar; for example, the λ_{max} values in acetonitrile are respectively 388 nm and 375 nm for DHPDQ and DPDQ (Sec.3.3). This indicates that the twist angle of DHPDQ in solution must be similar to that in the other compounds. In the solid state, DPDQ and the other non-H-bonded systems have a slight yellow colour, consistent with the λ_{max} observed in the solution. However, DHPDQ crystals and powder are distinctly lighter in colour, being almost white. This we take as indicative of the slightly increased absorption energy of these molecules in the solid state, which is a consequence of the increased twist angle. Thus the H- bond tethers on the DHPDQ molecule, appear to have contributed to a higher absorption energy and hence a larger transparency window for this material in the visible range.

Our earlier computational analysis of DPDQ (Sec.2.4) has focused on the strong dependence of hyperpolarisability, β on the twist angle, 0. It was found that the β went through a maximum at 0 ~ 55°. When 0 is ~70^{o},

the p would be approximately 40% lower. The β values calculated for the crystal structure geometries of DPDQ and other systems are all approximately -50 to -54 x 10^{-30} esu. The β value calculated for the molecular structure of DHPDQ in its crystalline state is -31.3 x 10^{-30} esu. The decrease in β due to the enhanced twist is quite consistent with the trend predicted earlier. Thus we find that the H-bond matrix in crystals of DHPDQ has led to strong modification of the molecular structure which has contributed positively to the absorption energies, but negatively to the molecular hyperpolarisability. Molecular structure exerting a crucial control on the crystal structure is a commonly observed and well-studied phenomenon. The present observation however is rather a rare and interesting case where the crystal structure of a molecular material has had a profound influence on the molecular structure and hence on the molecular property. This could be described as an instance of molecular engineering through crystal design !

Powder SHG measurements were carried out on DHPDQ following similar procedures as described earlier. The SHG intensity saturated for particle sizes of ~250 μ, at about 13 U; similar SHG was found for crystals as well, indicating that this material also is phase-matchable. We believe that the H-bond has played a dual role in leading to this moderate SHG. As described above, it has exerted a strong influence on the molecular structure and hence on the molecular hyperpolarisability, the later being affected negatively. At the same time, the H-bond plays a critical role in determining the nature and rigidity of the crystal packing. In conjunction

with the molecular chirality, the intermolecular H-bonding interactions have led to a molecular packing motif wherein the dipole vectors are steered away from an antiparallel alignment. The cumulative effect of these two factors appears to dominate the observed solid state SHG. In Fig.6.6, we schematise this paradigm; we note that the novelty in our present study is the additional influence of the intermolecular H-bonding interaction on the molecular structure ( ) that is of strong consequence to the observed bulk NLO property.

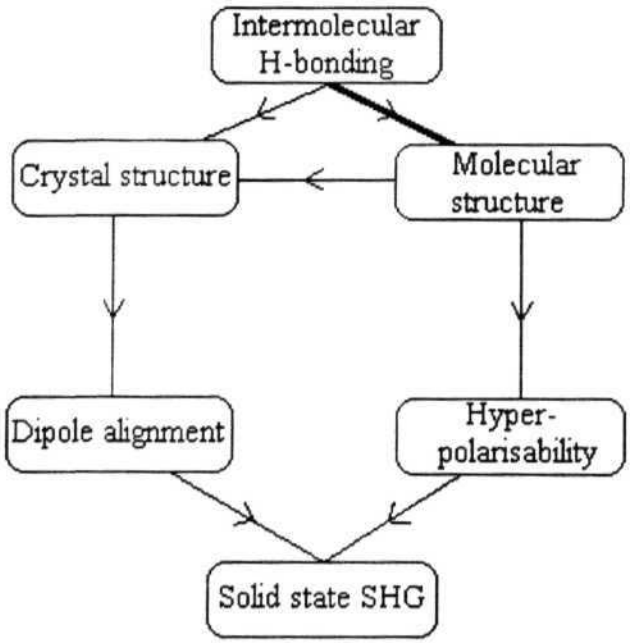

Figure 6.6: *Schematic diagram of various factors which contribute to the solid state SHG in materials*

We have examined further, the consequence of modifying the chiral nature and the intermolecular H-bond interactions in DHPDQ. First, we carried out the reaction of the racemic mixture of *3-(R)* and 3-(*S*)-hydroxypyrrolidine with TCNQ. A statistical mixture of *(R,R), (S,S)* and *(R,S)* products is expected to form. The product obtained, **13-*RS*** surprisingly showed solid state SHG, though quite weak (~1 U). This is indicative of a noncentric crystal lattice. One possible way that a noncentric lattice has formed is that an optically active product is formed by some imbalance in the statistical distribution mentioned above. However the product was found to be optically inactive ($[\alpha]_D^{29}$ (c = 0.03, MeOH) = 0°). Therefore we conclude that **13-*RS*** is indeed a racemate or meso form or mixture of both. The weak SHG obtained indicates that the H-bond interactions have led to the formation of a noncentric lattice. The mono-3-(*R*)-hydroxypyrrolidine derivative HPPDQ which is expected to have a very different H-bond network was also prepared in our laboratory. The SHG capability was found to be moderate (~ 4 U), but greatly reduced with respect to DHPDQ. This indicates the relevance of the chirality and multiple H-bond options available in DHPDQ. Since both attempts led to reduced SHG capability, and further since neither gave good crystalline material, we have not proceeded further with their investigations. We note however, that both DHPDQ-*RS* and HPPDQ had the usual light yellow colour of the push-pull quinonoid materials, in strong contrast to DHPDQ, again indicating that the unique H-bonded structure of DHPDQ and its enhanced twist angle give rise to the higher energy absorption in this interesting material.

6.4 INFLUENCE OF THE PLACEMENT OF THE STEREOGENIC CENTRE AND ENHANCED SHG IN DMPDQ (12)

In Sec.6.2 we have found that though noncentrosymmetry was achieved in MBPDQ (14), the molecular dipole vectors of adjacent NLO chromophores were nearly antiparallel. The low SHG capability of the material could be attributed to this. The derivatives **14-*R*** as well as 15 also did not show any improved SHG. The stereogenic centre in these molecules are on a side chain and the centre of symmetry in the unit cell is broken by small bond rotations rather than reorientation of the molecular dipoles. The stereogenic centre in a more rigid environment would force the near neighbour molecular dipoles to deviate further from an antiparallel arrangement. This was one of the motivations for the preparation of the PMPDQ (16) described in Sec.6.2. As anticipated, the SHG of this material showed great improvement over MBPDQ. The crystals of PMPDQ, however, showed poor refinement in the structure analysis as discussed above.

The logical extension to these investigations that we considered was the synthesis of DMPDQ (12). It was hoped that the presence of two methoxymethyl groups would create enough steric hindrance between molecules to prevent free motion of these ether chains and help in the crystal structure refinement. It was also hoped that increasing the number of stereogenic centres in a rigid framework would coax the molecular

dipoles further away from an antiparallel arrangement thus improving the solid state quadratic nonlinear optical properties.

Crystals of DMPDQ were grown from acetonitrile solution and the crystal structure analysis showed that the refinement went through smoothly in contrast to PMPDQ. The crystal belongs to the noncentric space group $P2_1$. The unit cell parameters and relevant structure analysis data are collected in Table 6.6 (the fractional coordinates of the asymmetric unit are presented in Tables A-8.1 to A-8.3). The important bond lengths, bond angles and dihedrals in the molecule are presented in Table 6.7. The bond lengths once again are clearly indicative of the benzenoid nature of the conjugation unit. The molecular structure and unit cell view along the *b* axis are shown in Fig.6.7. The molecular structure (Fig. 6.7(a) and Table 6.7) reveals that the molecular twist in DMPDQ is 54°.

Examination of interatomic distances in DMPDQ show that there are short distances of 2.501 A and 2.563A between aromatic ring H atoms and cyano group N atoms of neighbouring molecules along the *b* and *c* axes leading to molecular sheets approximately parallel to the *bc* plane. Such intermolecular interactions were not observed in MBPDQ or PMPDQ. Significantly, in none of these crystals have we found short atom-atom distances between molecules which have a non-antiparallel alignment of their dipole vectors; in DMPDQ for instance, these molecules

(a)

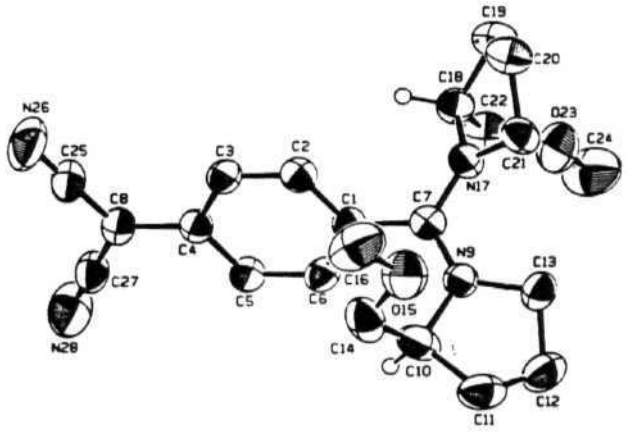

(b)

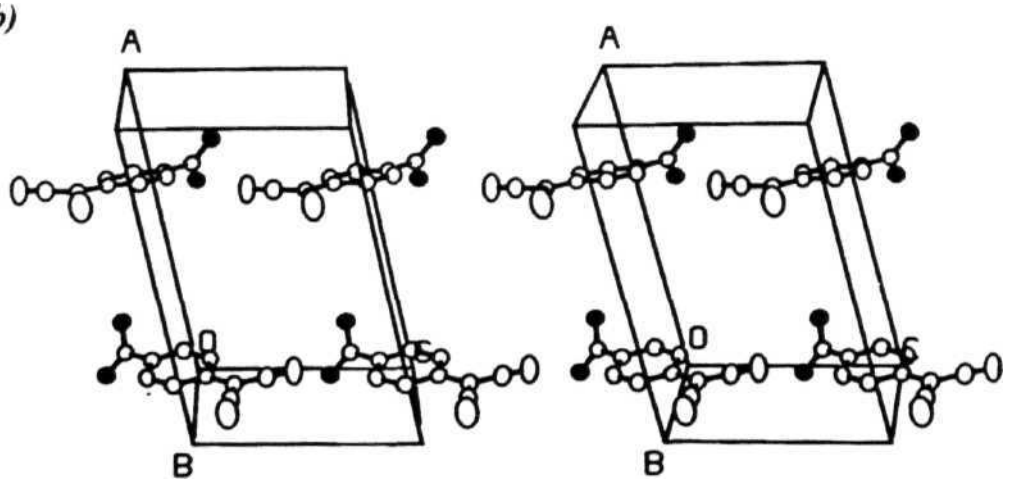

Figure 6.7: *(a) Molecular structure of DMPDQ from single-crystal x-ray analysis; H atoms of only the stereogenic centres are shown*
(b) stereoview of the unit cell along b axis; all atoms except N (shown as filled circle) of the methoxymethylpyrrolidine groups are omitted for clarity

Table 6.6: *Crystallographic data for DMPDQ*

molecular formula	$C_{22}H_{28}N_4O_2$
morphology	cubes
crystal system	monoclinic
space group	$P2_1$
a, Å	13.902(3)
b, Å	8.311(4)
c, Å	9.203(2)
β, deg.	102.26(1)
V, $Å^3$	1039.1(7)
Z	2
ρ_{calcd}, g cm^{-3}	1.22
$\mu(CuK_\alpha)$, cm^{-1}	6.01
no. of unique reflections	2115
no. of reflections with $I \geq 2\sigma_I$	2059
R	0.034
R_w	0.054

form neighbours along the *a* axis. This non-antiparallel alignment is **crucial for the bulk** NLO property and therefore it appears that the C-H···N intermolecular interactions do not to have any direct bearing on the SHG efficiencies **of** these materials, even though they perhaps exert a strong **stabilising** influence in the crystal packing in **DMPDQ.**

Table 6.7: *Significant bond lengths, bond angles and dihedral angles in DMPDQfrom single crystal x-ray analysis; the atom labellings are shown in Fig. 6.7 (a)*

	Distance (Å)		Angle (deg)
C(1) - C(2)	1.399	C(1) - C(7) - N(9)	121.7
C(1) - C(6)	1.398	C(1) - C(7) - N(17)	118.9
C(1) - C(7)	1.468	C(7) - N(9) - C(10)	124.3
C(2) - C(3)	1.377	C(7) - N(9) - C(13)	124.3
C(3) - C(4)	1.407	C(7) - N(17) - C(18)	123.5
C(4) - C(5)	1.407	C(7) - N(17) - C(21)	125.7
C(4) - C(8)	1.441	N(9) - C(7) - N(17)	119.3
C(5) - C(6)	1.377	C(10) - N(9) - C(13)	111.4
C(7) - N(9)	1.324	C(18) - N(17) - C(21)	110.7
C(7) - N(17)	1.339	C(1) - C(7) - N(9) - C(10)	20.4
C(8) - C(25)	1.399	C(1) - C(7) - N(17) - C(18)	33.4
C(8) - C(27)	1.392	C(2) - C(1) - C(7) - N(17)	53.8
C(25) - N(26)	1.146	C(3) - C(4) - C(8) - C(25)	4.7
C(27) - N(28)	1.155	C(5) - C(4) - C(8) - C(27)	3.7
		C(6) - C(1) - C(7) - N(9)	54.2

The SHG capability of DMPDQ was determined using the Kurtz - Perry powder method and gave the highest value ~ 55 U in this series of push-pull quinonoid systems, for powders with particle sizes in the range 50 - 200 μ. The saturation of the SHG intensity at higher particle sizes indicated that the material is phase-matchable. Examination of the crystal packing (Fig.6.7(b)) reveals that the dipoles of molecules stacked along the *a* axis are nearly perpendicular to each other, with the intervector angle being 103°. This is the strongest deviation from an antiparallel alignment achieved in this class of strongly zwitterionic diamino substituted dicyanoquinodimethanes and appears to be the basis for the strong solid state SHG observed. We present below a semi-quantitative analysis of the correlation between the solid state SHG and the molecular and crystal features in this class of push-pull quinonoids.

We have collected in Table 6.8. the inter vector angle, a between the near neighbour molecular dipoles (defined in Sec.6.1) in MBPDQ, PMPDQ, DHPDQ and DMPDQ; these are the systems which have shown strong solid state SHG and where crystal structure analysis have been carried out. It may be noted that MBPDQ and DMPDQ have only two molecules in the unit cell and the inter vector angle is unique. In PMPDQ and DHPDQ, there are four molecules per unit cell, and hence two inequivalent inter vector angles. If we assume that the polar axis of the crystals is along the net dipole vector of the molecules in the unit cell, the angle between this unique axis and the molecular dipoles are 84° in MBPDQ, 27.5° and 121.5° in PMPDQ, 6.1° and 119.6° in DHPDQ and

51.5° in DMPDQ. It is noteworthy that the angle in DMPDQ is quite close to the optimal angle for efficient SHG found in NPP. Table 6.8 also provides the calculated P(0) values (AM1) for the four molecules using the molecular structures obtained from the x-ray analysis. It is found that the p (0) of MBPDQ, PMPDQ and DMPDQ are nearly the same and that of DHPDQ is smaller for reasons discussed in Sec.6.3. Significantly, the solid state SHG capabilities show profound changes. A simple model of vector addition may be used to obtain a semi-quantitative understanding of the influence of the angle, a on the bulk SHG capability. The sum of two vectors with magnitude p and having an inter vector angle a, can easily be shown to be $f\beta$ where,/= $\{2(1+\cos\alpha)\}^{1/2}$. When two or more vectors are to be added to a vector, the relevant intervector angles, α_i, have to be used and this factor can be calculated by successive application of the above equation *ie.*,*f*= $\Pi\ \{2(1+\cos\alpha_i)\}$. The enhancement or reduction factor,/ for the four materials are also presented in Table 6.8; in the case of PMPDQ and DHPDQ, since there are four molecules each in the unit cell, we have taken into account, the addition of three vectors successively to an arbitrarily chosen initial vector.

The increased rigidity of the stereogenic centre environment appears to have improved the / factor on going from MBPDQ to PMPDQ. The increase in such centres leads to the highest value of / in DMPDQ. In DHPDQ, even though the number of stereogenic centres is similar to that in DMPDQ, the factor is only comparable to that in PMPDQ, presumably

because the stereogenic centres are further removed by a C atom, from the dipole axis; the H-bonding interactions of course complicate

Table 6.8: *The static β values, inter dipole vector angles, afrom crystal structure analysis, the computed enhancement/reduction factor, f andhe powder SHG values for four SHG active compounds*

compound	-β(0) (10^{-30} esu)	α (deg.)	*f*	*f*|β(0)| (10^{-30} esu)	powder SHG (U)
MBPDQ	51.0	168	0.21	10.7	3
DHPDQ	31.3	126, 114	0.89	27.8	13
PMPDQ	51.4	94, 149	0.99	50.4	28
DMPDQ	50.2	103	1.25	62.8	55

the picture further. Since the p values of MBPDQ, PMPDQ and DMPDQ are nearly the same, the SHG intensities of these materials follow the trend of/ illustrating the crucial influence of the dipole alignment on the NLO characteristic of the bulk material. Since DHPDQ has a different β value, to make a general comparison of all the compounds, we have to consider the /[3 values (since the sign is not relevant, we consider only the magnitudes of P). It is seen that the good *f* factor in DHPDQ is partially offset by its reduced β and leads to an *f*β value intermediate between MBPDQ and PMPDQ. We recall that the intermolecular H-bonding present in DHPDQ strongly influence both these factors, the *f* through the

direct effect on the crystal structure and (3 through the impact on the molecular structure. The solid state SHG observed in the four materials is now seen to have an excellent correlation to the $f\beta$ values. Fig.6.8 illustrates this elegant simple correlation. We believe that this empirical analysis provides a simple and semiquantitative basis for the commonly utilised dissection of the bulk NLO effect of molecular materials into the molecular and crystal packing contribution. Though the spirit behind this

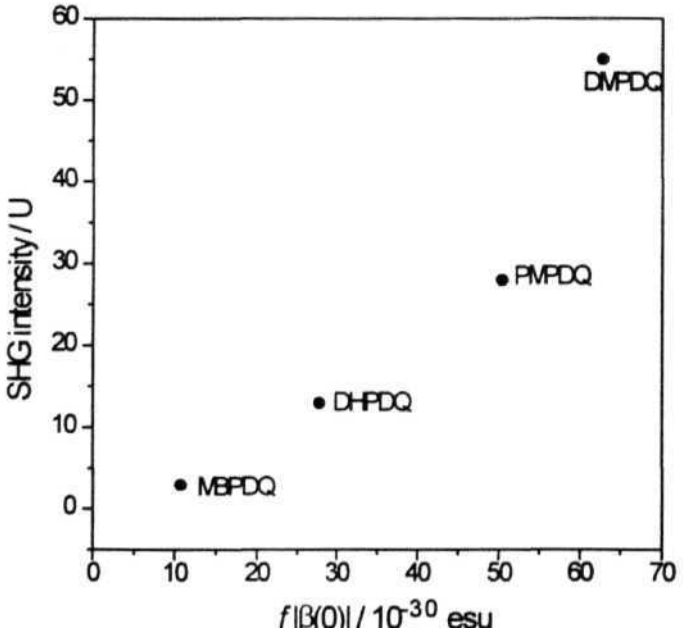

Figure 6.8: *The correlation of fβ with solid state SHG in four compounds DMPDQ (**12**), DHPDQ (**13**), MBPDQ (**14**) and PMPDQ (**16**)*

is the same as that in the oriented gas model, the treatment is simpler (and admittedly less rigorous) and directly useful for experimentalists working on a class of related systems.

6.5 CONCLUSION

We have presented in this Chapter the crystal structure details and powder SHG studies of MBPDQ, PMPDQ. DHPDQ and DMPDQ. DHPDQ is a unique entry in the sense that this material illustrated novel effects of intermolecular H-bonding that could be crucial to the fabrication of SHG active materials. DMPDQ is found to have the highest powder second harmonic generation capability (~ 55 U) in the series and this is in good accord with the progression of inter dipole vector angles towards an orthogonal orientation in this family of crystals. The improvement in the alignment of dipoles was achieved by controlling the placement of the stereogenic centres in these compounds. This opens up new avenues of investigation for the generation of noncentric crystal lattices of fundamental interest in the design of quadratic NLO molecular materials.

The ease of synthesis and crystallisation, transparency through most of the visible window, good thermal stability upto ~ 250°C and strong phase-matchable second harmonic generation are the positive features of the new molecular materials that we have presented here. These aspects should make this class of compounds, a significant entry into the field of

crystalline molecular materials with potential quadratic NLO applications. Though a variety of materials based on thin films, polymers *etc.* showing strong NLO characteristics have been reported in the literature, we believe that crystalline materials will continue to play an important role in the development of advanced materials and molecular devices because of the advantage they offer in terms of a direct insight into the structural aspects that is vital for fine tuning and improving the physical properties.

REFERENCES

1. Nicoud, J.-F.; Twieg, R.J. in *Nonlinear Optical Properties of Organic Molecules and Crystals;* Chemla, D.S.; Zyss, J. (Eds) Academic Press, New York, 1987, Vol.2, p. 221.
2. Twieg, R.J.; Azema, A.; Jain, K.; Cheng, Y.Y. *Chem. Phys. Lett.* **1982,** *92,* 208.
3. Heitler, L.R.; Hartzler, H.D.; Acker, D.S.; Benson, R.E. *J. Am. Chem. Soc.* **1962**, *84*, 3387.
4. Nicoud, J.F. *Mol. Cryst. Liq. Cryst.* **1988,***156,* 257.
5. Twieg, R.J.; Moret, E.; Jain, K. *IBM Tech. Dis. Bull* **1983,** *26,* 422.
6. Desiraju, G.R *Crystal Engineering: The Design of Organic Solids* Elsevier, Amsterdam, 1989.
7. Nicoud. J.-F.: Twieg, R.J. in *Nonlinear Optical Properties of Organic Molecules and Crystals;* Chemla, D.S.; Zyss, J. (Eds) Academic Press, New York, 1987, Vol.1, p. 259.
8. Zyss, J.; Nicoud, J.F.; Coquillay, M. *J. Chem. Phys.* **1984,** *81,* **4160.**
9. Bhattacharya, S.; Dastidar, P.; Guru Row, T.N. *Chem. Mater.* **1994,** *6*, 531.
10. Aakeroy, B.C.; Bahra, G.S.; Hitchcock, P.B.; Patell, Y.; Seddon, K.R. *J. Chem. Soc, Chem. Commun.* **1993,** 152.
11. Fuller, J.; Carlin, R.T.; Simpson, L.J.; Furtak, T.E. *Chem. Mater.* **1995,** 7, 909.
12. Huang, K.; Britton, D.; Etter, M.C.; Byrn, S.R. *J. Mater. Chem.* **1995,** *5,* 379

13. Knossow, M.; Mauguen, Y.; de Rango, C. *Cryst. Struct. Commun.* 1976,5,719.

14. Sarma, J.A.R.P.; Laxmikanth Rao, J.; Bhanuprakash, K. *Chem. Mater.* 1995, 7, 1843.

CHAPTER 7

OVERVIEW OF THE PRESENT WORK AND FUTURE PROSPECTS

Molecular materials are becoming increasingly important in the field of nonlinear optics. A large number of organic, organometallic and polymeric systems have been developed over the past several years. Though the molecular systems surpass conventional materials with regard to the efficiency and speed of the NLO responses, several problems such as mechanical and thermal stabilities, transparency *etc.* remain so that they are as yet not fully optimised for technological applications. Therefore the search for new materials in this area continues to be a fascinating and challenging problem.

We have presented in this thesis, a systematic investigation of a new class of molecular materials, diamino substituted dicyanoquinodimethanes, which are shown to be potential candidates for quadratic NLO applications; we have demonstrated in particular, the second harmonic generation capability of these materials. Though a wide variety of molecular structures have been investigated in the past for SHG applications, we are not aware of any previous detailed investigation of quinonoid molecular materials in this connection. Semiempirical computational studies we have carried out on these molecules revealed that they possess large molecular hyperpolarisabilities in view of the relatively small size of these molecules. These studies also provided useful insight into the influence of the molecular structure on the molecular nonlinear response. These computational studies led us to synthesise several members of this novel class of push-pull molecules and investigate experimentally their solid state SHG capability.

The theoretical analysis of the correlation of (3 to the quinonoid-benzenoid character of these molecules suggests ways to fine-tune the molecular hyperpolarisabilities of these formally quinonoid molecules by adjusting the push-pull effect. Another significant result from the semiempirical computational study is that the (3 as a function of the molecular twist goes through a maximum at the angle corresponding to the optimal geometry. The fact that most of these molecules manifest their highest possible values of β at the twist angle observed in their crystals is very encouraging for continuing efforts in the development of these molecular materials. The large computed hyperpolarisabilities of these molecules are supported by the results of the simple solvatochromic estimation of β_{2level} on several systems and calibration studies on a prototypical molecule by the EFISHG method.

At the material level, these push-pull quinonoid systems are found to have several positive features. They are very easy to synthesise; only one or two steps are involved in all the cases. Further, the synthetic protocol is amenable to the introduction of a wide variety of substituents. Due to their zwitterionic nature, their crystals possess strong electrostatic binding forces which leads to high thermal stability with typical melting points in the range 200 - 250°C; in this respect these materials are superior to most of the well known organic NLO materials. These compounds are transparent in most of the visible range (the λ_{max} and cutoff wavelengths are typically about 400 nm and 500 nm respectively). Therefore they are of potential interest in the fabrication of devices in the visible range.

The achiral compounds in this series have all crystallised in centrosymmetric crystal lattice and thus showed no SHG. This could be the result of the large ground state dipole moments of these molecules. We have however observed an interesting phenomenon of solvate switchable SHG in one of the polymorphic forms of the achiral derivative, DPDQ; this may have potential sensor applications. Introduction of chiral groups led to the successful preparation of noncentrosymmetric crystals in several candidates, such as MBPDQ, DHPDQ, PMPDQ and DMPDQ. They are found to have moderate to strong phase-matchable SHG capability ranging from 3 U - 55 U. The synthesis and investigation of these materials have not only led to the development of strongly SHG active novel molecular materials, but also revealed important aspects of material design. The crucial aspect of the placement of the stereogenic centre in these molecules that leads to improved dipole alignment and increased SHG has been analysed in terms of an enhancement/reduction factor. An interesting case of the dual influence of intermolecular H-bonding on molecular and crystal structure together determining the bulk SHG has been demonstrated in one of the systems.

The simplicity of the synthesis of these push-pull quinonoid compounds allows a wide variety of new derivatives to be prepared for further investigations on these materials. A new series of compounds currently under investigation in our laboratory involves generation of axial chirality in the molecule by appropriate derivatisation. Such an approach has not been attempted, to the best of our knowledge in the fabrication of

molecular NLO materials. Another interesting recent observation in the ongoing work in our laboratory is the strong SHG from push-pull quinonoid materials having moderately long alkyl chains on the amino groups. The origin of noncentricity in these basically achiral systems is under investigation. This may open up new approaches to the problem of generating noncentric crystal lattices. Recently there has been a report of SHG observed in a condensation product between tetracyanoethylene (TCNE) and bridged ferrocene dimer.[1] It would be interesting to synthesise the corresponding compound with TCNQ in place of TCNE; the topology of the product would be quite crucial in determining its NLO properties.

Another synthetic variation on the push-pull quinonoid compounds that would be interesting to study is the replacement of the TCNQ by related acceptors with shorter extent of conjugation such as TCNE and those with longer extent of conjugation such as the tetracyano derivatives of 9,10- or 2,6-anthraquinodimethane. " We note that some donor substitutions on TCNE have been carried out to create push-pull olefines, by earlier workers and their NLO properties investigated briefly.` In view of the investigations we have carried out on the TCNQ-derived systems, further exploration of these TCNE derived systems may be warranted.

The crystals of the various push-pull quinonoid compounds that we have grown were adequate for x-ray structure analysis. However, their relatively small sizes do not permit detailed investigations of the nonlinearity tensor components, the phase-matching directions, electro-optic

effects *etc*.. Crystal growth using specialised techniques are being planned in our laboratory. Of late, there has been enormous interest in the fabrication of Langmuir-Blodgett films of NLO chromophores. The push-pull quinonoid compounds with long chain amines are easily prepared following the synthetic protocols we have used. Preparation of LB films of these systems are under way in our laboratory. We note that LB films of some related compounds recently studied by Ash well *et at* have shown promising NLO properties. Doped polymers are known to be efficient NLO systems considering their large figure of merit and are suitable for device applications. The push-pull quinonoid molecules are suitable candidates for doping into polymers and electric field poling, in view of the high thermal stabilities of these chromophores. Incorporation of these molecules into suitable polymer host matrices through covalent linkage and subsequent poling to create robust NLO materials would also be a promising approach.

The discussion presented above shows that the investigations presented in this thesis have led to the fabrication of a new class of molecular materials capable of efficient SHG with great potential for further development and ultimately, perhaps technological application.

REFERENCES

1. Benito, A.; Cano, J.; Martinez-Manez, R.; Paya, J.; Soto, J.; Julve, M.; LlQret, F.; Marcos, M.D.; Sinn, E. *J. Chem. Soc, Dalton Trans.* **1993**, 1999.
2. Kini, A.M.; Cowan, D.O.; Gerson, F.; Mockel, R. *J. Am. Chem. Soc.* **1985,***107,* 556.
3. Yanagimoto, T.; Takimiya, K.; Otsubo, T.; Ogura, F. *J. Chem. Soc, Chem. Commun.* **1993,** 519.
4. Adhikesavulu, D.; Kamath, N.U.; Venkatesan, K. *Proc Indian Acad. Sci. (Chem. Sci.)***1983**,*92,* 449.
5. *Nonlinear Optical Properties of Organic Molecules and Crystals,* Chemla, D.S.; Zyss, J. (Eds), Academic Press, New York, 1987, p.247.
6. Ashwell, G.J.; Dawnay, E.J.C.; Kuczynski, A.P.; Szablewski, M.; Sandy, I.M. *J. Chem. Soc, Faraday Trans.* **1990,** *86,* 1117.
7. (a) Eaton, D.F. *Science* **1991,** *253,* 281. (b) Marder, S.R.; Perry, J.W. *Science* **1994,** *263,* 1706.

APPENDIX

Table A-1.1: ***Atomic coordinates and equivalent*** *isotropic* ***displacement parameters for DPIDQ (9).*** U_{eq} ***is defined as one third*** *of the trace of* ***the orthogonalised*** U_{ij} *tensor* (e.s.d's are in parantheses)

Atom	x/a	y/b	z/c	U_{eq}
Molecule A				
C(1)	0.6735(1)	0.44307(8)	0.5709(2)	3.41(4)
C(2)	0.6158(1)	0.47805(8)	0.4510(2)	3.72(5)
C(3)	0.5459(1)	0.4268(1)	0.3145(2)	3.97(5)
C(4)	0.5298(1)	0.33756(9)	0.2903(2)	3.72(5)
C(5)	0.5898(1)	0.30326(8)	0.4102(2)	3.85(5)
C(6)	0.6594(1)	0.35469(9)	0.5464(2)	3.79(5)
C(7)	0.7445(1)	0.49869(8)	0.7197(2)	3.31(4)
C(8)	0.4549(1)	0.2840(1)	0.1483(2)	4.44(5)
N(9)	0.80754(9)	0.56450(7)	0.7080(1)	3.73(4)
C(10)	0.8560(1)	0.5584(1)	0.5744(2)	4.50(5)
C(11)	0.8422(1)	0.6318(1)	0.4936(2)	5.60(7)
C(12)	0.8766(2)	0.7163(1)	0.6172(2)	6.60(8)
C(13)	0.8230(2)	0.7189(1)	0.7493(2)	6.34(8)
C(14)	0.8404(1)	0.6458(1)	0.8308(2)	4.76(6)
N(15)	0.74390(8)	0.48395(7)	0.8633(1)	3.46(4)
C(16)	0.8334(1)	0.5130(1)	1 0092(2)	4.34(5)
C(17)	0.8554(1)	0.4414(1)	1 0932(2)	5.09(6)
C(18)	0.7615(1)	0.4027(1)	1 1309(2)	5.27(6)
C(19)	0.6743(1)	0.3709(1)	0.9767(2)	4.83(6)
C(20)	0.6511(1)	0.44283(9)	0.8945(2)	3.97(5)
C(21)	0.4020(1)	0.3188(1)	0.0242(2)	5.24(6)
N(22)	0.3590(1)	0.3490(1)	-0.0768(2)	7.39(7)
C(23)	0.4327(1)	0.1957(1)	0.1322(2)	5.03(6)
N(24)	0.4164(1)	0.1232(1)	0.1232(2)	6.96(7)
Molecule B				
C(1')	0.1560(1)	0.08195(8)	0.7435(2)	3.26(4)
C(2')	0.0538(1)	0.04178(8)	0.7006(2)	3.47(5)
C(3')	-0.0263(1)	0.08760(9)	0.6847(2)	3.57(5)
C(4')	-0.0093(1)	0.17684(8)	0.7128(1)	3.23(4)
C(5')	0.0945(1)	0.21679(8)	0.7587(2)	3.38(4)

Table A-1.1 (contd...)

C(6')	0.1742(1)	0.17057(8)	0.7720(2)	3.45(4)
C(7')	0.2420(1)	0.03305(8)	0.7542(2)	3.23(4)
C(8')	-0.0935(1)	0.22466(9)	0.6945(2)	3.78(5)
N(9')	0.24635(9)	-0.02757(7)	0.8364(1)	3.71(4)
C(10')	0.2050(1)	-0.0237(1)	0.9770(2)	4.57(6)
C(11')	0.1311(1)	-0.1031(1)	0.9577(2)	5.41(7)
C(12')	0.1803(2)	-0.1821(1)	0.9225(2)	6.15(8)
C(13')	0.2209(2)	-0.1827(1)	0.7771(3)	6.53(8)
C(14')	0.2959(1)	-0.1032(1)	0.8001(2)	5.12(6)
N(15')	0.31364(8)	0.05055(7)	0.6805(1)	3.51(4)
C(16')	0.4219(1)	0.0367(1)	0.7334(2)	4.65(6)
C(17')	0.4941(1)	0.1172(1)	0.7497(2)	5.70(7)
C(18')	0.4725(1)	0.1498(1)	0.5975(2)	5.81(7)
C(19')	0.3607(1)	0.1613(1)	0.5438(2)	4.99(6)
C(20')	0.2893(1)	0.0805(1)	0.5295(2)	4.04(5)
C(21')	-0.1958(1)	0.1827(1)	0.6525(2)	4.28(5)
N(22')	-0.2781(1)	0.1450(1)	0.6175(2)	6.11(6)
C(23')	-0.0767(1)	0.3130(1)	0.7107(2)	4.50(6)
N(24')	-0.0617(1)	0.3857(1)	0.7246(2)	6.64(7)

Table A-1.2: *Hydrogen coordinates and isotropic displacement parameters for DPIDQ (9)*

Atom	x/a	y/b	z/c	U_{eq}
Molecule A				
H(2)	0.6250	0.5381	0.4641	4.5
H(3)	0.5076	0.4520	0.2345	4.8
H(5)	0.5820	0.2432	0.3967	4.6
H(6)	0.6987	0.3296	0.6258	4.5
H(101)	0.9279	0.5581	0.6167	5.4
H(102)	0.8255	0.5068	0.4956	5.4
H(111)	0.8823	0.6291	0.4187	6.7
H(112)	0.7712	0.6275	0.4372	6.7

Table A-1.2 (contd...)

H(121)	0.9493	0.7239	0.6642	7.9
H(122)	0.8598	0.7609	0.5647	7.9
H(131)	0.8492	0.7711	0.8288	7.6
H(132)	0.7509	0.7159	0.7029	7.6
H(141)	0.8012	0.6472	0.9067	5.7
H(142)	0.9118	0.6500	0.8856	5.7
H(161)	0.8925	0.5316	0.9781	5.2
H(162)	0.8188	0.5589	1.0820	5.2
H(171)	0.8775	0.3984	1.0245	6.1
H(172)	0.9088	0.4632	1.1918	6.1
H(181)	0.7777	0.3565	1.1789	6.3
H(182)	0.7410	0.4446	1.2043	6.3
H(191)	0.6936	0.3270	0.9057	5.8
H(192)	0.6143	0.3490	1.0019	5.8
H(201)	0.6262	0.4843	0.9623	4.8
H(202)	0.5994	0.4208	0.7940	4.8
Molecule B				
H(2')	0.0395	-0.0184	0.6820	4.2
H(3')	-0.0952	0.0583	0.6539	4.3
H(5')	0.1095	0.2771	0.7808	4.1
H(6')	0.2433	0.1994	0.8013	4.1
H(101')	0.2609	-0.0170	1.0718	5.5
H(102')	0.1696	0.0240	0.9882	5.5
H(111')	0.1117	-0.1004	1.0551	6.5
H(112')	0.0713	-0.1064	0.8704	6.5
H(121')	0.2358	-0.1820	1.0141	7.4
H(122')	0.1301	-0.2314	0.9003	7.4
H(131')	0.2551	-0.2307	0.7601	7.8
H(132')	0.1643	-0.1869	0.6844	7.8
H(141')	0.3160	-0.1044	0.7036	6.1
H(142')	0.3553	-0.1000	0.8876	6.1
H(161')	0.4345	0.0220	0.8353	5.6
H(162')	0.4338	-0.0083	0.6554	5.6
H(171')	0.4866	0.1600	0.8358	6.8
H(172')	0.5631	0.1058	0.7747	6.8

Table A-1.2 (contd...)

H(181')	0.5154	0.2030	0.6180	7.0
H(182')	0.4873	0.1101	0.5137	7.0
H(191')	0.3483	0.2063	0.6212	6.0
H(192')	0.3471	0.1753	0.4412	6.0
H(201')	0.2964	0.0374	0.4436	4.9
H(202')	0.2200	0.0914	0.5058	4.9

Table A-2.1: *Atomic coordinates and equivalent isotropic displacement parameters for DPZDQ (**10**)*

Atom	x/a	y/b	z/c	U_{eq}
Molecule A				
C(1)	0.1531(1)	0.57475(8)	0.2278(1)	2.77(4)
C(2)	0.1808(1)	0.66633(8)	0.2604(2)	3.01(4)
C(3)	0.1065(1)	0.71925(8)	0.2631(1)	2.93(4)
C(4)	0.0003(1)	0.68369(8)	0.2309(1)	2.80(4)
C(5)	-0.0275(1)	0.59107(8)	0.1965(2)	3.06(4)
C(6)	0.0470(1)	0.53862(8)	0.1951(1)	2.88(4)
C(7)	0.2316(1)	0.51714(8)	0.2254(1)	2.87(4)
C(8)	-0.0795(1)	0.73783(9)	0.2309(2)	3.21(4)
N(9)	0.30585(8)	0.53325(7)	0.1539(1)	3.24(4)
C(10)	0.4087(1)	0.5040(1)	0.1981(2)	4.20(5)
C(11)	0.4955(1)	0.5808(1)	0.2254(2)	5.02(6)
N(12)	0.4810(1)	0.6195(1)	0.0826(2)	5.02(5)
C(13)	0.3835(1)	0.6540(1)	0.0489(2)	4.69(6)
C(14)	0.2927(1)	0.5793(1)	0.0173(2)	3.66(5)
N(15)	0.22633(8)	0.44719(7)	0.2956(1)	3.21(4)
C(16)	0.1910(1)	0.4465(1)	0.4402(2)	3.66(5)
C(17)	0.1004(1)	0.3711(1)	0.4105(2)	3.94(5)
N(18)	0.1183(1)	0.28576(8)	0.3392(2)	4.35(5)
C(19)	0.1569(1)	0.2911(1)	0.2012(2)	4.37(5)
C(20)	0.2531(1)	0.3625(1)	0.2344(2)	4.00(5)
C(21)	-0.0584(1)	0.8295(1)	0.2406(2)	3.74(5)

Table A-2.1 (contd...)

N(22)	-0.0413(1)	0.90435(9)	0.2477(2)	5.57(6)
C(23)	-0.1841(1)	0.6990(1)	0.2088(2)	3.62(5)
N(24)	-0.2686(1)	0.6650(1)	0.1912(2)	5.53(6)
Molecule B				
C(1')	0.6629(1)	0.93809(8)	1.0590(2)	3.18(4)
C(2')	0.6111(1)	0.97780(8)	0.9368(2)	3.47(4)
C(3')	0.5422(1)	0.92797(9)	0.7947(2)	3.57(5)
C(4')	0.5202(1)	0.83545(8)	0.7682(2)	3.25(4)
C(5')	0.5753(1)	0.79602(8)	0.8900(2)	3.46(5)
C(6')	0.6453(1)	0.84603(9)	1.0313(2)	3.42(4)
C(7')	0.7315(1)	0.99153(8)	1.2135(2)	3.04(4)
C(8')	0.4449(1)	0.7845(1)	0.6218(2)	3.68(5)
N(9')	0.79737(9)	1.06348(7)	1.2126(1)	3.36(4)
C(10')	0.8513(1)	1.0678(1)	1.0877(2)	4.10(5)
C(11')	0.8422(1)	1.1513(1)	1.0225(2)	5.14(6)
N(12')	0.8722(1)	1.2317(1)	1.1485(2)	5.49(5)
C(13')	0.8155(1)	1.2235(1)	1.2653(2)	4.99(6)
C(14')	0.8289(1)	1.1433(1)	1.3417(2)	4.04(5)
N(15')	0.72605(8)	0.96957(7)	1.3521(1)	3.20(4)
C(16')	0.6307(1)	0.92095(9)	1.3736(2)	3.58(5)
C(17')	0.6553(1)	0.8410(1)	1.4456(2)	4.20(5)
N(18')	0.7407(1)	0.8625(1)	1.5959(2)	4.72(5)
C(19')	0.8329(1)	0.9137(1)	1.5761(2)	4.47(5)
C(20')	0.8140(1)	0.9947(1)	1.5045(2)	3.84(5)
C(21')	0.3986(1)	0.8260(1)	0.4973(2)	3.94(5)
N(22')	0.3631(1)	0.8627(1)	0.3968(2)	5.44(5)
C(23')	0.4180(1)	0.6921(1)	0.5999(2)	4.43(6)
N(24')	0.3973(1)	0.6170(1)	0.5856(2)	6.57(7)

Table A-2.2: *Hydrogen coordinates and isotropic displacement parameters for DPZDQ (10)*

Atom	x/a	y/b	z/c	Ueq
Molecule A				
H(2)	0.2525	0.6925	0.2812	3.6
H(3)	0.1278	0.7815	0.2872	3.5
H(5)	-0.0992	0.5646	0.1738	3.7
H(6)	0.0263	0.4764	0.1717	3.5
H(101)	0.4170	0.4812	0.2940	5.0
H(102)	0.4100	0.4591	0.1124	5.0
H(111)	0.4948	0.6243	0.3149	6.0
H(112)	0.5617	0.5615	0.2488	6.0
H(N12)	0.5430	0.6624	0.1045	6.0
H(131)	0.3846	0.6972	0.1394	5.6
H(132)	0.3757	0.6798	-0.0437	5.6
H(141)	0.2890	0.5386	-0.0781	4.4
H(142)	0.2290	0.6025	0.0022	4.4
H(161)	0.2481	0.4400	0.5269	4.4
H(162)	0.1683	0.5006	0.4683	4.4
H(171)	0.0882	0.3671	0.5114	4.8
H(172)	0.0394	0.3843	0.3396	4.8
H(N18)	0.1713	0.2672	0.4245	5.2
H(191)	0.1751	0.2359	0.1666	5.2
H(192)	0.1018	0.3028	0.1170	5.2
H(201)	0.2711	0.3645	0.1371	4.8
H(202)	0.3109	0.3499	0.3129	4.8
Molecule B				
H(2')	0.6236	1.0402	0.9516	4.2
H(3')	0.5086	0.9569	0.7127	4.3
H(5')	0.5642	0.7336	0.8749	4.1
H(6')	0.6823	0.8175	1.1112	4.1
H(101')	0.9237	1.0657	1.1331	4.9
H(102')	0.8240	1.0185	1.0008	4.9
H(111')	0.8866	1.1553	0.9546	6.2
H(112')	0.7710	1.1481	0.9605	6.2
H(N12')	0.9516	1.2348	1.2042	6.6

Table A-2.2 (contd...)

H(131')	0.8398	1.2748	1.3492	6.0
H(132')	0.7427	1.2200	1.2127	6.0
H(141')	0.7857	1.1401	1.4115	4.8
H(142')	0.9006	1.1478	1.4024	4.8
H(161')	0.6046	0.9589	1.4440	4.3
H(162')	0.5786	0.9020	1.2712	4.3
H(171')	0.5937	0.8142	1.4657	5.0
H(172')	0.6742	0.8007	1.3692	5.0
H(N18')	0.7128	0.8951	1.6702	5.7
H(191')	0.8836	0.9326	1.6797	5.4
H(192')	0.8606	0.8763	1.5071	5.4
H(201')	0.8760	1.0191	1.4826	4.6
H(202')	0.7965	1.0371	1.5793	4.6

Table A-3.1: *Atomic coordinates and equivalent isotropic displacement parmeters for DMDQ (11)*

Atom	x/a	y/b	z/c	U_{eq}
C(1)	0.7197(1)	0.25024(8)	0.1274(2)	2.89(5)
C(2)	0.6682(1)	0.17290(8)	0.0638(2)	3.05(5)
C(3)	0.5625(1)	0.15562(8)	0.0648(2)	3.00(5)
C(4)	0.5027(1)	0.21387(8)	0.1311(1)	2.87(5)
C(5)	0.5563(1)	0.29097(8)	0.1971(2)	3.09(5)
C(6)	0.6616(1)	0.30879(8)	0.1943(2)	3.02(5)
C(7)	0.8327(1)	0.26909(8)	0.1261(1)	2.79(5)
C(8)	0.3910(1)	0.19601(9)	0.1292(2)	3.34(5)
N(9)	0.91030(9)	0.20830(7)	0.1754(1)	3.07(4)
C(10)	0.9086(1)	0.1446(1)	0.2983(2)	3.66(6)
C(11)	0.9312(1)	0.0542(1)	0.2496(2)	4.31(6)
O(12)	1.03194(9)	0.05156(7)	0.2094(1)	4.74(5)
C(13)	1.0250(1)	0.1085(1)	0.0799(2)	4.71(7)
C(14)	1.0100(1)	0.2017(1)	0.1222(2)	3.93(6)
N(15)	0.85727(9)	0.34687(7)	0.0783(1)	2.99(4)

Table A-3.1 (contd...)

C(16)	0.9661(1)	0.3879(1)	0.1330(2)	3.58(6)
C(17)	0.9510(1)	0.4797(1)	0.1842(2)	4.54(7)
O(18)	0.8807(1)	0.52943(6)	0.0621(1)	4.60(5)
C(19)	0.7747(1)	0.4916(1)	0.0154(2)	4.42(7)
C(20)	0.7788(1)	0.3996(1)	-0.0408(2)	3.53(6)
C(21)	0.3391(1)	0.1185(1)	0.0624(2)	3.52(6)
N(22)	0.2994(1)	0.0541(1)	0.0078(2)	4.99(6)
C(23)	0.3303(1)	0.2546(1)	0.1932(2)	3.90(6)
N(24)	0.2824(1)	0.3030(1)	0.2489(2)	6.07(7)

Table A-3.2: *Hydrogen coordinates and isotropic displacement parmeters for DMDQ (11)*

Atom	x/a	y/b	z/c	U_{eq}
H(2)	0.7068	0.1319	0.0191	3.6
H(3)	0.5288	0.1027	0.0198	3.6
H(5)	0.5188	0.3 13	0.2446	3.7
H(6)	0.6954	0.3618	0.2384	3.6
H(101)	0.9632	0.1597	0.3925	4.4
H(102)	0.8384	0.1454	0.3166	4.4
H(111)	0.8732	0.0369	0.1610	5.2
H(112)	0.9354	0.0151	0.3344	5.2
H(131)	1.0906	0.1037	0.0492	5.7
H(132)	0.9642	0.0915	-0.0053	5.7
H(141)	1.0025	0.2376	0.0325	4.7
H(142)	1.0720	0.2198	0.2042	4.7
H(161)	1.0110	0.3560	0.2193	4.3
H(162)	0.9997	0.3891	0.0499	4.3
H(171)	1.0206	0.5075	0.2164	5.4
H(172)	0.9203	0.4775	0.2703	5.4
H(191)	0.7451	0.4915	0.1025	5.3
H(192)	0.7290	0.5252	-0.0676	5.3
H(201)	0.8008	0.4001	-0.1348	4.2
H(202)	0.7078	0.3743	-0.0613	4.2

Table **A-4.1:** *Atomic coordinates and equivalent isotropic displacement parameters for DPDQ-A (8)*

atom	x/a	y/b	z/c	U_{eq}
Molecule A				
C(1)	0.9550(1)	0.2830(2)	0.66826(8)	3.91(8)
C(2)	0.8812(1)	0.3644(3)	0.66878(9)	4.30(9)
C(3)	0.8598(1)	0.3892(3)	0.71645(9)	4.17(9)
C(4)	0.9108(1)	0.3366(2)	0.76676(8)	3.80(8)
C(5)	0.9845(1)	0.2561(3)	0.76569(8)	3.97(9)
C(6)	1.0056(1)	0.2296(3)	0.71782(9)	4.07(9)
C(7)	0.9771(1)	0.2531(2)	0.61662(8)	3.87(8)
C(8)	0.8880(1)	0.3656(3)	0.81716(9)	4.16(9)
N(9)	0.9226(1)	0.1789(2)	0.57689(7)	4.26(7)
C(10)	0.9179(2)	0.1877(3)	0.5178(1)	5.1(1)
C(11)	0.8282(2)	0.1446(4)	0.4915(1)	6.3(1)
C(12)	0.8099(2)	0.0207(4)	0.5291(1)	6.6(1)
C(13)	0.8517(2)	0.0839(3)	0.5855(1)	5.4(1)
N(14)	1.0516(1)	0.3021(2)	0.61189(7)	4.11(7)
C(15)	1.1013(2)	0.4236(3)	0.6477(1)	5.4(1)
C(16)	1.1665(2)	0.4680(4)	0.6187(1)	6.1(1)
C(17)	1.1841(2)	0.3133(4)	0.5938(1)	6.0(1)
C(18)	1.0976(2)	0.2439(3)	0.5730(1)	5.2(1)
C(19)	0.8095(2)	0.4256(3)	0.8178(1)	5.5(1)
N(20)	0.7445(2)	0.4726(4)	0.8179(1)	9.2(2)
C(21)	0.9441(1)	0.3346(3)	0. 679(1)	4.6(1)
N(22)	0.9913(2)	0.3092(3)	0.9092(1)	6.7(1)
Molecule B				
C(1')	0.4759(1)	0.2083(2)	0.25350(8)	3.67(8)
C(2')	0.5512(1)	0.1495(2)	0.24541(8)	3.89(8)
C(3')	0.5679(1)	0.1595(3)	0.19550(9)	4.09(9)
C(4')	0.5108(1)	0.2289(2)	0.15017(8)	4.03(9)
C(5')	0.4355(1)	0.2886(2)	0.15893(8)	4.00(8)
C(6')	0.4187(1)	0.2776(2)	0.20861(8)	3.78(8)
C(7')	0.4570(1)	0.2034(2)	0.30672(8)	3.65(8)
C(8')	0.5276(1)	0.2368(3)	0.09759(9)	4.6(1)
N(9')	0.5134(1)	0.2498(2)	0.35121(7)	3.92(7)

Table A-4.1 (contd...)

C(10')	0.5149(2)	0.2046(3)	0.4076(1)	5.3(1)
C(11')	0.6050(2)	0.2340(4)	0.4384(1)	6.5(1)
C(12')	0.6273(2)	0.3806(3)	0.4110(1)	5.7(1)
C(13')	0.5889(1)	0.3459(3)	0.35150(9)	4.37(9)
N(14')	0.3814(1)	0.1524(2)	0.30941(7)	4.41(8)
C(15')	0.3278(2)	0.0445(3)	0.2689(1)	5.5(1)
C(16')	0.2567(2)	0.0081(4)	0.2941(1)	7.0(1)
C(17')	0.2462(2)	0.1595(4)	0.3217(1)	7.0(2)
C(18')	0.3357(2)	0.2040(3)	0.3493(1)	5.8(1)
C(19')	0.6042(2)	0.1819(3)	0.0902(1)	5.5(1)
N(20')	0.6683(2)	0.1359(4)	0.0861(1)	8.0(1)
C(21')	0.4660(2)	0.2867(3)	0 0511(1)	5.2(1)
N(22')	0.4130(2)	0.3259(3)	0.0138(1)	7.1(1)

Table A-4.2: *Hydrogen coordinates and isotropic displacement parameters for DPDQ-A (8)*

Atom	x/a	y/b	z/c	U_{eq}
Molecule A				
H(2)	0.8457	0.4028	0.6355	5.2
H(3)	0.8090	0.4434	0.7156	5.0
H(5)	1.0207	0.2192	0.7990	4.8
H(6)	1.0558	0.1736	0.7184	4.9
H(101)	0.9302	0.2911	0.5078	6.1
H(102)	0.9555	0.1148	0.5083	6.1
H(111)	0.7922	0.2332	0.4895	7.5
H(112)	0.8221	0.1035	0.4558	7.5
H(121)	0.7510	0.0090	0.5242	7.9
H(122)	0.8335	-0.0779	0.5232	7.9
H(131)	0.8716	0.0002	0.6104	6.5
H(132)	0.8139	0.1477	0.5987	6.5
H(151)	1.0673	0.5117	0.6510	6.5
H(152)	1.1267	0.3821	0.6829	6.5

Table A-4.2 (contd...)

H(161)	1.1453	0.5446	0.5912	7.3
H(162)	1.2159	0.5075	0.6436	7.3
H(171)	1.2097	0.3305	0.5648	7.2
H(172)	1.2191	0.2471	0.6205	7.2
H(181)	1.0999	0.1320	0.5733	6.2
H(182)	1.0718	0.2797	0.5371	6.2
O(1W)	1.1039(2)	0.0528(3)	0.9566(1)	8.8(1)
Molecule B				
H(2')	0.5913	0.1020	0.2750	4.7
H(3')	0.6195	0.1185	0.1913	4.9
H(5')	0.3956	0.3376	0.1296	4.8
H(6')	0.3670	0.3178	0.2129	4.5
H(101')	0.4777	0.2683	0.4214	6.3
H(102')	0.5005	0.0968	0.4096	6.3
H(111')	0.6099	0.2524	0.4760	7.8
H(112')	0.6399	0.1478	0.4347	7.8
H(121')	0.6865	0.3936	0.4185	6.9
H(122')	0.6031	0.4722	0.4222	6.9
H(131')	0.6270	0.2882	0.3365	5.2
H(132')	0.5735	0.4407	0.3314	5.2
H(151')	0.3077	0.0948	0.2345	6.6
H(152')	0.3576	-0.0485	0.2647	6.6
H(161')	0.2069	-0.0186	0.2670	8.4
H(162')	0.2711	-0.0756	0.3198	8.4
H(171')	0.2198	0.2372	0.2959	8.4
H(172')	0.2144	0.1447	0.3475	8.4
H(181')	0.3554	0.1501	0.3830	7.0
H(182')	0.3411	0.3145	0.3553	7.0
O(2W)	0.7320(2)	-0.1332(3)	0.0431(1)	11.2(2)

Table A-5.1: *Atomic coordinates and equivalent isotropic displacement parameters for DPDQ-C (8)*

Atom	x/a	y/b	z/c	U_{eq}
C(1)	0.4970(4)	0.7793(3)	0.6206(6)	3.2(2)
C(2)	0.5389(3)	0.7150(3)	0.6989(5)	3.2(2)
C(3)	0.6365(4)	0.6907(3)	0.6951(6)	3.5(2)
C(4)	0.6971(4)	0.7310(3)	0.6130(6)	3.7(2)
C(5)	0.6549(4)	0.7957(3)	0.5341(6)	4.2(2)
C(6)	0.5568(4)	0.8198(3)	0.5370(6)	3.8(2)
C(7)	0.3910(3)	0.8048(3)	0.6213(5)	3.1(2)
C(8)	0.8005(4)	0.7057(4)	0.6100(7)	4.9(3)
N(9)	0.3123(3)	0.7581(2)	0.5775(5)	3.1(2)
C(10)	0.2133(4)	0.7621(3)	0.6264(6)	3.7(2)
C(11)	0.1762(4)	0.6808(3)	0.6113(7)	4.9(3)
C(12)	0.2142(5)	0.6514(3)	0.4740(7)	4.8(3)
C(13)	0.3179(4)	0.6872(3)	0.4885(6)	3.8(2)
N(14)	0.3775(3)	0.8751(2)	0.6676(5)	3.5(2)
C(15)	0.4594(4)	0.9215(3)	0.7669(8)	4.9(3)
C(16)	0.4056(5)	0.9913(3)	0.796(1)	5.9(3)
C(17)	0.3204(5)	1.0006(3)	0.648(1)	6.2(3)
C(18)	0.2813(4)	0.9200(3)	0.6173(7)	4.6(2)
C(19)	0.8397(5)	0.6377(5)	0.680(1)	6.3(4)
N(20)	0.8700(5)	0.5823(5)	0.743(1)	9.1(4)
C(21)	0.8632(5)	0.7515(5)	0.5382(8)	6.2(3)
N(22)	0.9115(5)	0.7900(6)	0.4788(9)	9.5(4)
Cl(1)	0.3556(2)	0.5359(1)	0.2412(3)	9.0(1)
Cl(2)	0.5422(2)	0.4714(1)	0.1921(3)	9.6(1)
Cl(3)	0.5479(2)	0.6107(2)	0.3584(3)	10.8(2)
C(23)	0.4793(6)	0.5551(5)	0.211(1)	6.9(4)

Table A-5.2: *Hydrogen coordinates and isotropic displacement parameters for DPDQ-C (S)*

Atom	x/a	y/b	z/c	U_{eq}
H(2)	0.4995	0.6872	0.7567	3.8
H(3)	0.6631	0.6459	0.7490	4.2
H(5)	0.6945	0.8237	0.4771	5.1
H(6)	0.5296	0.8643	0.4822	4.6
H(101)	0.2236	0.7793	0.7299	4.4
H(102)	0.1657	0.7946	0.5608	4.4
H(111)	0.2056	0.6527	0.7016	5.9
H(112)	0.1030	0.6783	0.5924	5.9
H(121)	0.2203	0.5978	0.4779	5.8
H(122)	0.1686	0.6660	0.3803	5.8
H(131)	0.3299	0.6986	0.3898	4.6
H(132)	0.3712	0.6550	0.5425	4.6
H(151)	0.4880	0.8960	0.8609	5.8
H(152)	0.5130	0.9327	0.7153	5.8
H(161)	0.3766	0.9857	0.8833	7.1
H(162)	0.4513	1.0335	0.8107	7.1
H(171)	0.2669	1.0335	0.6634	7.4
H(172)	0.3476	1.0193	0.5649	7.4
H(181)	0.2512	0.9123	0.5110	5.6
H(182)	0.2323	0.9079	0.6763	5.6
H(23)	0.4713	0.5826	0.1169	8.3

Table A-6.1: *Atomic coordinates and equivalent isotropic displacement parameters for MBPDQ*

Atom	x/a	y/b	z/c	U_{eq}
C(1)	0.6082(2)	0.3000	0.8543(2)	3.58(9)
C(2)	0.5661(2)	0.3739(4)	0.9628(2)	3.8(1)
C(3)	0.4607(2)	0.3574(5)	0.9905(2)	3.8(1)
C(4)	0.3927(2)	0.2654(4)	0.9110(2)	3.57(9)
C(5)	0.4357(2)	0.1916(5)	0.8015(2)	3.8(1)
C(6)	0.5408(2)	0.2083(4)	0.7741(2)	3.66(9)

Table A-6.1 (contd...)

C(7)	0.7204(2)	0.3181(4)	0.8270(2)	3.9(1)
C(8)	0.2830(2)	0.2458(5)	0.9421(3)	4.3(1)
N(9)	0.7913(2)	0.2881(5)	0.9165(2)	4.06(9)
C(10)	0.9050(2)	0.3097(6)	0.8974(3)	5.4(1)
C(11)	0.9546(2)	0.2697(7)	1.0270(3)	5.8(1)
C(12)	0.8784(2)	0.1461(6)	1.0838(3)	5.6(1)
C(13)	0.7717(2)	0.2112(5)	1.0427(3)	4.4(1)
N(14)	0.7513(2)	0.3652(5)	0.7100(2)	5.0(1)
C(15)	0.6829(3)	0.4436(5)	0.6131(2)	4.9(1)
C(16)	0.7378(4)	0.5959(6)	0.5606(4)	7.4(2)
C(17)	0.6503(2)	0.3268(5)	0.5057(2)	4.7(1)
C(18)	0.5555(3)	0.3580(6)	0.4419(3)	5.7(1)
C(19)	0.5237(4)	0.2630(6)	0.3376(3)	7.1(2)
C(20)	0.5874(5)	0.1349(7)	0.2980(3)	7.6(2)
C(21)	0.6783(4)	0.1001(7)	0.3598(4)	7.6(2)
C(22)	0.7129(3)	0.1965(7)	0.4645(4)	6.5(2)
C(23)	0.2467(2)	0.3007(6)	1.0611(3)	5.0(1)
N(24)	0.2186(3)	0.3489(8)	1.1581(3)	7.7(2)
C(25)	0.2108(2)	0.1748(6)	0.8548(3)	5.7(1)
N(26)	0.1515(2)	0.1179(9)	0.7823(4)	9.1(2)

Table A-6.2: *Hydrogen coordinates and isotropic displacement parameters for MBPDQ (14)*

Atom	x/a	x/b	x/c	U_{eq}
H(2)	0.6106	0.4367	1.0186	4.5
H(3)	0.4339	0.4094	1.0649	4.5
H(5)	0.3915	0.1291	0.7453	4.6
H(6)	0.5678	0.1568	0.6997	4.4
H(101)	0.9294	0.2356	0.8336	6.5
H(102)	0.9203	0.4204	0.8730	6.5
H(111)	1.0223	0.2217	1.0176	6.9
H(112)	0.9602	0.3662	1.0788	6.9

Table A-6.2 (contd...)

H(121)	0.8897	0.0382	1.0503	6.7
H(122)	0.8852	0.1434	1.1747	6.7
H(131)	0.7470	0.2909	1.1020	5.3
H(132)	0.7221	0.1235	1.0348	5.3
H(114)	0.8288	0.3669	0.6958	6.0
H(15)	0.6209	0.4796	0.6544	5.8
H(161)	0.8012	0.5635	0.5208	8.8
H(162)	0.6930	0.6490	0.4992	8.8
H(163)	0.7534	0.6705	0.6288	8.8
H(18)	0.5119	0.4457	0.4703	6.8
H(19)	0.4590	0.2856	0.2940	8.5
H(20)	0.5666	0.0703	0.2257	9.1
H(21)	0.7196	0.0091	0.3323	9.2
H(22)	0.7782	0.1730	0.5065	7.8
N(27)	0.9778(4)	0.377(2)	0.6055(4)	15.7(6)
C(28)	1.0028(6)	0.399(1)	0.504(1)	11.2(4)
C(29)	1.0349(5)	0.417(1)	0.3657(5)	10.9(4)
H(291)	1.0835	0.3324	0.3449	13.0
H(292)	0.9745	0.4088	0.3112	13.0
H(293)	1.0670	0.5225	0.3542	13.0

Table A-7.1: *Atomic coordinates and equivalent isotropic displacement parameters for PMPDQ (16)*

Atom	x/a	y/b	z/c	U_{eq}
C(1)	0.6434(6)	0.314(1)	0.605(1)	5.8(3)
C(2)	0.6742(7)	0.202(1)	0.609(1)	6.9(3)
C(3)	0.7321(6)	0.176(1)	0.705(1)	6.1(3)
C(4)	0.7643(6)	0.252(1)	0.799(1)	5.8(2)
C(5)	0.7331(6)	0.355(1)	0.788(1)	6.1(3)
C(6)	0.6730(7)	0.385(1)	0.698(1)	6.2(3)
C(7)	0.5781(7)	0.342(1)	0.499(1)	5.6(2)
C(8)	0.8285(7)	0.216(1)	0.893(1)	6.2(3)

Table A-7.1 (contd...)

N(9)	0.5963(6)	0.3299(8)	0.371(1)	6.9(2)
C(10)	0.5336(8)	0.307(1)	0.261(2)	10.0(4)
C(11)	0.5826(9)	0.267(1)	0.153(1)	8.8(3)
C(12)	0.663(1)	0.264(2)	0.190(2)	13.1(5)
C(13)	0.6828(8)	0.318(1)	0.316(1)	7.8(3)
N(14)	0.5062(6)	0.3831(7)	0.541(1)	6.3(2)
C(15)	0.467(1)	0.350(2)	0.669(2)	9.9(4)
C(16)	0.389(1)	0.420(1)	0.689(2)	9.7(4)
C(17)	0.395(1)	0.510(1)	0.575(2)	8.7(4)
C(18)	0.4468(8)	0.451(1)	0.467(1)	7.4(3)
C(19)	0.450(2)	0.207(3)	0.633(4)	23(3)
O(20)	0.413(2)	0.194(2)	0.510(3)	25(2)
C(21)	0.403(1)	0.089(2)	0.504(2)	12(1)
C(22)	0.8542(8)	0.109(1)	0.912(1)	7.5(3)
N(23)	0.8775(8)	0.023(1)	0.917(1)	10.3(4)
C(24)	0.863(1)	0.293(1)	0.979(1)	8.5(4)
N(25)	0.892(1)	0.361(1)	1.044(1)	11.7(4)

Table A-7.2: *Hydrogen coordinates and isotropic displacement parameters for PMPDQ (16)*

Atom	x/a	y/b	z/c	U_{eq}
H(2)	0.6550	0.1476	0.5447	7.7
H(3)	0.7517	0.1023	0.7078	7.3
H(5)	0.7538	0.4087	0.8482	7.2
H(6)	0.6517	0.4589	0.7007	7.3
H(101)	0.4917	0.2566	0.2891	12.4
H(102)	0.5059	0.3751	0.2336	12.4
H(111)	0.5632	0.1918	0.1301	9.9
H(112)	0.5755	0.3100	0.0726	9.9
H(121)	0.6800	0.1882	0.1971	15.8
H(122)	0.6956	0.2993	0.1226	15.8
H(131)	0.7112	0.3838	0.3051	9.4

Table A-7.2 (contd...)

H(132)	0.7162	0.2687	0.3739	9.4
H(15)	0.5060	0.3577	0.7427	11.3
H(161)	0.3367	0.3760	0.6780	11.6
H(162)	0.3861	0.4520	0.7772	11.6
H(171)	0.3388	0.5303	0.5440	9.9
H(172)	0.4222	0.5737	0.6092	9.9
H(181)	0.4762	0.5003	0.4074	8.5
H(182)	0.4120	0.4030	0.4089	8.5
H(191)	0.4981	0.1698	0.6552	24.8
H(192)	0.4061	0.1866	0.7082	24.8
H(211)	0.3680	0.0563	0.5742	15.0
H(212)	0.3749	0.0698	0.4182	15.0
H(213)	0.4557	0.0448	0.5033	15.0

Table A-8.1: *Atomic coordinates and equivalent isotropic displacement parameters for DMPDQ (**12**)*

Atom	x/a	y/b	z/c	U_{eq}
C(1)	0.7488(1)	0.4000	1.1030(2)	3.16(6)
C(2)	0.7324(1)	0.3404(3)	0.9576(2)	3.46(6)
C(3)	0.7339(1)	0.4417(3)	0.8397(2)	3.42(6)
C(4)	0.7494(1)	0.6082(3)	0.8602(2)	3.09(6)
C(5)	0.7649(1)	0.6660(3)	1.0070(2)	3.38(6)
C(6)	0.7659(1)	0.5647(3)	1.1257(2)	3.41(6)
C(7)	0.7513(1)	0.2855(3)	1.2252(2)	3.13(6)
C(8)	0.7490(1)	0.7139(3)	0.7359(2)	3.59(7)
N(9)	0.8286(1)	0.2742(3)	1.3371(2)	3.46(5)
C(10)	0.9295(1)	0.3310(4)	1.3313(2)	4.47(8)
C(11)	0.9884(2)	0.2860(4)	1.4864(3)	5.30(1)
C(12)	0.9143(2)	0.2838(4)	1.5830(3)	5.50(1)
C(13)	0.8253(2)	0.2075(4)	1.4846(2)	4.42(8)
C(14)	0.9659(2)	0.2540(4)	1.2048(3)	5.30(1)
O(15)	0.9511(1)	0.0873(3)	1.2078(2)	5.90(8)

Table A-8.1 (contd...)

C(16)	0.9767(2)	0.0088(7)	1.0865(3)	7.40(2)
N(17)	0.6753(1)	0.1852(3)	1.2196(2)	3.37(5)
C(18)	0.5720(1)	0.2283(4)	1.1519(2)	3.75(7)
C(19)	0.5185(2)	0.0666(4)	1.1383(3)	5.00(1)
C(20)	0.5984(2)	-0.0606(4)	1.1628(3)	5.01(9)
C(21)	0.6818(1)	0.0181(3)	1.2729(2)	4.13(8)
C(22)	0.5336(2)	0.3472(4)	1.2496(3)	4.72(9)
O(23)	0.5436(1)	0.2781(4)	1.3900(2)	6.26(9)
C(24)	0.5083(3)	0.3760(8)	1.4915(5)	8.70(2)
C(25)	0.7404(2)	0.6558(4)	0.5911(2)	4.38(8)
N(26)	0.7327(2)	0.6087(5)	0.4722(2)	7.10(1)
C(27)	0.7584(2)	0.8799(4)	0.7540(2)	4.44(9)
N(28)	0.7662(3)	1.0176(4)	0.7683(3)	7.40(1)

Table A-8.2: *Hydrogen coordinates and equivalent isotropic displacement parameters for DMPDQ (12)*

Atom	x/a	y/b	z/c	U_{eq}
H(2)	0.7202	0.2289	0.9401	4.1
H(3)	0.7242	0.3982	0.7422	4.1
H(5)	0.7751	0.7779	1.0247	4.1
H(6)	0.7782	0.6072	1.2238	4.1
H(10)	0.9290	0.4446	1.3200	5.4
H(111)	1.0179	0.1830	1.4848	6.4
H(112)	1.0381	0.3638	1.5210	6.4
H(121)	0.9370	0.2212	1.6698	6.6
H(122)	0.9000	0.3898	1.6107	6.6
H(131)	0.7665	0.2377	1.5143	5.3
H(132)	0.8307	0.0935	1.4852	5.3
H(141)	1.0341	0.2759	1.2150	6.4
H(142)	0.9306	0.2964	1.1130	6.4
H(161)	0.9652	-0.1035	1.0929	8.9
H(162)	0.9378	0.0497	0.9966	8.9

Table A-8.2 (contd...)

H(163)	1.0443	0.0269	1.0879	8.9
H(18)	0.5684	0.2732	1.0560	4.5
H(191)	0.4799	0.0578	1.2115	6.0
H(192)	0.4774	0.0555	1.0422	6.0
H(201)	0.5769	-0.1559	1.2031	6.0
H(202)	0.6180	-0.0854	1.0725	6.0
H(211)	0.7435	-0.0287	1.2687	4.9
H(212)	0.6716	0.0112	1.3716	4.9
H(221)	0.4662	0.3698	1.2091	5.7
H(222)	0.5706	0.4441	1.2566	5.7
H(241)	0.5452	0.4730	1.5064	10.4
H(242)	0.4409	0.4004	1.4533	10.4
H(243)	0.5148	0.3210	1.5836	10.4

Table A-9.1: *Atomic coordinates and equivalent istotropic displacement parameters for DHPDQ (13)*

Atom	x/a	y/b	z/c	U_{eq}
O(1)	0.7501(2)	0.4569(1)	0.3870(3)	5.7(1)
O(2)	0.6772(2)	0.6903(1)	0.9648(2)	5.57(9)
C(1)	0.4351(2)	0.4938(1)	0.7593(3)	3.30(8)
C(2)	0.3289(2)	0.4737(1)	0.7022(3)	3.8(1)
C(3)	0.2635(2)	0.4173(1)	0.7766(3)	3.80(9)
C(4)	0.3034(2)	0.3783(1)	0.9119(2)	3.31(8)
C(5)	0.4105(2)	0.3997(1)	0.9677(3)	3.69(9)
C(6)	0.4754(2)	0.4560(1)	0.8928(3)	3.64(9)
C(7)	0.5047(2)	0.5553(1)	0.6803(3)	3.33(8)
C(8)	0.2375(2)	0.3169(1)	0.9869(3)	3.9(1)
N(9)	0.5533(2)	0.5370(1)	0.5455(2)	4.1(1)
C(10)	0.5584(2)	0.4534(1)	0.4891(4)	4.8(1)
C(11)	0.6342(2)	0.4582(2)	0.3452(3)	4.6(1)
C(12)	0.6076(3)	0.5396(2)	0.2826(3)	5.3(1)
N(13)	0.6051(3)	0.5903(1)	0.4283(3)	4.6(1)

Table A-9.1 (contd...)

N(14)	0.5125(2)	0.6251(1)	0.7495(2)	3.51(7)
C(15)	0.5941(2)	0.6892(1)	0.7140(3)	4.4(1)
C(16)	0.5998(3)	0.7332(1)	0.8673(3)	4.6(1)
C(17)	0.4810(3)	0.7293(1)	0.9288(4)	5.0(1)
C(18)	0.4458(2)	0.6447(1)	0.8935(3)	4.4(1)
C(19)	0.1481(2)	0.2784(2)	0.9088(3)	4.7(1)
N(20)	0.0765(2)	0.2461(2)	0.8435(4)	7.1(2)
C(21)	0.2671(2)	0.2867(2)	1.1317(3)	4.5(1)
N(22)	0.2923(2)	0.2615(2)	1.2529(3)	6.8(1)

Table A-9.2: *Hydrogen coordinates and is to tropic displacement parameters for DHPDQ (13)*

Atom	x/a	y/b	z/c	U_{eq}
H(O1)	0.7771	0.3994	0.4058	6.7
H(O2)	0.6833	0.7197	1.0625	6.6
H(2)	0.3007	0.4991	0.6107	4.6
H(3)	0.1905	0.4046	0.7361	4.6
H(5)	0.4394	0.3750	1.0594	4.4
H(6)	0.5483	0.4692	0.9328	4.4
H(101)	0.4849	0.4346	0.4623	5.7
H(102)	0.5909	0.4198	0.5663	5.7
H(11)	0.6164	0.4180	0.2713	5.5
H(121)	0.5360	0.5402	0.2311	6.4
H(122)	0.6650	0.5570	0.2123	6.4
H(131)	0.6797	0.6055	0.4587	5.6
H(132)	0.5599	0.6363	0.4130	5.6
H(151)	0.5669	0.7223	0.6322	5.2
H(152)	0.6664	0.6684	0.6858	5.2
H(16)	0.6238	0.7864	0.8528	5.5
H(171)	0.4332	0.7660	0.8761	6.0
H(172)	0.4792	0.7395	1.0382	6.0
H(181)	0.4653	0.6104	0.9775	5.2
H(182)	0.3664	0.6414	0.8741	5.2

List of Publications :

1. **M.Ravi,** A.Samanta and T.P.Radhakrishnan, "Excited State Dipole Moments from an Efficient Analysis of Solvatochromic Stokes Shift Data", J. *Phys. Chem.* **1994,** *98,* 9133.

2. **M.Ravi,** T.Soujanya. A.Samanta and T.P.Radhakrishnan, "Excited State Dipole Moments of Some Coumarin dyes from a Solvatochromic Method using the Solvent Polarity Parameter", E_T^N, *J. Chem. Soc. Faraday Trans.* **1995,** 97, 2739.

3. **M.Ravi,** D.N.Rao. S.Cohen, I.Agranat and T.P.Radhakrishnan, "A New Class of Nonlinear Optical Materials Based on Push - Pull Quinonoid Molecules", *Curr. Sci. (India)* **1995,** *68,* 1119.

4. **M.Ravi** and T.P.Radhakrishnan, "Analysis of the Large Hyperpolarizabilities of Push -Pull Quinonoid Molecules", *J. Phys. Chem.* **1995,** *99,* 17624.

5. **M.Ravi,** D.N.Rao. S.Cohen, I.Agranat and T.P.Radhakrishnan, "Strong Optical Second Harmonic Generation in a Chiral Diaminodicyanoquinodimethane System", *J. Mater. Chem.* **1996, *6,* 1119.**

6. **M.Ravi,** S.Cohen, I.Agranat and T.P.Radhakrishnan, "Molecular and Crystal Structures of a Class of Push - Pull Quinonoid Compounds with Potential Nonlinear Optical Applications", *Struct. Chem.* **1996,** 7, 225.

7. **M.Ravi,** D.N.Rao, S.Cohen, I.Agranat and T.P.Radhakrishnan, "Solvate Switchable Powder Second Harmonic Generation in a Push - Pull Quinonoid System",./. *Mater. Chem.* **1996,** *6,* 1853.

8. **M.Ravi,** D.N.Rao, S.Cohen, I.Agranat and T.P.Radhakrishnan, "Push - Pull Quinonoid Compounds : Enhanced Powder SHG Utilizing the Effect of Chiral Centres on the Dipole Alignment", *Chem. Mater.* **1997,** P, 830..

9. **M.Ravi,** "A Simple Method for the Estimation of Hyperpolarizabilities: Application to Diamino Substituted Dicyanoquinodimethane Molecules", *Synth. Metals* (submitted).

10. **M.Ravi,** P.Gangopadhyay, D.N.Rao, S.Cohen, I.Agranat and T.P.Radhakrishnan, "Dual Influence of H-bonding on the Solid State SHG in a Quinonoid Molecular Material" (manuscript under preparation).

Posters/Lectures presented and Meetings /Workshops attended :

1. **M.Ravi,** D.N.Rao and T.P.Radhakrishnan, "New Organic molecules of interest as TICT and NLO systems", *Trombay Symposium on Radiation and Photochemistry* (TSRP-94), BARC, Bombay, Jan. 1994.

2. **M.Ravi,** D.N.Rao and T.P.Radhakrishnan, "Second Harmonic Generation in Novel Organic Materials", *National Laser Symposium*, IRDE, Dehradun, Feb., 1995.

3. Workshop on Electrodeposition of Thin Films, IUC, Indore, Jan., 1995.

4. Indo-Japanese joint workshop on Molecular Level Design of Molecular Materials and Functions, NCL, Pune, March, 1996.

5. Presented a lecture at the Workshop on Nonlinear Optics, CAT, Indore, July, 1996.

6. **M.Ravi,** S.Venugopal Rao, V.Nirmal Kumar, D.N.Rao and T.P.Radhakrishnan, "Quinonoid Molecular Materials for Nonlinear Optics: EFISHG study of Molecular Hyperpolarizabilities", *Physics of Materials*, University of Hyderabad, Hyderabad, March, 1997.